2022年 2月
博士學位論文

Exploration of optimal processes on amine plasma-polymerization and plasma sterilization for biomedical applications

朝 鮮 大 學 校 大 學 院

齒醫生命工學科

李 昌 珉

Exploration of optimal processes on amine plasma-polymerization and plasma sterilization for biomedical applications

의생명 응용을 위한 아민 플라즈마 중합 및
플라즈마 살균에 관한 최적공정 탐색

2022年 2月 25日

朝 鮮 大 學 校 大 學 院

齒 醫 生 命 工 學 科

李 昌 珉

Exploration of optimal processes on amine plasma-polymerization and plasma sterilization for biomedical applications

指導敎授 金 炳 勳

이 論文을 工學 博士學位申請 論文으로 提出함

2021年 10月

朝鮮大學校 大學院

齒醫生命工學科

李 昌 珉

李昌珉의 博士學位論文을 認准함

委員長　朝鮮大學校　敎　授　崔 漢 喆　印

委　員　全南大學校　敎　授　鞠 旻 錫　印

委　員　朝鮮大學校　敎　授　金 熙 中　印

委　員　朝鮮大學校　敎　授　安 相 建　印

委　員　朝鮮大學校　敎　授　金 炳 勳　印

2022年　1月

朝鮮大學校 大學院

Contents

LIST OF TABLES ---------- v
LIST OF FIGURES ---------- vi
ABSTRACT (ENGLISH) ---------- x iii

1. General Introduction ---------- 1

2. Backgrounds ---------- 3
2.1. Bone tissue Engineering ---------- 3
2.2. Biomaterals ---------- 5
2.2.1. Polymers ---------- 8
2.2.2. Metals ---------- 12
2.3. Plasma surface modifications (PSM) ---------- 15
2.3.1. Plasma ---------- 15
2.3.2. Sources and discharge of plasma generation ---------- 16
2.3.2.1. Microwave (MW) plasma ---------- 16
2.3.2.2. Radio frequency (RF) plasma ---------- 16
2.3.2.3. Dielectric barrier discharge (DBD) ---------- 17
2.3.3. Plasma surface treatment ---------- 19
2.3.3.1. Surface cleaning ---------- 19
2.3.3.2. Surface treatment ---------- 21
2.3.4. Plasma-polymerization ---------- 24
2.4. Plasma sterilization ---------- 26
2.5. Applications of plasma ---------- 29

3. Part Ⅰ: HDPE surface modification by amine plasma-polymerization using three kinds of monomers ---------- 30
3.1. Introduction ---------- 30
3.2. Materials ---------- 33
3.2.1. Preparation of high density polyethylene samples -------- 33
3.2.2. Amine monomers ---------- 33

3.2.3. Low-pressure RF plasma deposition ---------- 33
3.3. Methods ---------- 35
3.3.1. Plasma-polymerization ---------- 35
3.3.2. Surface characterizations ---------- 36
3.3.2.1. Contact angle ---------- 36
3.3.2.2. Amine concentration measurement ---------- 36
3.3.3. Mesenchymal stem cells (MSCs) proliferation ---------- 37
3.3.3.1. Mesenchymal stem cell culture ---------- 37
3.3.3.2. Cell proliferation ---------- 37
3.4. Results ---------- 39
3.4.1. Surface characterizations ---------- 39
3.4.1.1. Allylamine plasma-polymerization for process optimization 39
3.4.1.2. Cyclopropylamine plasma-polymerization for process optimization ---------- 43
3.4.1.3. 1,2-Diaminocyclohexane plasma-polymerization for process optimization ---------- 48
3.4.1.4. Amine concentration analysis after amine plasma-polymerization ---------- 53
3.4.2. Proliferation of mesenchymal stem cells ---------- 56
3.5. Discussions ---------- 57
3.6. Conclusions ---------- 60

4. Part Ⅱ: Preosteoblast behaviors on Ti surface with modified by amine plasma-polymerization using APPJ device -------- 61
4.1. Introduction ---------- 61
4.2. Materials ---------- 63
4.2.1. Titanium ---------- 63
4.2.2. Amine monomers ---------- 63
4.3. Methods ---------- 64
4.3.1. Atmospheric pressure plasma jet setup ---------- 64
4.3.2. Gas species analysis in plasma plume ---------- 64
4.3.3. Electrical characteristic of plasma discharge ---------- 64

4.3.4. Surface characterizations ---------- 66
4.3.4.1. Contact angles ---------- 66
4.3.4.2. Surface topologies and roughness ---------- 66
4.3.4.3. Surface chemistry ---------- 66
4.3.5. Preosteoblast *in vitro* evaluations ---------- 67
4.3.5.1. Cell culture ---------- 67
4.3.5.2. Cell proliferation ---------- 67
4.3.5.3. Cell viability ---------- 68
4.3.5.4. Focal adhesion ---------- 68
4.3.5.5. Cell differentiation ---------- 69
4.3.5.6. Bone mineralization ---------- 70
4.3.5.7. Western blotting ---------- 70
4.3.6. Statistical analysis ---------- 70
4.4. Results ---------- 71
4.4.1. Surface characterizations ---------- 71
4.4.2. Biological response of MC3T3-E1 cells ---------- 91
4.5. Discussions ---------- 98
4.6. Conclusions ---------- 100

5. Part Ⅲ: Feasibility of CAP on the eradication of *P. gingivalis* bioflim for periodontitis treatment ---------- 101
5.1. Introduction ---------- 101
5.2. Materials ---------- 103
5.3. Methods ---------- 105
5.3.1. CAP setup ---------- 105
5.3.2. Gas species analysis in plasma plume ---------- 108
5.3.3. *P. gingivalis* culture ---------- 110
5.3.4. *P. gingivalis* CFU assay ---------- 111
5.3.5. Human gingival fibroblast culture ---------- 111
5.3.6. Morphological analysis ---------- 111
5.3.7. ROS generation in PBS ---------- 112
5.3.8. Live and dead cell Staining ---------- 112

5.4. Results ---------- 113
5.4.1. Gas species analysis in plasma plume ---------- 113
5.4.2. *P. gingivalis* biofilm formation ---------- 113
5.4.3. Generation of ROS by CAP ---------- 113
5.4.4. Antibacterial activity of CAP ---------- 117
5.4.5. Live and dead cell activity of *P. gingivalis* -------- 117
5.4.6. Viability of HGF-1 cells after CAP treatment -------- 120
5.5. Discussions ---------- 122
5.6. Conclusions ---------- 124

6. ABSTRACT (KOREAN) ---------- 125

7. References ---------- 129

LIST OF TABLES

Table 2.1. Manufacturing methods and materials that have been used in the construction of porous scaffolds to replace bone damage ---------- 4

Table 2.2. List of common medical devices and materials by FDA ---------- 10

Table 3.1. Amine plasma-polymerization conditions (Nozzle diameter: 3.5 mm) ---------- 35

Table 3.2. Low and high amine concentrations ---------- 55

Table 4.1. Conditions of plasma discharge ---------- 85

Table 5.1. Characterization of frequency and power of CAP ---------- 107

LIST OF FIGURES

Figure 2.1. Evolution of biomaterials ---------- 6

Figure 2.2. Plasma cleaning application from dental materials by Relyon plasma company equipment ---------- 19

Figure 2.3. Schematic diagram of plasma cleaning works to contaminated surface ---------- 20

Figure 2.4. Roles of the physical mechanism on the effect of microbubbles and plasma-derived NO in biofilm dispersal ---------- 28

Figure 3.1. Photographs of HDPE disk sample used in this study ---------- 34

Figure 3.2. Constitutional formula of plasma-polymerization monomers, (a) Allylamine, (b) Cyclopropylamine, (c) 1,2-Diaminocyclohexane -------- 34

Figure 3.3. Schematic diagram and actual image of low-pressure plasma system ---------- 34

Figure 3.4. The effect of chamber inside pressure on the surface distribution patterns of allylamine polymeric thin film. The pressure inside the chamber was varied from 30 to 100 mTorr; (a) 30 mTorr, (b) 40 mTorr, (c) 50 mTorr, (d) 60 mTorr, and (e) 100 mTorr. Plasma-polymerization was performed on the 19 cm diameter stanless steel plate and set up by 80W power using 3.5 mm nozzle diameter ---------- 40

Figure 3.5. The effect of chamber inside pressure and plasma power on the surface distribution patterns of allylamine polymeric thin film. The pressure inside the chamber was selected to be 30 and 60 mTorr; (a-c) 30 mTorr, (d-f) 60 mTorr. Also, plasma power varied from 30 to 90 W; (a, d) 30 W, (b, e) 60 W, (c, f) and 90 W. Plasma-polymerization was performed on the 19 cm diameter stainless steel plate using 3.5 mm nozzle diameter --- 41

Figure 3.6. The effect of distance from center on the amine concentration distributions. (a) Sample positions marked on surface. (b) Contact angles as a function of distances from center and positions marked on surface. (c) The

effect of distance from center to positions on the changes of amine concentrations. Plasma-polymerization was carried out at 60 W power and 30 mTorr chamber pressure ---------- 42

Figure 3.7. The effect of pressure inside the chamber on the surface distribution patterns of cyclopropylamine polymeric thin film. The pressure inside the chamber was varied from 30 to 50 mTorr. (a) 30 mTorr, (b) 35 mTorr, (c) 40 mTorr, (d) 45 mTorr, and (e) 50 mTorr. Plasma-polymerization was performed on the 19 cm diameter stainless steel plate and set up by 60 W power using 3.5 mm nozzle diameter ---------- 44

Figure 3.8. Effect of chamber pressure on the changes of amine concentration distributions. The pressure inside the chamber was varied from 30 to 50 mTorr. (a) sample positions marked on surface, (b) 30 mTorr, (c) 35 mTorr, (d) 40 mTorr, (e) 45 mTorr, and (f) 50 mTorr. Plasma-polymerization was carried out at 60 W power using 3.5 mm nozzle diameter ---------- 45

Figure 3.9. Effect of plasma power on the changes of amine concentration distributions. The plasma power was varied from 50 to 70 W; (a) Sample positions marked on surface, (b) 50 W, (c) 60 W and (d) 70 W. Plasma-polymerization was carried out at 40 mTorr chamber pressure using 3.5 mm nozzle diameter ---------- 46

Figure 3.10. Effect of distance from center on the changes of amine concentration. (a) Sample positions marked on surface, (b) Contact angles. (c) Plots of amine concentrations vs. distance from nozzle. Plasma-polymerization was carried out at 60 W power and 40 mTorr chamber pressure ---------- 47

Figure 3.11. The effect of chamber inside pressure on the changes of surface distribution patterns of 1,2-diaminocyclohexane polymeric thin film. The pressure inside the chamber was varied from 5 to 45 mTorr; (a) 5 mTorr, (b) 10 mTorr, (c) 15 mTorr, (d) 20 mTorr, (e) 25 mTorr, (f) 30 mTorr,

(g) 35 mTorr, (h) 40 mTorr and (i) 45 mTorr. Plasma-polymerization was performed on the 19 cm diameter stainless steel plate and set up by 50 W power using 2 mm nozzle diameter ---------- 49

Figure 3.12. The effect of plasma power and nozzle diameter on the changes of surface distribution patterns of 1,2-diaminocyclohexane polymeric thin film. The plasma power was selected to be 50 and 80 W; (a-d) 50 W, and (e-h) 80 W. Also, nozzle diameter varied from 0.5 mm to 3.5 mm; (a, e) 0.5 mm, (b, f) 1 mm, (c, g) 2 mm, and (d, h) 3.5 mm. Plasma-polymerization was performed on the 19 cm diameter stainless steel plate and set up by 10 mTorr chamber pressure ---------- 50

Figure 3.13. FT-IR results of 1,2-diaminocyclohexane plasma-polymerization after washed by water or 70% ethanol. (a) no washed. (b) deionized water at 25℃, 100 rpm for 1 h. (c) 70% ethanol for 5 min. (d) Comparison of each samples of 8 cm distance from center. Plasma-polymerization was carried out at 80 W power and 10 mTorr chamber pressure ---------- 51

Figure 3.14. The effect of distance from center on the changes of amine concentration distributions. (a) Sample positions marked on surface. (b) Contact angles. (c) Plots of amine concentrations vs. distance from center. Plasma-polymerization was carried out at 80 W power and 10 mTorr chamber pressure ---------- 52

Figure 3.15. (a) HDPE disks with low and high amine concentration dyed by orange II. (b) FT-IR spectrum of disks treated with various monomers. (AA-H, allylamine high amine concentration; CPA-H, cyclopropylamine high amine concentration; DACH-H, 1,2-diaminocyclohexane high amine concentration; AA-L, allylamine low amine concentration; CPA-L, cyclopropylamine low amine concentration; DACH-L, 1,2-diaminocyclohexane low amine concentration) ---------- 54

Figure 3.16. The effect of monomers on the changes of contact angles of the samples. (AA-H, allylamine high amine concentration; CPA-H,

cyclopropylamine high amine concentration; DACH-H, 1,2-diaminocyclohexane high amine concentration; AA-L, allylamine low amine concentration; CPA-L, cyclopropylamine low amine concentration; DACH-L, 1,2-diaminocyclohexane low amine concentration) ---------- 55

Figure 3.17. The effect of various monomers and amine concentrations on the MSCs proliferation. (AA-H, allylamine high amine concentration; CPA-H, cyclopropylamine high amine concentration; DACH-H, 1,2-diaminocyclohexane high amine concentration; AA-L, allylamine low amine concentration; CPA-L, cyclopropylamine low amine concentration; DACH-L, 1,2-diaminocyclohexane low amine concentration) ---------- 56

Figure 4.1. Experimental specimen and monomer. (a) Ti disk and (b) chemical structure of cyclopropylamine ---------- 63

Figure 4.2. Schematic diagram and photograph of the atmospheric pressure plasma jet device components ---------- 65

Figure 4.3. Gas species analyzing device. Optical emission spectrometer (left) and optical fiber (right) ---------- 65

Figure 4.4. Device for analyzed electrical characteristics of plasma discharge. Oscilloscope (left) and high voltage probe (middle) and current probe (right) ---------- 65

Figure 4.5. Amine concentrations as a function of (a) frequencies (distance between nozzle and sample is 4 mm, He flow rate 300 sccm, and CPA flow rate 2 sccm), (b) voltages (same condition as (a)), (c) CPA flow rate and distance at 14 kV and 50 kHz (M is CPA flow rate and D is distance of reactor and sample), (d) He flow rate and frequency (Electrode A was electrode position 52 mm and Electrode B was electrode position 37 mm; He 300 sccm and 30 kHz denote 300-30) ---------- 74

Figure 4.6. Amine concentrations as a function of (a) He flow rate and electrode position at 12 kV (distance between nozzle and sample 2 mm, frequency 50 kHz, monomer flow rate 20 sccm), (b) He flow rate and

polymerization time (distance between nozzle and sample 2 mm, frequency 50 kHz, CPA flow rate 20 sccm), (c) Number of plasma-polymerization sites on the amine concentration (voltage 12 kV, frequency 50 kHz, distance between nozzle and sample 2 mm, He flow rate 400 sccm, monomer flow rate 20 sccm). (d) The effect of plasma-polymerization time on the cell proliferation (voltage 12 kV, frequency 50 kHz, distance between nozzle and sample 2 mm, He flow rate 400 sccm, monomer flow rate 20 sccm) ----- 75

Figure 4.7. The effect of single or double grounds and the flow rate of monomers on the amine concentration (S, single ground; D, double ground; CPA flow rate 5 sccm denote S-5; -10, monomer flow rate 10 sccm; -15, monomer flow rate 15 sccm; -20, monomer flow rate 20 sccm) ---------- 76

Figure 4.8. Generation of a plasma flame with increasing He gas flow rate at a fixed monomer flow rate. Monomer flow rate was fixed at 10 and 20 sccm ---------- 78

Figure 4.9. The effect of various parameters on the changes of amine concentration. (a) Applied voltage at 50 kHz frequency. (b) Monomer flow rate. (c) Frequency. (d) Plasma-polymerization time. (e) The effect of polymerization time on the changes of amine concentration on the disks. --- 79

Figure 4.10. The effect of frequency on the changes of waveform 12 kV voltage. (a) 40 kHz. (b) 50 kHz, (c) 60 kHz, and (d) 70 kHz. (e) plasma power vs. frequency. The waveform was measured by changing the frequency by every 10 kHz from 40 to 70 kHz ---------- 81

Figure 4.11. The effect of voltages on the changes waveform at 50 kHz frequency (a) 8 kV, (b) 10 kV, (c) 12 kV, and (d) 14 kV. (e) Plots of voltage vs. plasma power. The voltage was measured from 8 to 14 kV in every 2 kV increments ---------- 82

Figure 4.12. The effect of monomer flow rate on the changes of waveform at 12 kV voltage and 50 kHz frequency. (a) 5 sccm, (b) 10 sccm, (c) 15 sccm, and (d) 20 sccm. (e) Plots of monomer flow rate vs. plasma power.

The voltage was fixed at 12 kV and the frequency was set at 50 kHz, and the flow rate of the monomer was increased from 5 to 20 sccm in steps of 5 sccm ---------- 83

Figure 4.13. Contact angles measurement. (a) before sterilization, (b) after sterilization ---------- 86

Figure 4.14. Optical emission spectroscopy of plasma flame. (a) He gas plasma, (b) amine plasma-polymerization plasma ---------- 87

Figure 4.15. Changes of surface topologies with increased plasma -polymerization times (a) and root mean square roughness (b) ---------- 88

Figure 4.16. Analysis of elements on the surface using XPS, (a) XPS wide spectrum, (b) carbon element, and (c) nitrogen element ---------- 89

Figure 4.17. Analysis of amine plasma-polymerization surface elements using XPS. (a) C 1s. (b) N 1s ---------- 90

Figure 4.18. Fluorescence images of early-adherent cells (green is Paxillin; orange is Rhodamine; blue is DAPI, 4hr after seeding) ---------- 92

Figure 4.19. Proliferation of MC3T3-E1 cells on amine plasma-polymerized surfaces. (**p<0.01) ---------- 93

Figure 4.20. Live-dead cell staining of MC3T3-E1 cells on the amine plasma-polymerization surface (Live cell is green and dead cell is red) ---------- 94

Figure 4.21. The effect of treatment time on the changes of ALP activity at 7 and 14 d ---------- 95

Figure 4.22. The effect of treatment time on the changes of calcium deposition. (a) Alizarin red S staining, (b) Plots of treatment time vs. Alizarin red S - 96

Figure 4.23. Western blot analysis of osteogenic protein expression ---------- 97

Figure 5.1. Surface morphologies of SLA treated Ti disks ---------- 104

Figure 5.2. Schematic diagram and actual image for treating cold atmospheric plasma on the Ti surface with *P. gingivalis* grown ---------- 106

Figure 5.3. Gas species analyzing device. Optical emission spectrometer (left) and optical fiber (right) ---------- 109

Figure 5.4. Optical emission spectroscopy spectra of the CAP pillars. (a) Effect of oxygen supply. (b) Effect of energy level ---------- 114

Figure 5.5. Morphological observations of biofilm formation on the surface of Ti disks. (a) FE-SEM image. (b) Uninoculated Ti surface. (c) Fluorescence image of *P. gingivalis* on Ti disks surface ---------- 115

Figure 5.6. ROS generation in PBS (0.01 M, pH 7.4) by CAP treatment. (a) Effect of treatment time (intensity, 9, energy level, 7). (b) Effect of energy level (treatment time was 60 sec). Relative ROS levels were measured with SOSG reagents ---------- 116

Figure 5.7. CFU analysis of *P. gingivalis*. (a) Images of surviving bacteria after CAP treatment. (b) Effect of treatment time on viability of *P. gingivalis* (9-7 in Table 5.1). (c) Effect of energy on viability of *P. gingivalis* (treatment time: 60 sec) ---------- 118

Figure 5.8. Effect of CAP device treatment time on *P. gingivalis* survival rate of Ti disk. *P. gingivalis* on Ti disk was treated with the CAP device and then stained with *P. gingivalis* live and dead cell dyes. Green and red represent live and dead bacteria, respectively ---------- 119

Figure 5.9. Viability and intracellular ROS levels of HGF-1 after CAP treatment. Effect of treatment time (a) and energy level (b) on viability of HGF-1. Effect of treatment time (c) and energy level (d) on intracellular ROS levels in HGF-1 ---------- 121

ABSTRACT (ENGLISH)

Exploration of optimal processes on amine plasma-polymerization and plasma sterilization for biomedical applications

Chang-Min Lee
Advisor: Prof. Byung-Hoon Kim, Ph.D.
Department of Biodental Engineering
Graduate School of Chosun University

Recently, plasma technology was extensively applied in various biomedical field such as biomaterial surface modifications, sterilization, and cancer therapy etc. In present study, we performed the amine plasma surface modification on high-density polyethylene (HDPE) medical grade polymer and Ti dental implant to enhancing the biocompatibility. In addition, we sterilized the *P. gingivalis*, cause of periimplantitis using cold atmospheric pressure plasma jet.

HDFE polymer has been widely used as bone substitute material in bone defect reconstruction. However, HDPE has a hydrophobic nature, resulting in poor bioactivities such as cell adhesion and proliferation. Therefore, we carried out amine plasma-polymerization on HDPE surface to induce the surface functionalization using an allylamine (AA), cyclopropylamine (CPA), and 1,2-diaminocyclohexane (DACH) monomer.

The purpose of the first study was to optimize the amine plasma-polymerization process through the analysis of surface characterized and then investigate the mesenchymal stem cell (MSC) proliferation in this process.

Optimization of plasma-polymerization was found out by changing process conditions such as chamber pressure, plasma power, monomer injection nozzle diameter, and sample position in plasma chamber. After amine plasma-polymerization on HDPE, surface characterizations were analyzed using FT-IR, XPS, AFM, and contact angle. In addition, amine concentration on the HDPE surface was examined the Orange II method, and MSC proliferation was evaluated by MTT assay.

The results were as follows.

1. From result of FT-IR analysis, it was confirmed that amine polymeric thin film deposited on HDPE was partially removed with water or alcohol.
2. Contact angles of HDPE were decreased regardless of the type of monomers, as the distance from the nozzle increased. Amine concentration on the HDPE surface was changed with the distance from the nozzle. The distribution of the amine concentration with the distance showed a different pattern depending on each monomer, but the dispersion was reduced at a distance of 7 cm.
3. Amine concentrations on HDPE surface were distributed from 5 nmol/mm^2 to 100 nmol/mm^2. FT-IR result indicated that the NH band at 1640 cm^{-1} showed an increase in the band with the increase in the amine concentration. Contact angles were decreased with increasing concentration in AA and CPA monomer, but there was no difference in DACH monomer.
4. MSC proliferation was improved in amine plasma-treated samples compared to non-treated samples. In particular, on the 18 d, the cell proliferation of plasma-polymerized HDPE using AA and CPA monomer increased more than 2 times as compared to that of the pristine HDPE. At low and high amine concentrations, cell proliferation increased with increasing concentration in AA and CPA monomer. However, for DACH monomer, there was no difference of proliferation to increase of the amine concentration.

Taken together, we suggest that amine plasma-polymerization technique has potential

and usefulness to apply for bone tissue engineering.

In the second study, we designed and fabricated the atmospheric pressure plasma jet (APPJ) device to apply for surface modification of Titanium (Ti) dental implant. Ti implant surface was modified by amine plasma-polymerization using CPA monomer. To optimize the APPJ design, we considered as design variables such as shape of plasma reactor, He gas flow rate, CPA monomer flow rate, applied voltage, frequency, electrode position, and ground electrode. And then, Ti implant surface was characterized by amine concentration, contact angle, XPS, AFM, and *in vitro* test were evaluated through MC3T3-E1 preosteoblast cell proliferation, initial adhesion, and differentiation.

The results were as follows.

1. The I-shape reactor deposited more amine groups to the sample surface than the Y-shape reactor. At a monomer flow rate over 5 sccm, there was no change in the amine concentration on the surface by the number of grounds. As the monomer flow rate increased, the amine concentration on the surface increased at 15 sccm, but decreased at 20 sccm.
2. As the applied voltage to the reactor was increased, the amine concentration on the surface increased, but decreased at 16 kV. As the frequency increased, the amine concentration on the surface increased, and there was no change in increase or decrease beyond 60 kHz.
3. Optimization conditions were a voltage of 12 kV, a frequency of 50 kHz, a He gas flow rate of 1 slm, and a monomer flow rate of 10 sccm. After amine plasma-polymerization, contact angles were 12.3˚ or less compared to 59˚ of the control. After 1 d, it was confirmed that the contact angle of plasma-polymerized Ti surface showed 34˚ or less
4. Roughness of amine-polymerized Ti surface was greatly reduced, and the RMS roughness of the surface also decreased. XPS analysis indicated that nitrogen and carbon were increased in the amine-polymerized Ti surface compared to the pristine Ti surface.
5. As a result of examining cell proliferation, the 4 min sample showed the highest

proliferation on 2 and 3 d. As a result of observing the initial cell adhesion morphology using fluorescence staining, there was no significant difference in the cell morphology, but the luminescence of paxillin, an initial adhesion factor, was more strongly expressed on the amine surface sample. As a result of confirming cytotoxicity using the Live-Dead cell reagent, there was no toxicity on the surface of the amine polymerization.

6. Cell differentiation on the amine-polymerized Ti surface increased to less than 30% over 14 d. The bone calcification of the amine-polymerized sample was reduced compared to the untreated sample. Western blot showed that ALP and OPN were strongly expressed in some amie polymerized samples. RUX2 showed no significant difference in all samples.

We have successfully developed a simple and low-cost APPJ device to apply for enhancing the oseointegration of Ti implant, and optimal amine plasma-polymerization was derived. It is expected that APPJ can be used in the surface treatment of commercial Ti implants in the future.

In the third study, we investigated the bactericidal effect of Sandblast, Large-Grit, and Acid Etching (SLA)-treated Ti surface by FEDBD plasma. *P. gingivalis* is well known as the main microorganism caused peri-implantitis. Therefore, we performed sterilization and remove experiment for *P. gingivalis* biofilm and evaluated the cytotoxicity of human gingival fibroblast-1 (HGF-1) cells.

The results were as follows.

1. As the oxygen concentration in the plasma gas and plasma intensity increased, the generation of OH radicals increased.
2. ROS generation was increased as the plasma irradiation time and plasma intensity increased.
3. As the plasma irradiation time and plasma intensity was increased, *P. gingivalis* colony and biofilm decreased.
4. There was no significant effect on the HGF-1 survival rate until 60 sec of plasma exposure, but the survival rate decreased after 90 sec. Cell viability decreased as

the ROS inside the cell increased.

Plasma sterilization was confirmed to be very effective method in treating peri-implantitis through *P. gingivalis* sterilization experiment.

In conclusions, surface modification and sterilization using plasma technology could provide the introduction of functionalization on biomaterial having poor bioactivity, and bactericidal effect. It was that plasma technology will have infinite applications in the biomedical field.

1. General Introduction

Tissue engineering is the study of restoring, maintaining, or improving the function of tissues or organs damaged by accidents or aging. Tissue engineering is composed of three main factors include cells, scaffolds, and growth factors. For successful tissue regeneration, it is important to select cells suitable for the tissue to be regenerated, design a scaffold with a shape and structure suitable for the structure of the tissue, and select growth factors suitable for the characteristics of the tissue. Recently, tissue engineering is being studied in a variety of fields, from the regeneration of organ tissue, which is soft tissue, to bone, which is hard tissue [1].

In particular, the mostly clinical used research is in the field of bone regeneration, where bone diseases and bone tissue damage due to aging, obesity, and accidents are increasing [2].

Extensive studies have reported the considerable shortcomings, limitations, and complications of current clinical treatments for bone repair and regeneration; these include autologous and allogenic transplantations using autografts and allografts [3].

The challenging history of grafting procedures has led to increasing demand for alternative treatments. Failure rates of nearly 20% due to infections, hematoma, immunological rejection, sensory loss and prolonged pain was reported in the last decade [4-6].

Synthetic biomaterial devices represent a promising alternative to bone grafts, able to remove immunological reactions and mitigate inflammatory responses. Specifically, polyethylene (PE) has demonstrated a more consistent, efficient, low-cost alternative to some bone grafts able to replace tissue lost and, in only some cases, restore tissue function.

PE represent the most popular plastic globally, due to its easy and cheap manufacturing processes, and also represents a versatile biomaterial with significant clinical impact. PE is categorized by its density and branching and as such, several types of PE exist ranging from ultra-high-molecular-weight to medium- and low-density PE, each with varying thermal, mechanical, chemical, electrical and optical properties relevant for biological mimicry.

As representative commercial product using HDPE, MEDPOR® implants, developed by Porex Corp (Fairburn, GA, USA) and now owned by Stryker (Kalamazoo, MI, USA), have largely dominated the market [7, 8]. Overall, PE is a highly versatile and adaptable biomaterial utilized extensively in pre-clinical studies and clinical practice, demonstrating superior performance compared to autografting and other biomaterial implants, and becoming recognized as the 'gold standard' in a wide range of treatment [9].

In recent years, scaffolds for bone regeneration have been widely developed and it can be designed as a patient-tailored shape and fabricated 3D printing technique.

Plasma surface modification is a versatile and economic surface-modification technique that alters the functionality of biomaterials. The advantage of this technique is that we can attach various functional polymers on the desired surface site. A prime attribute of these processes is that materials of different chemistry than the original substrate can be incorporated into the biomaterial component so that specific beneficial in vivo behaviors can be attained [10, 11]. Bio-integration is the ideal outcome expected of an artificial implant. This implies that the phenomena that occur at the interface between the implant and host tissues do not induce any deleterious effects such as chronic inflammatory response or formation of unusual tissues [12].

In this study, we investigated the surface modification of high-density polyethylene (HDPE) by polymerization process using low-pressure plasma. Furthermore, surface of titanium (Ti) disks was coated with amine functional group to regulate cell reaction on the surface of a Ti disks using atmospheric pressure plasma. Additionally, antibacterial efficacy of cold atmospheric plasma (CAP) was also evaluated using *Porphyromonas gingivalis* (*P. gingivalis*) periodontitis model onto Ti disks.

2. Backgrounds

2.1. Bone tissue engineering

In recent years, bone tissue engineering is rapidly developing due to the development of 3D bio-printing technology. Bio-printing has the ability that it can be customized for each patient tissue structure. [13]. Bone tissue engineering strives to replicate the osteoconductive, osteoinductive, and osteogenic properties of bone [14]. Despite advancements in manufacturing synthetic bone and soft tissue composites, their clinical applications have limited.

Tissue engineering could provide a single-stage solution for surgical treatment of segmental long bone defects. The ideal engineered graft would be osteoconductive, osteoinductive, promote osteogenesis and angiogenesis, allow load transfer with weight-bearing activities, and be biocompatible with host tissue. Many promising constructs exist, but none meet all of the qualities outlined above. As shown in Table 2.1, the list of materials and manufacturing methods that have been trialed in attempt to create a better engineered bone scaffold are quite extensive [15].

Table 2.1. Manufacturing methods and materials that have been used in the construction of porous scaffolds to replace bone damage [15]

Rigid porous scaffolds	
Manufacturing	Materials
▪ Molding ▪ Foaming ▪ Leaching ▪ Template-casting ▪ Machining ▪ Layer-by-layer assembly ▪ Lithographic techniques ▪ Additive manufacturing	▪ Metals (titanium, tantalum, magnesium) ▪ Ceramics (Calcium phosphate, calcium hydroxyapatite, calcium sulfate, Beta-TCP, etc.) ▪ Polyesters ▪ Polyurethanes ▪ Polycarbonates ▪ polyanhydrides ▪ Polyphosphazenes ▪ Polypropylene fumarates

2.2. Biomaterials

Biomaterials can be extracted from nature or made artificially through a variety of chemical approaches using polymers, bioceramics, metals, and so on. Accordingly, biomaterials may constitute part or all of a living structure or biomedical device that performs, enhances, or replaces natural functions. Various biomaterials constituting the scaffolds (natural and synthetic materials, biodegradable and permanent materials, etc.) have been studied [16]. Most of these are research subjects for use as bioabsorbable suture materials, which were known in the medical field before the advent of tissue engineering.

Bones are the functional tissue, to provide structural support, protect vital organs, store minerals, helps in multi-directional motion and bear load of our body [17]. Bone implants are fabricated through biomaterials which are categorized as: (a) first generation, (b) second generation, and (c) third generation biomaterials. First generation implants are bioinert, second generation implants are biodegradable, bioinert and bioactive. Third generation implants focuses on stimulating specific cellular response at molecular level along with the properties of second generation [17] (Figure 2.1).

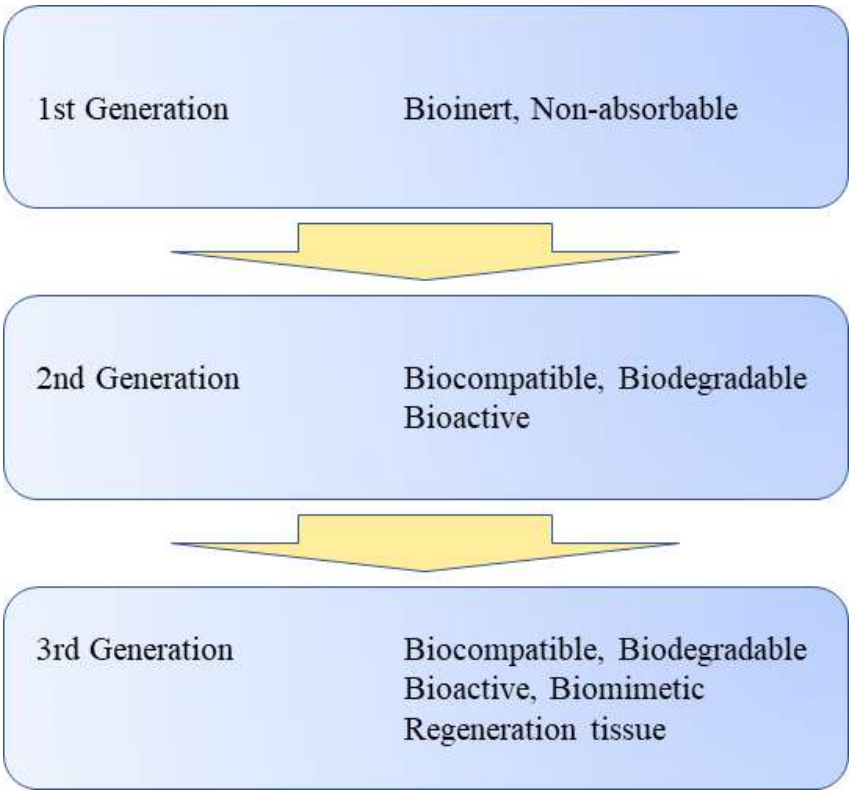

Figure 2.1. Evolution of biomaterials [17].

Biocompatibility is clearly important, although it is important to note that "biocompatibility" is not an intrinsic property of a material, but depends on the biologic environment and the leeway that exists with respect to tissue reaction. Similarly, the material must be neither cytotoxic nor systemically toxic. Therefore, it is important to be aware of the potential toxicity of the materials' breakdown products, as well as of residual unreacted cross-linking agents (e.g., glutaraldehyde), reactive groups on polymers (e.g., aldehydes, amides, hydrazides), and similar issues.

As alluded to above, the mechanical properties for biomaterials in tissue engineering are determined by the target environment and delivered cells. In general, the properties of the construct should match those of the surrounding tissue: e.g., relatively tough in bone, softer in pliable tissues. The properties will also be defined by the delivered cells' need for porosity for in-growth, delivery of nutrients, or protection from the environment, perhaps especially in the case of non-autologous transplants.

2.2.1. Polymer

The biomaterials used in tissue engineering can be broadly classified as synthetic polymers, which includes relatively hydrophobic materials such as the hydroxyacid [a family that includes poly(lactic-co-glycolic) acid, PLGA], polyanhydride, and others; naturally occurring polymers, such as complex sugars (hyaluronan, chitosan); and inorganics (hydroxyapatite). There are also functional or structural classifications, such as whether they are hydrogels, injectable, surface modified, capable of drug delivery, by specific application, and so on [18].

Natural polymer

Natural materials used as biomaterials include proteins such as collagen, fibrin, and gelatin, and polysaccharides such as hyaluronan, agarose, alginate, and chitosan. Scaffolds made of natural materials generally have good biological compatibility, but lack mechanical stability, and problems with the supply, processing, and disease transmission potential of natural materials may arise [19].

Synthetic polymer

Polymeric biomaterials play important roles in a wide variety of medical devices, diagnostic systems, and pharmaceutical formulations. During the past few decades, tremendous amounts of new polymeric biomaterials have been developed in association with the emergence and fast growth of the field of tissue engineering and regenerative medicine. These polymeric scaffolds, most often made of biodegradable synthetic polymers and natural macromolecules, play a pivotal role in tissue engineering and are used in the regeneration of essentially all tissue types [20].

Polylactone and complexes such as polylactic acid (PLA), polyglycolic acid (PGA), and polycaprolactone (PCL), which are representative synthetic polymers used as biomaterials, are most commonly used as fixtures because of their excellent biocompatibility [21].

Polylactic acid, a synthetic polymer well known for sutures, is a polyester that breaks down in the body to form lactic acid that can be easily removed from the body [22].

Polyglycolic acid composed of biodegradable aliphatic polyester is also used in various medical fields, and it can be degraded in 2-4 weeks in body [23].

Polycaprolactone decomposes very slowly compared to PLA. Degradation *in vivo* was observed for up to 3 years. Therefore, it is widely used in long-term implantation and drug release control applications [24].

Polyesters, which are mainly used, have disadvantages including immune rejection due to reduced bioactivity. In addition, polylactic acid and polyglycolic acid are decomposed by hydrolysis to generate carbon dioxide and lower the pH to create an acidic environment. In severe cases, it can induce tissue necrosis [25].

Polyethylene has many advantages as a biomaterial for medical implants and has been extensively applied to the fabrication of porous high-density polyethylene implant for facial and cranial reconstruction [26].

Other kinds of devices and materials in used with the U.S. Food and Drug Administration were given in Table 2.2.

To overcome this limitation, recently, a composite material has been developed by integrating polyester and hydrogel materials. Hydrogels are hydrophilic, capable of absorbing water, and often exhibit superior biocompatibility compared to hydrophobic polymers (such as polyester). However, hydrogels exhibit weak mechanical strength and can be easily deformed under pressure or water vapor conditions, so they are often used by mixing with materials with mechanical strength such as ceramics [27].

Table 2.2. List of common medical devices and materials by FDA [28]

FDA Category	Common Devices	Synthetic Polymer Material Used
Anesthesiology	• Epidural catheters	• Polythylene • Polytetrafluoroethylene • Polyamide
Cardiovascular	• Pacemaker • Implantable cardioverter/defibrillator • Left Ventricular Assist Device • Mechanical heart valves • Artificial blood vessels • Catheters	• Polypropylene • Polyethylene • Polytetrafluoroethylene • Polyamide • Polyethyleneterephthalate • Polydimethylsiloxane • Polyhydroxyalkanoates
Dental	• Dentures • Dental implants	• Polymethylmethacrylate
Ear, nose, and throat	• Cochlear implants • Staples implant • Nasal implants for nose reconstruction	• Polydimethylsiloxane • Liquid crystal polymer • Polyethylene • Parylene • Silicone
Gastroenterology and urology	• Penile implants • Neurostimulator in sacral nerve stimulation • Foley catheter • Artificial urinary sphincter implant • Hernia or vagina mesh	• Polydimethylsiloxane • Polyethylene • Polytetrafluoroethylene • Polyamide • Polyhydroxyalkanoates • Silicone
General and plastic surgery	• Synthetic blood vessels • Breast implants • Cheek, jaw, and chin implants • Lip implant • Titanium surgical implant • Hip implant	• Polyethylene • Polyethyleneterephthalate • Polytetrafluoroethylene • Silicone • Polydimethylsiloxane

Hematology and pathology	• Central venous access device • Peripherally inserted central catheter	• Polyethylene • Polytetrafluoroethylene • Polyamide
Neurology	• Implantable pulse generator for deep brain stimulation • Neuroprosthetics • Cognitive prostheses • Catheters	• Poluimides • Polydimethylsiloxane • Parylene • Liquid crystal polymer • SU-8 • Polyethylene • Polytetrafluoroethylene • Polyamide • Polyhydroxyalkanoates
Obsteric and gynecologic	• Intrauterine device (IUD) • Intravaginal rings • Etonogestrael-releasing contraceptive implant • Urogynecologic surgical mesh implants • Fetal micro-pacemaker	• Silicone • Polyurethane • Polypropylene
Ophthalmic	• Dexamethasone intravitreal implant • Retinal prosthesis • Artificial intraocular lens • Glaucoma valve • Fluocinolone opthalmic implant • Orbital implant • Catheters	• Polymethylmetacrylate • Polyethylene • Polytetrafluoroethylene • Polyamide
Orthopedic	• Orthopedic implants	• Polyethylene • Polyether ether ketone • Polyhydroxyalkanoates

2.2.2. Metals

Ti and Ti alloy

Titanium (Ti) has been used for a long time in the medical implant field due to its high corrosion resistance in various media such as seawater and aqua regia, as well as non-toxicity and biocompatibility in the human body. For many years, commercially pure Ti as well as some alloys such as binary and tertiary Ti alloys have been used. Ti6Al4V is the most used Ti alloy in dentistry [29].

Ti implant

Since the 1960s, Ti has become a popular metallic biomaterial because of its properties for many biomechanical applications including dentistry. The use of bone-anchored titanium implants has become routine treatment modalities in dentistry. Chemical and biological interactions between the coated titanium surface and the host tissue start with binding of water molecules, ions and biomolecules, followed by mineralization at the implant surface. Therefore, the initial state of the titanium surface is decisive for the tissue regeneration around the implant [30].

Ti Surface treatment

Apart from surgical procedures, the success of implants is highly dictated by the surface properties of the implant material that influence molecular interactions, cellular response and thereby, bone regeneration [30].

Plasma spray coating

Plasma spraying technique generally involves thick layer of depositions, such as hydroxyapatite (HA) and titanium (Ti). The coating process includes spraying thermally melted materials on the implant substrates. A combination of HA coating on Ti alloys substrate has received many attentions due to their attractive properties such as good biocompatibility and mechanical properties [31].

Grift blasting

Another route for roughening the surface is grit blasting, through pressurised particle projection either using ceramic materials or silica onto the implant surface. Materials such as sand, hydroxyapatite, alumina, or TiO_2 particles are usually employed for the purposes [31].

Acid etching

In acid etching, the use of acids on metal surfaces is not only to clean the surface but also to modify the roughness. A strong acid like hydrofluoric (HF), nitric (HNO_3), and sulphuric (H_2SO_4) or a combination of these acids is commonly used in this technique. Acid etched surfaces had increased cell adhesion and bone formation, thus enhancing the osseointegration [31].

Dual Acid Etching (DAE)

Similar to acid etching, the DAE is also able to treat the surface via chemical or acid whether in sequence or with the combination of both. Rapid osseointegration can be achieved by dual etching through micro rough surface. A comparative study between a machined surface and those using HF and HCl/H_2SO_4 (DAE) has shown the acid treated surface has greater resistance to reverse torque removal and better osseointegration [31].

Sandblast, Large-Grit, and Acid Etching (SLA)

SLA is used to induce surface erosion by applying a strong acid onto the blasted surface. This treatment combines blasting with large-grit sand particles and acid etching sequentially to obtain macro roughness and micro pits to increase the surface roughness as well as osseointegration [31].

Plasma Immersion Ion Implantation [32]

Since the PIII technique enables to embed a great variety of elements into the near-surface region of the various substrates, it offers unique advantages for surface modification technologies of biomaterials (Lin *et al.*, 2019). The most valuable feature

of PIII is that the concentration and depth distribution of the implanted ions in the substrate can be strictly controlled by adjusting the implantation parameters (Jin *et al.*, 2014). In addition, it has been demonstrated that it can enhance the hardness, corrosion resistance, wear resistance, bioactivity, and antibacterial properties of biomaterials (Chen *et al.*, 2020).

Plasma Immersion Ion Implantation and Deposition [32]

The PIII&D method, invented in 1987 by Conrad *et al.* (1987), it has become a routine surface modification method. It has the advantage to levitate the retained dose levels that were limited by the sputtering because of ion implantation. Therefore, using PIII&D with relatively low cost, a three-dimensional film with strong adhesion, thick and without stress is possible to be produced (Yang *et al.,* 2007).

Physical Vapor Deposition [32]

Physical vapor deposition implies a physical coating strategy, involving the evaporation of solid metal under the vacuum environment and depositing it on a conductive substrate (Hauschild *et al.*, 2015). Generally, vacuum evaporation, ion plating, and sputter coating, etc. are among the main methods of PVD. Among them, magnetron sputtering technology has been extensively studied and it results in the formation of high-quality films over a large area and at a relatively low substrate temperature (Nemati *et al.*, 2018; Hamdi *et al*., 2019).

2.3. Plasma surface modifications (PSM)

2.3.1. Plasma

Plasma is defined as a form of fourth matter in nature completely different from solid, liquid, and gas. That is an ionized state in which ions and electrons are separated at high temperature. In other words, when the temperature exceeds a certain temperature, the substance passes through the gaseous state and the gas molecules therein violently collide to cause ionization. As a result, a large number of positive ions and electrons are generated, leading to a randomly moving state. When gas molecules or atoms are ionized, positive ions and electrons are always generated in pairs, so the number of positive ions and electrons in the plasma is almost the same, so that the overall electrical quasi-neutral state is maintained. Therefore, a gas in an ionized state with the same density of ions and electrons can be defined as plasma.

Plasma states that can be observed in the surroundings include fluorescent lamps used as lighting lamps and neon signs commonly seen on the street. Plasma is also the flash of lightning that occurs frequently during rain showers. The aurora that occurs in the night sky in the Arctic region can be seen as the light displayed by plasma. Systematic studies of plasma began with the research of Irving Langmuir and his colleagues in the 1920s. Langmuir also introduced the term "plasma" as a description of ionized gas in 1928 [33].

2.3.2. Sources and discharge of plasma generation

As previously mentioned, for surface modification treatments, various plasma sources are available. Each of them has its own characteristics such as density, temperature, chemical composition, etc., and leads to different results. The choice of the proper source for the specific task requires the study of the characteristics of the various plasmas [34].

2.3.2.1. Microwave (MW) plasma [34]

MW discharges are electrical discharges generated by electromagnetic waves with frequencies between 300 MHz and 10 GHz. MW discharges represent a simple way of plasma generation both with high (> 100 W/cm^3) and low (< 1 W/cm^3) power levels and can be used over a wide region of operating pressures (from 10^{-3} Pa up to atmospheric pressure). Nowadays, these discharges are widely used for generation of quasi-equilibrium and non-equilibrium plasmas for different applications because of the simplicity of control of the plasma internal structure by means of changes of the plasma characteristics and the possibility of plasma generation both in small and large chambers. The plasma absorbed power can be high enough and runs up to 90% of the incident power.

2.3.2.2. Radio frequency (RF) plasma [34]

RF discharges usually operate in the frequency range f = 1−100 MHz. The power coupling in RF discharges can be accomplished in different ways: capacitively coupled discharges and inductively coupled discharges.

Capacitively coupled plasma (CCP)

CCP is generated with high-frequency RF electric fields, typically 13.56 MHz. In its simplest form, the RF voltage is applied across two parallel metal plates, generating an oscillating electric field between them. This field accelerates electrons leading to an ionization avalanche. The parallel electrodes which are separated by a distance of a few centimeters may be in contact with the discharge or insulated from it by a dielectric.

Gas pressures are typically in the range 1 ~ 10^3 Pa. In a capacitively coupled RF discharge, the electron density is in the range n_e = 10^9 ~ 10^{10} cm^{-3} and densities up to 10^{11} cm^{-3} are possible at higher frequencies.

Inductively coupled plasma (ICP)

ICP is similar to CCP but the electrode consists of a coil wrapped around the discharge volume that inductively excites the plasma. ICP is excited by an electric field generated by a transformer from an RF current in a conductor. The changing magnetic field of this conductor induces an electric field in which the plasma electrons are accelerated. ICPs can achieve high electron densities (ne = 10^{12} cm^{-3}) at low ion energies.

2.3.2.3. Dielectric barrier discharge (DBD) [34]

Dielectric barrier discharges (silent discharges) are non-equilibrium discharges that can be conveniently operated over a wide temperature and pressure range. DBDs are characterized by the presence of one or more insulating layers in the current path between metal electrodes in addition to the discharge space. At a sufficient AC voltage, electrical breakdown occurs in many independent thin current filaments. These short-lived micro discharges have properties of transient high pressure glow discharges with electron energies ideally suited for exciting or dissociating background gas atoms and molecules.

Due to charge build up on the dielectric, the field at the location of a micro discharge is reduced within a few nanoseconds after breakdown thus terminating the current flow at this location. The current density in a micro discharge channel can reach 100 to 1000 Acm^{-2}. Due to the short duration, this normally results in very little transient gas heating in the remaining channel. The dielectric barrier limits the amount of charge and energy deposited in a micro discharge and distributes the micro discharges over the entire electrode surface. As long as the external voltage is rising, additional micro discharges will occur at new positions because the presence of residual charges on the dielectric has reduced the electric fields at positions where micro

discharges have already occurred. When the voltage is reversed, however, the next micro discharges will form in the old micro discharge locations.

Its flexibility with respect to geometrical configuration, operating medium and operating parameters is unprecedented. Conditions optimized in laboratory experiments can easily be scaled up to large industrial installations.

Although DBD configurations can be operated between line frequency and microwave frequencies the typical operating range for most technical DBD applications lies between 500 Hz and 500 kHz.

Plasma can be used in the continuous wave (CW) or pulsed mode. In the continuous wave mode, plasma with a specific power is turned on for a specific amount of time. In the pulsed mode, plasma is intermittently generated with a fixed duty cycle (Δ).

$$\Delta = t_{on} / t_{on} + t_{off} \quad (1)$$

where t_{on} is the time during which the plasma is turned on and t_{off} is the time during which the plasma is turned off. The mean power (P_{mean}) is then defined by equation (2) and represents the average energy dissipated in the plasma period, with P_{peak} the power injected during t_{on}.

$$P_{mean} = \Delta * P_{peak} \quad (2)$$

2.3.3. Plasma surface treatment

2.3.3.1. Surface cleaning

Plasma cleaning has been proven effective for critical surface treatments and can effectively clean surfaces without having a negative impact on other properties of the surface. Plasma cleaning decomposes chemical and biological contaminants at the nano-scale, reducing contamination by up to 6 times, including solvent cleaning residues, compared to conventional wet cleaning methods. Plasma cleaning creates a clean surface that can be glued or further treated without further removal of residues. It is based on the effects of ultra-violet lights and active species from the plasma. Ultra-violet light generated in the plasma is very effective in removing surface contaminants composed of organic bonds. The second cleaning operation is performed by active species generated in the plasma. These species can react with organic pollutants to form primarily water and carbon dioxide, or act like molecular sandblasts and break down organic contaminants. The cleaning method using plasma is one of the methods widely used in various fields of biomaterials such as dental or orthopedic materials. Figure 2.2 and 2.3 shown the plasma cleaning process with equipment photograph and schematic diagram.

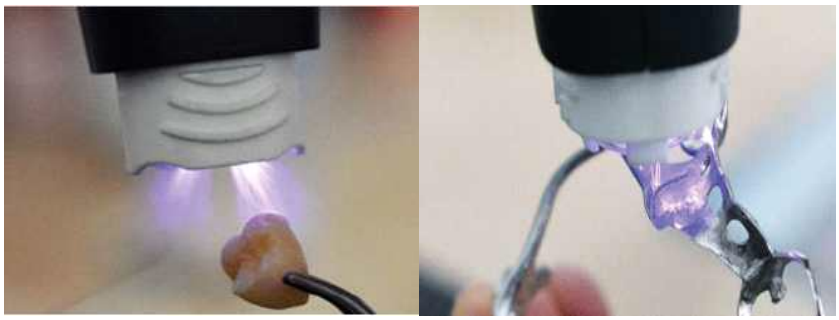

Figure 2.2. Plasma cleaning application from dental materials by Relyon plasma company equipment [35].

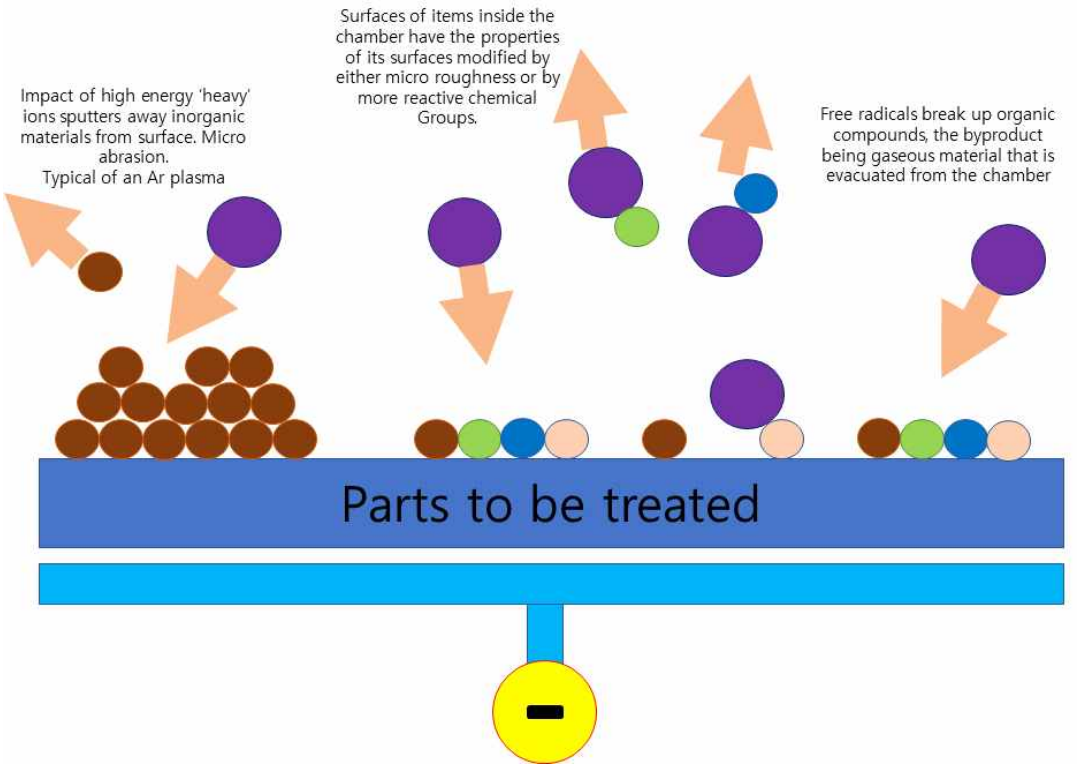

Figure 2.3. Schematic diagram of plasma cleaning works to contaminated surface [36].

2.3.3.2. Surface treatment [18]

Cells are sensitive to the environment in which they exist, responding to chemical cues, and morphologic aspects of the surfaces with which they are in contact. Although the common synthetic polymeric scaffolds have great advantages in terms of their manufacturing process and the reproducibility of their degradability and other properties, they suffer from a lack of those finer cues. One approach to providing them is by modifying their surfaces, by physical adsorption of compounds, or by chemical modification. Apart from immobilizing proteins or other compounds for specific biologic effects (e.g., adhesion), this approach can also be used to increase polymer hydrophilicity to repel proteins and perhaps reduce the tendency toward adhesion (e.g., in the peritoneum). Another common type of surface modification is micro- or nanopatterning to create structured cellular arrays and influence cell behavior.

In recent years, numerous advances have been performed in developing plasma surface treatments to modify the physicochemical features of polystyrene surface without varying its bulk property. Various gas plasma treatments were used to produce desired polystyrenes surface properties. For example, oxygen-plasma treatment can increase the surface energy of polystyrene surface, whereas inert gas plasma can induce cross-linking at polystyrene surface. Hence, atmospheric-pressure-plasma-based processes are the potential candidate in PS surface pretreatments as it alters the polymer surface outermost layer without changing its bulk properties. Furthermore, atmospheric-pressure plasmas have a significant function in simultaneously combining polymer surface modification and bio-decontamination with the inherent advantages of gas-phase processes [37].

Poly(ethylene terephthalate) (PET) is now one of the most recommended polymers for engineering purposes, due to its excellent properties (i.e. transparency, mechanical strength, gas permeability and chemical resistance), which are useful in many areas of technological interest. Unfortunately, PET is not always suitable due to its low surface free energy, which affects its wettability and thus any process involving surface interactions, as in printability, biocompatibility and adhesion. This is an important issue, bearing in mind the role played by the wetting behavior of polymers in a wide range

of potential applications, not only industrial (e.g., nanoparticles grafting), but also biomedical areas (e.g., tissue engineering). The key role of wettability has been highlighted in the literature dealing with these topics. Thus, Rimpelova *et al*. [38] show the need of significantly increasing the hydrophilicity of polyethylene plates as a requisite to improve the adhesion and growth of fibroblasts. Other papers (see Kasálková *et al.* [39]) endorse the potential benefit of grafting of nanoparticles onto the activated polymers.

To overcome the problem brought to the fore above, the surface energy content of any polymer, PET plates included, needs to be increased without changing other bulk properties of the material. A myriad of scholarly papers has tried to improve wettability of a number of mainly hydrophobic polymers. In addition to current methods of surface modification, as chemical, thermal, mechanical or electrical treatments, plasma treatment has become a popular method with an advantage over the traditional wet chemical procedures. Apart from being an environmentally friendly technique because it neither needs water nor chemicals, plasma treatment is also a very versatile working method that can be used with polymer surfaces of different nature and shape. The efficiency of plasmas is based on the ability of active species such as ions, electrons, atoms or free radicals to induce chemical and physical modifications on the surface. The so-called cold, or low-temperature plasmas, have been found to be most suitable to modify surface properties of polymers of interest in industry, such as adhesivity, hydrophobicity, oleophobicity and hydrophilicity. Although the success of oxygen plasma is obvious, air and noble gases as well as plasma of different gases and vapors like O_2, N_2, NH_3, H_2O, CO_2 can also be used. The mechanisms of surface modification after plasma treatment differ depending on the type of gas. In case of noble gases, they do not incorporate new chemical species on the surface, and the main mechanisms are selective bond breakage and possible desorption of short chain species. During the treatment with gases other than noble gases, the predominant mechanism is functionalization (*i.e.*, surface formation of new chemical groups). In any case, it is known that surface modifications induced on the plates after plasma activation are not sustainable over time and may change during sample storage. Wetting properties undergo important modifications, manifested by changes in surface free energy, which, in turn, determine

the values of the contact angles of liquid drops placed onto the surface. Ageing after plasma activation is also related to the undesirable effect of the so-called hydrophobic recovery of polymers. This makes the study of the ageing effect on the surface properties of plasma pretreated polymer samples an issue open for discussion. Morent *et al.* [40] found, that the effect of film storage time was the smallest for the argon-plasma treated polymers and the largest for the air plasma. It was explained by the highest crosslinking effect caused by argon plasma treatment. There is no paper in the literature which would explain this problem by changes in surface free energy using two different calculation approaches. So, the novelty of this paper lies in its methodology: both advancing and receding contact angle of probe liquids are measured and applied to calculate surface free energy by means of two different approaches; they explain the specific role played by the different plasma gases used for treatment of PET plates [41].

2.3.4. plasma-polymerization [42]

Since a few decades, polymeric materials have played a central role in regenerative medicine and tissue engineering as artificial tissue replacements and organ transplantation devices. Chemical and topographical surface modifications of biomaterials are often required to achieve an overall better biocompatibility.

Non-thermal plasma is a non-invasive, solvent-free alternative for modifying polymeric surface properties without affecting the bulk of the material. Plasma-polymerization of organic compounds has proven to be an effective tool for thin film production with specific surface chemistries, useful for biomedical applications. These polymer layers have received a growing interest in tissue regeneration and biomolecules immobilization processes. Many different types of chemical functional groups can be introduced.

Non-thermal plasmas have gained a great interest in plasma deposition of thin polymeric coatings. A plasma pre-treatment was used before the deposition of the monomer to increase the adhesion between the polymer surface and the plasma polymerized coatings due to the presence of reactive sites. The polymerization itself can be performed via two different processes: Plasma induced graft polymerization and plasma-polymerization.

The plasma induced graft polymerization of vinyl monomers has been found to be an attractive method of chemically modifying the surfaces of polymeric materials. Polymers can be treated with an inert-gas plasma and then exposed to oxygen to generate hydroperoxide active species that may initiate the grafting of a desired monomer.

Nowadays, plasma-polymerization is an inexpensive and versatile tool that can be used to coat almost any substrate with a variety of different surface chemistries. Compared to plasma induced graft polymerization, it follows a different surface modification strategy. Gaseous or liquid precursors undergo a sort of polymerization process through a free radical initiation reaction. They are exposed to plasma and subsequently converted into reactive fragments, which can initiate polymerization and in turn recombine to polymers. This results in the production of thin films (so-called plasma polymers) with unique chemical and physical properties. They are pinhole free, highly cross-linked, thermally stable, chemically inert coatings and strongly bonded to

the surface. They will not necessarily have a chemical structure and composition comparable to polymers obtained by conventional polymerization techniques. This technique is useful in many applications such as packaging, textiles, corrosion protection etc. It has also found a broad field of application in the biomedical field including all sorts of implants as well as sensors, wound dressings, contact lenses, etc.

2.4. Plasma sterilization

In the field of medicine, sterilization of medical equipment is an important procedure for preventing infectious diseases. Recently, plasma sterilization methods have been developed as secure sterilization methods and have already been used for sterilizing medical equipment [43-48]. After the treatment, active oxygen species instantaneously change to oxygen molecules. Therefore, this method is safe for the human body and harmless to the environment [49].

Currently, sterilization of medical instruments is mainly performed by high-pressure steam sterilization, ethylene oxide gas sterilization, hydrogen peroxide sterilization. However, high-pressure steam sterilization cannot be used for materials with a low heat resistance and moisture resistance. Further, ethylene oxide gas sterilization and hydrogen peroxide sterilization have drawbacks such as requiring a long processing time and using carcinogenic gasses. The plasma sterilization method has attracted attention in recent years as a new sterilization method to solve these problems. In the plasma sterilization method, microorganisms are sterilized by physical and chemical reactions due to active species, metastables, ultraviolet rays and high-energy charged particles. The plasma sterilization method has advantages over conventional sterilization methods, such as being performed at a low temperature, requiring only a short treatment time, and being non-toxic. So far, many kinds of plasma sterilization devices have been developed and tested for sterilization of microorganisms [41-45, 50].

Sterilization is a physical or chemical process that exterminates or inactivates microorganisms [47]. The worldwide accepted definition for medical devices to be considered sterile is the security assurance level (SAL). The SAL is a statistical parameter that refers to the probability of one surviving viable microorganism after sterilization. For medical devices, SAL needs to be below 10^{-6}, meaning 1 in 1,000,000 chance. Sterilization plays a major role in health-care facilities to prevent the spread of disease. Current sterilization methods include using autoclave or heat, ethylene oxide gas, hydrogen peroxide gas plasma, and radiation [47]. These sterilization methods have their limitations. The use of an autoclave or heat is not advisable for heat-sensitive materials because they may be disfigured. Ethylene oxide can be used for

heat-sensitive materials, but it presents a risk in its toxicity.

Surfaces treated with ethylene oxide require an airing time before they are safe to handle [43]. The use of hydrogen peroxide also requires a long processing time and a long ventilation time [43]. Gamma rays have been used in radiation sterilization. Using radiation requires protection for the operators and a special site to perform it. Plasma sterilization presents an option that is low temperature, efficient, and non-toxic. The existing hydrogen peroxide gas plasma process is 'partially' plasma sterilization (Figure 2.4) [51]. This process includes two phases: a diffusion phase and a plasma phase [47, 51]. First, the sterilization chamber is evacuated, and hydrogen peroxide solution is injected from a cassette and is vaporized in the sterilization chamber. The hydrogen peroxide vapor diffuses through the chamber and initiates the inactivation of microorganisms on all the surfaces exposed to the sterilant. Second, a gas plasma is created in the chamber. The residual hydrogen peroxide is then broken apart by the plasma, which aids in the removal of hydrogen peroxide residuals from the sterilizer load in order to make the contents safe for handling and use. Hence, the hydrogen peroxide plasma treatment is a direct gas plasma sterilization. In the past 15 years, low-temperature pure gas plasma sterilization has attracted great interest because of the unique characteristics of plasmas. Plasma is quasi-neutral ionized gas, known as the fourth state of matter. A large number of gas ions (e.g. O_2^+), atoms (e.g. O), and excited species (e.g. O^*, O_2^*) can be created in a plasma. These gas species are highly reactive and can effectively destroy or inactivate bacteria. Current literature agrees that there are three mechanisms by which plasma sterilizes a surface: ultra-violet (UV) irradiation of genetic material, chemical reactions with the plasma species, and plasma ion sputtering [52].

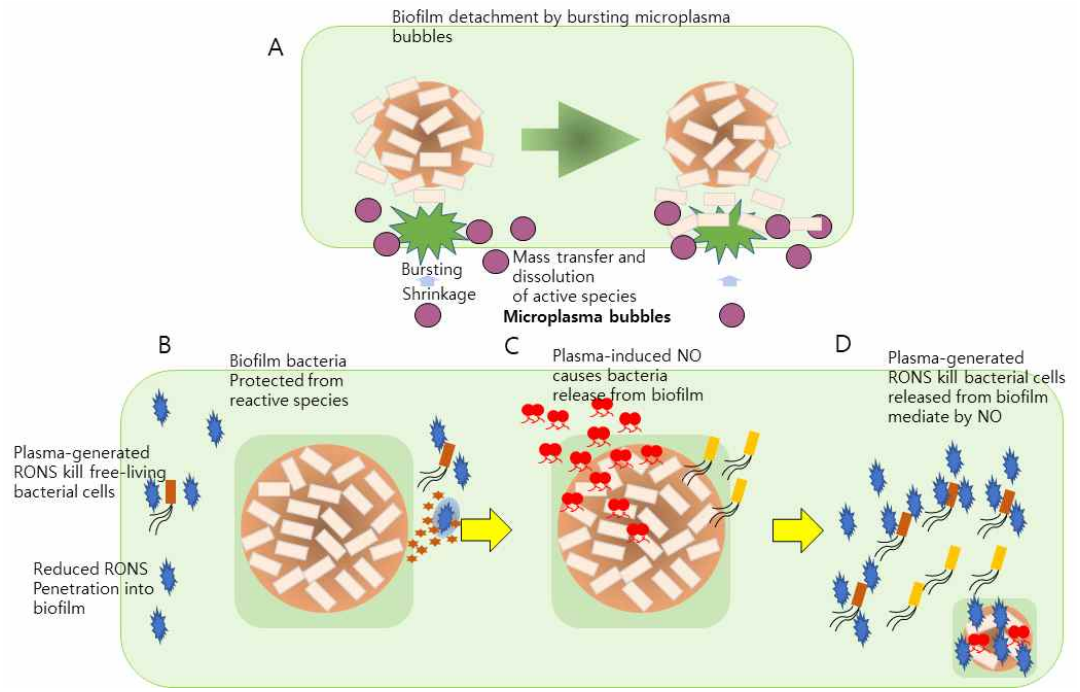

Figure 2.4. Roles of the physical mechanism on the effect of microbubbles and plasma-derived NO in biofilm dispersal [51].

2.5. Applications of plasma

Plasma research in various fields has not ceased recently. Plasma technology has great significance in that it can be applied to various fields, is eco-friendly, and is future-oriented. Comprehensively, it is divided into semiconductor, aerospace industry, biotechnology, nanotechnology, and information technology fields. It is recognized as an eco-friendly technology because there is almost no waste from plasma generation and it is used to purify greenhouse gases and polluting gases.

3. Part Ⅰ: HDPE surface modification by amine plasma-polymerization using three kinds of monomers

3.1. Introduction

Surface modification is a promising option for modulating the biological response of material surface, and there are various physical or chemical techniques to enhance the roughness, hydrophilicity, surface charge, surface energy, reactivity and biocompatibility [53-56].

For example, surface plasma modification enhances attachment of human umbilical vein endothelial cell (HUVEC) of polyurethane copolymer [57]. Furthermore, surface coating and patterning technologies using nanomaterials can be used to enhance the potential and durability of dental implant [58]. Among various technologies for surface modification, plasma technology was introduced to enhance the biological response *in vitro/in vivo* by attaching various functional groups such as carboxyl, hydroxyl, and primary amine to the surface of the material [33, 57-59].

Low-pressure plasma technology has been extensively used for surface modification of various materials and for deposition of specific functional groups on the material surface [60-62].

The advantage of this technology is able to process huge amount of surface simultaneously. Therefore, plasma technology can be considered as an useful method for formation of polymeric materials by using plasma state of monomers and/or reactive species.

Especially, plasma-polymerization is a useful technique for ultrathin films deposited onto material surface having various properties from surface energy to biocompatible functional groups [60-62]. These film properties can be controlled and changed *in situ*. Furthermore, ultrathin films formed by plasma-polymerization can be applicable in deposition of specific molecules on the top of existing materials, addition of specific

features to the surface, and controlling the biological activity of the surface [63-65].

High density polyethylene (HDPE), which is a synthetic biomaterial, have been investigated as a three-dimensional scaffold for bone defect reconstruction [66, 67]. Since HDPE provide excellent mechanical properties, low cost and appropriate structure as a biomaterial, it has been used to reconstruct bone defects [66, 67]. However, disadvantages of HDPE such as inert, hydrophobic, no functional groups, poor reactivity limit its application as a biomaterial [68, 69]. From these reasons, many scientists have been investigated to modify surface of HDPE to have functional and bioactive surfaces [68-70]. For example, Kim *et al.* reported that collagen was successfully grafted with HDPE/poly(ethylene-co-acrylic acid) (PEAA) composites and then HDPE/PEAA/collagen scaffold provided excellent foundation for proliferation of osteoblast cells [68].

Plasma-polymerization of amine-based monomers is an efficient way to prepare bioactive amino functionalized polymer surfaces.

Especially, primary amine ($-NH_2$) functional groups can promote covalent immobilization with biomolecules such as protein like antibodies, collagen, and DNA. Moreover, protonated amines can introduce a localized positive charge in aqueous solution at physiological pH value, which can potentially be used for electrostatic interactions with negatively charged cells and proteins and is propitious to promote cell adhesion and proliferation.

Mesenchymal stem cells (MSCs) may be the best choice for regenerative medicine to check the cellular response on the amine rich surface. In particular, MSCs was cell of great interest in regenerative medicine because of their low immunogenicity and self-renewal capacity [71].

In order to successfully carry out the amine plasma-polymerization under low pressure RF plasma, plasma process needs to be optimized. Process variables include pressure inside the reactor, precursor flow rate, processing time, reaction gas flow rate, and a uniform product can be produced by optimizing these variables.

The aim of this study was to optimize the amine plasma-polymerization on the HDPE surface using low-pressure RF plasma equipment and to verify the effect of amine surface modification through the proliferation of MSCs. In present study, allylamine (AA), cyclopropylamine (CPA), and 1,2-diaminocyclohexane (DACH) were

used as monomers for plasma-polymerization.

3.2. Materials

3.2.1. Preparation of high density polyethylene samples

Commercial HDPE (ORBILAN, Rosendahl, Germany) was used as a substrate material. HDPE disk was purchased with a diameter of 32 mm and a thickness of 5 mm. Sample were ultrasonically cleaned in acetone for 10 min and deionized water for 10 min subsequently (Figure 3.1).

3.2.2. Amine monomers

Three monomers were selected for use in plasma-polymerization. All monomers have amine groups of primary amines, include AA (241075, Sigma-Aldrich, 99% purity, St. Louis, MO, USA), CPA (A13844, Alfa Aesar, 98% purity, Haverhill, MA, USA), and DACH (132551, Sigma-Aldrich, 99% purity, St. Louis, MO, USA) (Figure 3.2).

3.2.3. Low-pressure RF plasma deposition

Plasma-polymerization was performed by radio frequency (RF) discharge device (UM1000134-001A mini plasma station, PLASMART, Korea), and its schematic diagram was shown in Figure 3.3. The inside of the chamber was maintained in a vacuum state using a rotary pump (GHP-800K, Kodivac, Korea). The flow rate of argon (Ar) gas required for pre-treatment and post-treatment was controlled by MFC. Plasma power was generated through a 13.56 MHz RF generator and adjusted with auto impedance matcher (Figure 3.3).

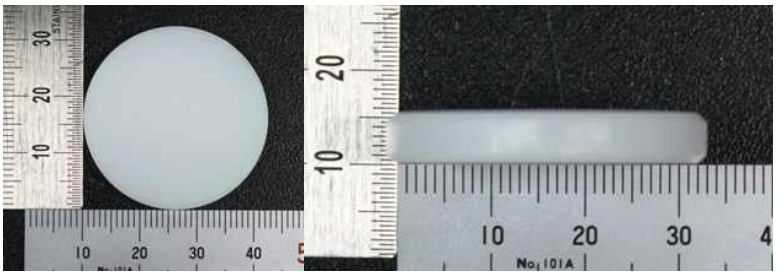

Figure 3.1. Photographs of HDPE disk sample used in this study.

(a) **(b)** **(c)**

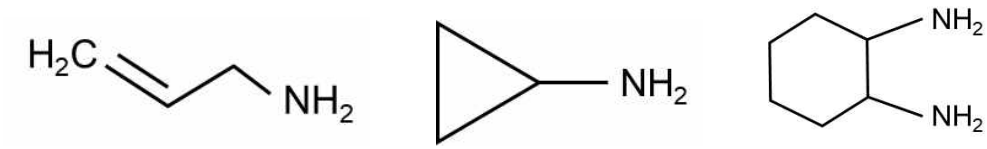

Figure 3.2. Constitutional formula of plasma-polymerization monomers, (a) Allylamine, (b) Cyclopropylamine, (c) 1,2-Diaminocyclohexane.

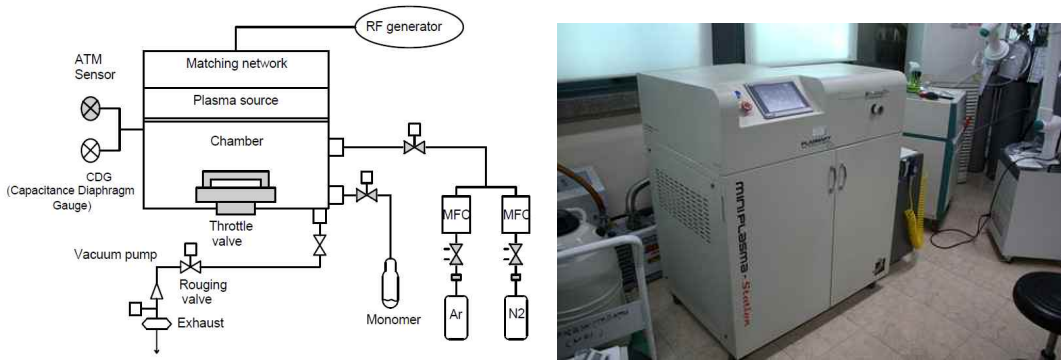

Figure 3.3. Schematic diagram and actual image of low-pressure plasma system.

3.3. Methods

3.3.1. Plasma-polymerization

HDPE surface modification was carried out by depositing an ultra-thin polymeric layer containing amine groups on the surface through plasma-polymerization using AA, CPA, and DACH monomers. HDPE samples were pretreated by Ar gas at 15 mTorr for 20 sccm (standard cubic centimeter per minute) and a RF power of 30 W for 10 sec. Plasma-polymerization was carried out at a discharge power of 60W (for AA and CPA), 80W (for DACH) and reactor pressure of 30 mTorr (for AA), 40 mTorr (for CPA), 10 mTorr (for DACH), respectively. After plasma-polymerization, poly amine thin film was formed on the HDPE surface. These specimens were desinated as follows: AA-H, AA-L, CPA-H, CPA-L, DACH-H, DACH-L (Table 3.1).

Table 3.1. Amine plasma-polymerization conditions (Nozzle diameter: 3.5 mm)

Monomers	Plasma power (W)	Reactor pressure (mTorr)	Distanc from center (cm)
Allylamine (AA)	60	30	7
Cyclopropylamine (CPA)	60	40	7
1,2-Diaminocyclohexane (DACH)	80	10	7

3.3.2. Surface characterizations

3.3.2.1. Contact angle

The contact angle was examined using a GSX (Surfacetech, Korea) equipped with a CCD camera. After 4 sec of dropping 7 μL of deionized water on the surface, the GSX instrument automatically measures the contact angle. The contact angles were extracted from the captured images using the Surfacetech software (version 1.1.5.6) and averaged over multiple readings (n = 3).

3.3.2.2. Amine concentration measurement [72]

Amine concentration was investigated by Orange II method. The Orange II sodium salt (Orange II, 195235, Sigma-Aldrich, 85% purity, USA) was diluted to a concentration of 14 mg/mL in pH 3 water for binding to amine functional groups. Sample surfaces were place in contact with the Orang II solution for 30 min at 40℃. After 30 min, each sample was washed two times with pH 3 water to remove any dye that did not adsorb onto the surface. The dye was desorbed from sample in a pH 10 water. Desorbed samples were measured for absorbance at a wavelength of 560 nm using an enzyme-linked immunosorbent assay (ELISA) reader (Epoch, BioTek, Winooski, VT, USA).

3.3.3. Mesenchymal stem cells (MSCs) proliferation

3.3.3.1. Mesenchymal stem cell culture

MSCs (PT-5006, Lonza, Basel, Switzerland), a normal human adipose derived stem cells isolated from normal (non-diabetic) adult lipoaspirates collected during elective surgical liposuction procedures, were cultured in Dulbecco's modified eagle medium (DMEM, 11885084, Gibco, Waltham, MA, USA) growth media, DMEM supplemented with 10% fetal bovine serum (FBS, 26140079, Gibco, Waltham, MA, USA) and a penicillin-streptomycin solution (100 units/ml penicillin and 100 unit/mL streptomycin, 15140122, Gibco, Waltham, MA, USA) as antibiotic. MSCs were plated at 2.875×10^5 cells on 100 mm culture dish and were cultured until the cell reached 90% confluence. Trypsin-EDTA (CC-5012, Lonza, Basel, Switzerland) solution of 3 mL was added in the culture dishes to detach adhered cells. Detached cells were added in Trypsin neutralizing solution (TNS, CC-5002, Lonza, Basel, Switzerland) 6 mL and aspirated by gentle pipetting. The cell suspensions were each transferred to 15 mL conical tube and it was spun down at 210 × g (Allegra X-15R, Bechman coulter, Brea, CA, USA) for 5 min at room temperature. The supernatant were carefully sucked out. Cell pellets were resuspended with DMEM growth media of 5 mL. Appropriate aliquots of suspended cells were plated in 100 mm culture dish. They were serially subcultured through this procedure and passaged at each 90% confluence level. The 5 passages MSCs were used for this study. All procedures were carried out at 37℃ in a CO_2 incubator (MCO-15AC, Sanyo Electric, Osaka, Japan) containing 5% CO_2 mixed gas.

3.3.3.2. Cell proliferation

Cell proliferation was measured by WST-8 (CM-VA2500, Cellomax Cell Viability Assay Kit, Precaregene, Anyang-si, Korea) reagent. A water-soluble yellow dye that can be reduced to water-soluble orange formazan crystals by the dehydrogenase system of active cells. The third passages subcultured MSCs in 100 mm culture were detached with 3 mL of trypsin-EDTA and resuspended in 6 mL TNS to neutralize them. After centrifugation the cells were diluted to a final concentration of 3×10^4 cells/mL in the prepared DMEM growth media as determined by a cell counter (Countess™ II,

Thermo Fisher scientific, Waltham, MA, USA). Each of specimen (HDPE, AA-H, CPA-H, DACH-H, AA-L, CPA-L, and DACH-L) was sterilized by 70% ethanol. The specimens were put in 6 well plate and the cells were seeded at a density of 9×10^4 cells/well on them. After 6, 12, and 18 d of cultivation of cell, the cells were incubated with 300 μL of the WST-8 solution per well at 37℃ for 1 h. A 100 μL aliquot of the solution from each well was aspirated and poured onto a 96-well plate to measure the absorbance at 450 nm using an ELISA reader.

3.4. Results

3.4.1. Surface characterizations

3.4.1.1. Allylamine plasma-polymerization for process optimization

Since plasma-polymerization can be occurred by reaction of activated gas each other on the HDPE surface, internal pressure and power of plasma were adjusted to find optimal conditions for plasma-polymerization with AA, CPA, and DACH as shown in Figure 3.4. The internal pressure of the plasma reactor was varied from 30 to 60 mTorr with 10 mTorr intervals. The applied plasma power and nozzle size were fixed at 80W and 3.5 mm respectively. The polymer film produced by polymerization was the thickest at 30 and 60 mTorr.

Figure 3.5 shows the AA plasma-polymerization pattern in the reactor. Plasma power was selected as 30, 60, and 90 W, and internal pressure were set 30 mTorr to and 60 mTorr. The applied nozzle size was fixed at 3.5 mm. The polymer film produced by polymerization was the thickest and darkest at 60 W plasma power, 30 mTorr internal pressure.

Figure 3.6 shows the contact angle and amine concentration for distance from center. The contact angle decreased away from center. In addition, the highest concentration of amine was detected at a distance of 7 cm compared to other distances.

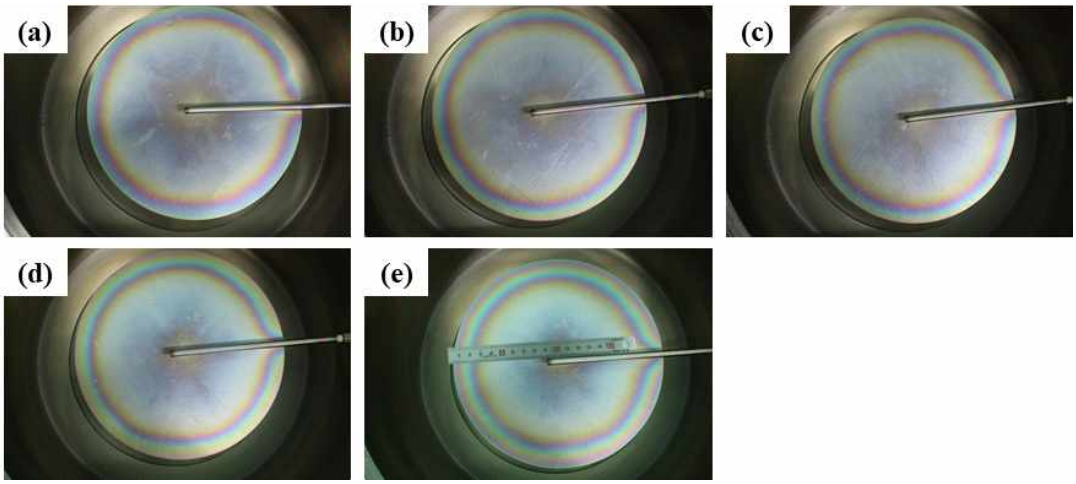

Figure 3.4. The effect of chamber inside pressure on the surface distribution patterns of allylamine polymeric thin film. The pressure inside the chamber was varied from 30 to 100 mTorr; (a) 30 mTorr, (b) 40 mTorr, (c) 50 mTorr, (d) 60 mTorr, and (e) 100 mTorr. Plasma-polymerization was performed on the 19 cm diameter stainless steel plate and set up by 80 W power using 3.5 mm nozzle diameter.

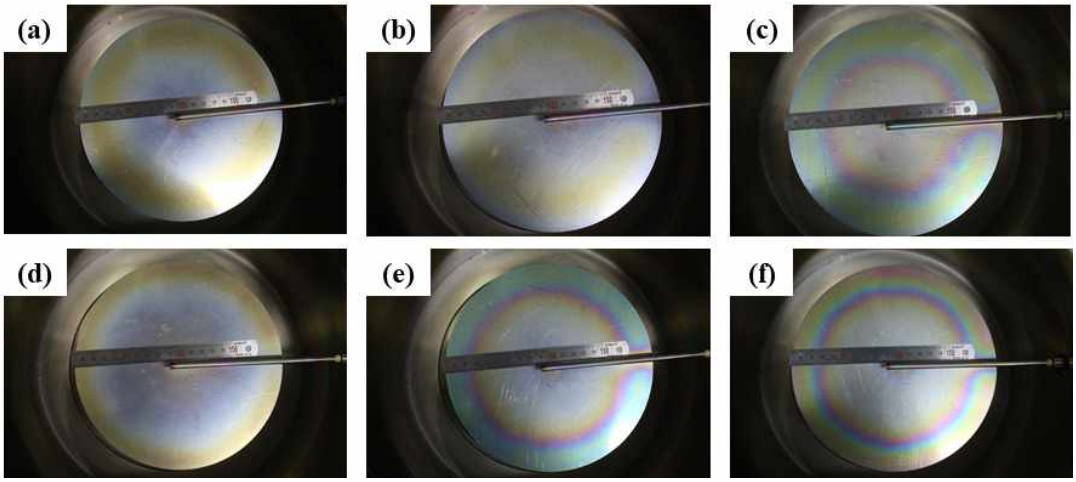

Figure 3.5. The effect of chamber inside pressure and plasma power on the surface distribution patterns of allylamine polymeric thin film. The pressure inside the chamber was selected to be 30 and 60 mTorr; (a-c) 30 mTorr, (d-f) 60 mTorr. Also, plasma power varied from 30 W to 90 W; (a, d) 30 W, (b, e) 60 W, and (c, f) 90 W. Plasma-polymerization was performed on the 19 cm diameter stainless steel plate using 3.5 mm nozzle diameter.

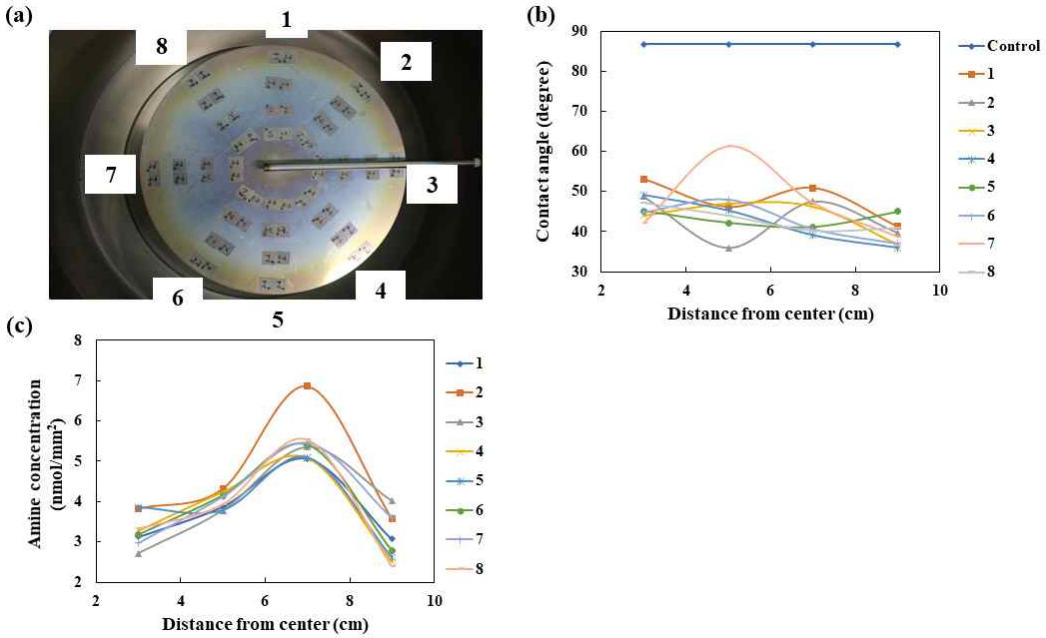

Figure 3.6. Effect of distance from center on the amine concentration distributions. (a) Sample positions marked on surface. (b) Contact angles as a function of distances from center and positions marked on surface. (c) The effect of distance from center to positions on the changes of amine concentrations. Plasma-polymerization was carried out at 60 W power and 30 mTorr chamber pressure.

3.4.1.2. Cyclopropylamine plasma-polymerization for process optimization

For CPA plasma-polymerization, since the amine distribution pattern on surface did not appear, the optimization of plasma-polymerization was determined by measuring the amine concentration on the surface for each condition.

Figure 3.7 shows that the effect of the plasma reactor internal pressure changed. The pressure increased by 5 mTorr from 30 mTorr to 50 mTorr. The applied plasma power was fixed at 60 W, and the nozzle size was fixed at 3.5 mm. There was no change in the surface due to polymerization, so it was impossible to confirm.

Figure 3.8 shows the amine concentration with internal pressure and position. The experimental conditions were the same as in Figure 3.7. As a result of measuring the amine concentration, it was confirmed that it came out most uniformly at 40 mTorr.

Figure 3.9 shows the amine concentration with plasma power and position. The power increased by 10 W from 50 W to 70 W. The internal pressure was fixed at 40 mTorr, and the nozzle size was fixed at 3.5 mm. As a result of measuring the amine concentration, it was confirmed that it came out most uniformly at 60 W.

Figure 3.10 shows the contact angle and amine concentration for distance from center. The contact angle decreased away from center. The amine concentration on the surface was increased from the distance of 7 cm from the center of the nozzle.

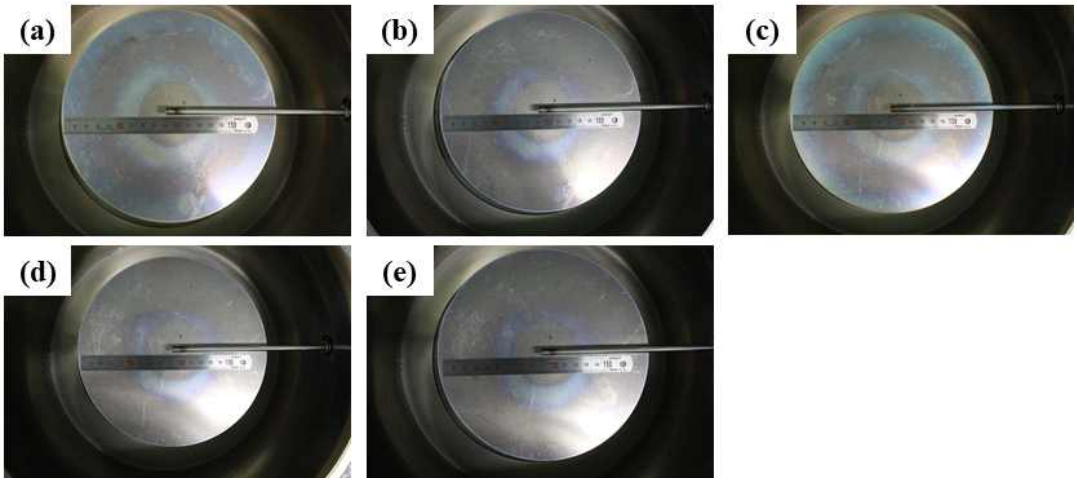

Figure 3.7. The effect of pressure inside the chamber on the surface distribution patterns of cyclopropylamine polymeric thin film. The pressure inside the chamber was varied from 30 to 50 mTorr. (a) 30 mTorr, (b) 45 mTorr, (c) 40 mTorr, (d) 45 mTorr, and (e) 50 mTorr. Plasma-polymerization was performed on the 19 cm diameter stainless steel plate and set up by 60 W power using 3.5 mm nozzle diameter.

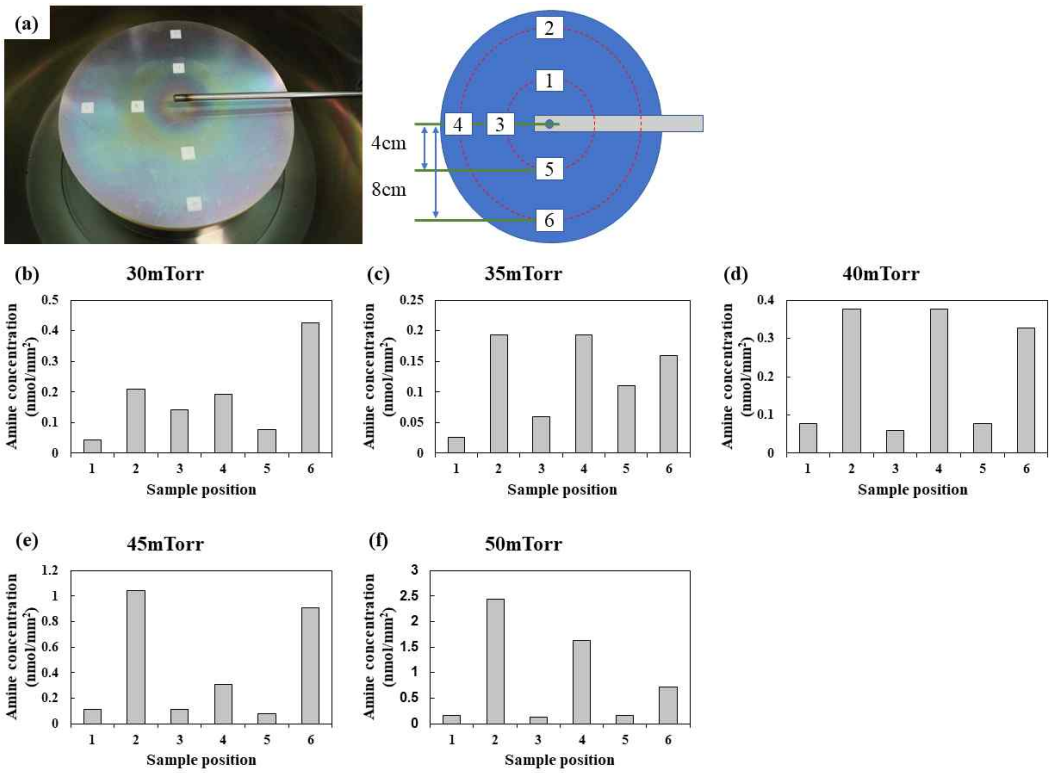

Figure 3.8. Effect of chamber pressure on the changes of amine concentration distributions. The pressure inside the chamber was varied from 30 to 50 mTorr. (a) sample positions marked on surface, (b) 30 mTorr, (c) 35 mTorr, (d) 40 mTorr, (e) 45 mTorr, and (f) 50 mTorr. Plasma-polymerization was carried out at 60 W power using 3.5 mm nozzle diameter.

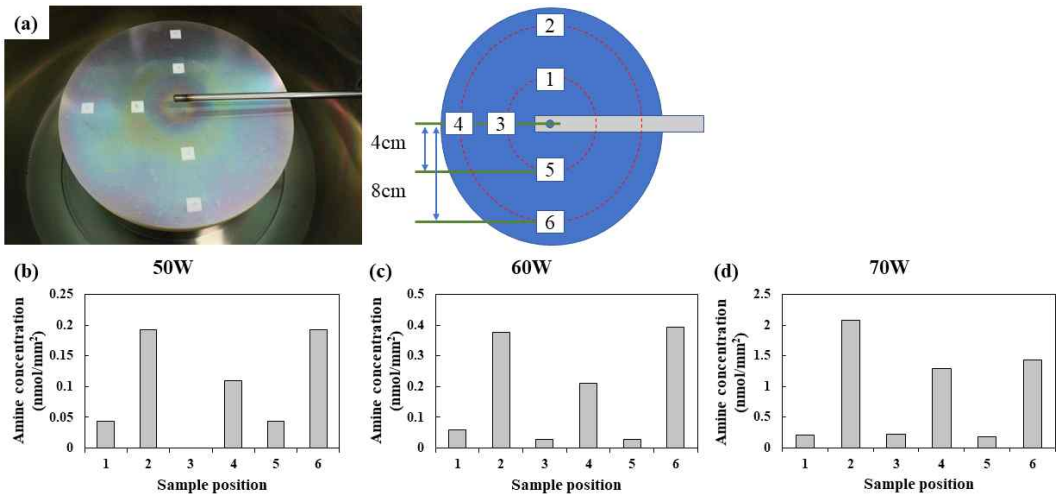

Figure 3.9. Effect of plasma power on the changes of amine concentration distributions. The plasma power was varied from 50 to 70 W; (a) Sample positions marked on surface, (b) 50 W, (c) 60 W and (d) 70 W. Plasma-polymerization was carried out at 40 mTorr chamber pressure using 3.5 mm nozzle diameter.

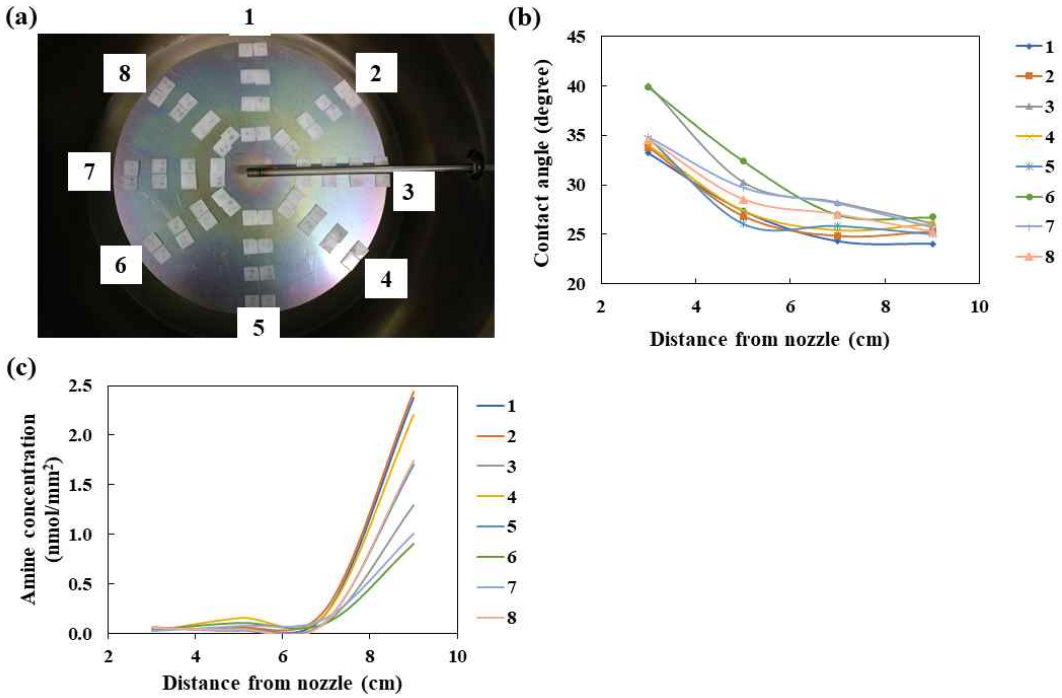

Figure 3.10. Effect of distance from center on the changes of amine concentration. (a) Sample positions marked on surface, (b) Contact angles. (c) Plots of amine concentrations vs. distance from nozzle. Plasma-polymerization was carried out at 60 W power and 40 mTorr chamber pressure.

3.4.1.3. 1,2-Diaminocyclohexane plasma-polymerization for process optimization

Figure 3.11 shows that the effect of the plasma reactor internal pressure changed. The pressure increased by 5 to 45 mTorr. The applied plasma power was fixed at 50 W, and the nozzle size was fixed at 2 mm. The polymer film produced by polymerization was the thickest and darkest at 10 mTorr. From this result, the internal pressure during DACH plasma-polymerization was fixed at 10 mTorr. Finally, amine concentration was investigated by changing plasma power and nozzle diameter.

Figure 3.12 shows the DACH plasma-polymerization pattern in the reactor. Plasma power was selected as 50 W and 80 W, and nozzle sizes were set to 0.5, 1, 2, and 3.5 mm. The applied internal pressure was fixed at 10 mTorr. The polymer film produced by polymerization was the thickest and darkest at 80 W plasma power, 3.5 mm nozzle size.

Figure 3.13 shows the DACH plasma-polymerization coating was stable in two kinds of liquid. In this experiment, linear low density polypropylene (LLDPP) was used for measuring for Fourier-transform infrared spectroscopy (FT-IR) after plasma-polymerization. The polymerized sample was measured three times in total, and the polymerized state, the state after 1 h at 25°C and 100 rpm, and the state after 5 min in 70% alcohol are indicated. All samples had amine groups on the sample surface and showed N-H band at 1640 cm^{-1}.

Figure 3.14 shows the contact angle and amine concentration for distance from center. The contact angle decreased from 5 cm to 9 cm. In addition, the amine concentration of surface was decreased as the distance from nozzle center.

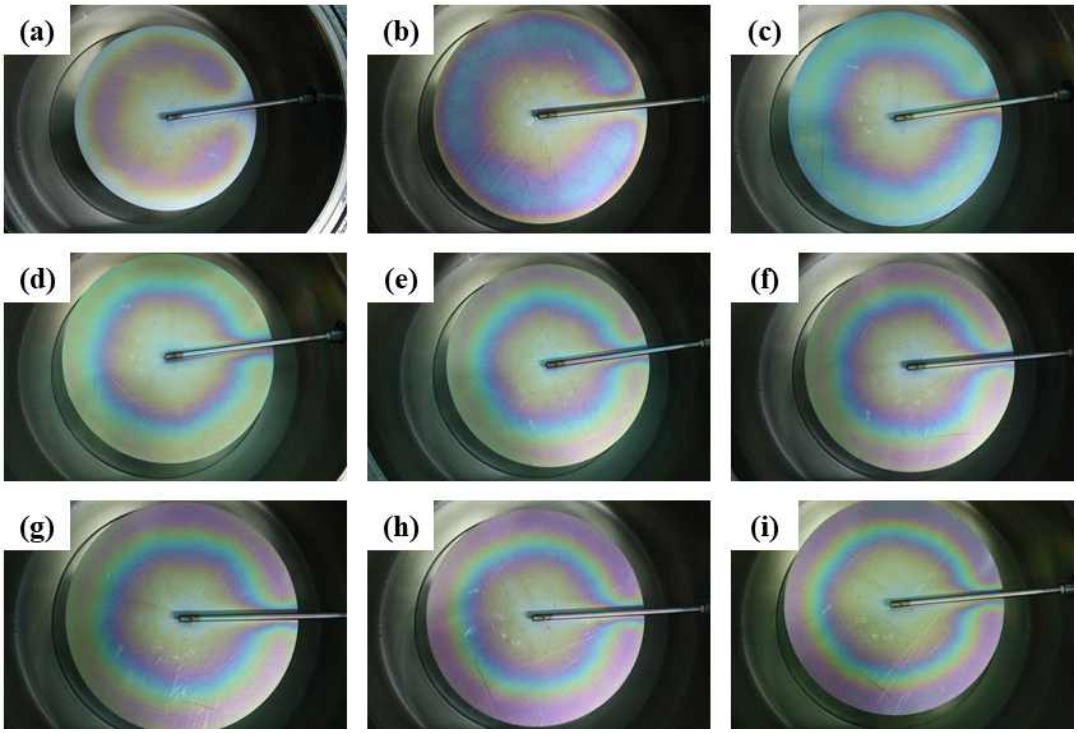

Figure 3.11. The effect of chamber inside pressure on the changes of surface distribution patterns of 1,2-diaminocyclohexane polymeric thin film. The pressure inside the chamber was varied from 5 to 45 mTorr; (a) 5 mTorr, (b) 10 mTorr, (c) 15 mTorr, (d) 20 mTorr, (e) 25 mTorr, (f) 30 mTorr, (g) 35 mTorr, (h) 40 mTorr and (i) 45 mTorr. Plasma-polymerization was performed on the 19 cm diameter stainless steel plate and set up by 50 W power using 2 mm nozzle diameter.

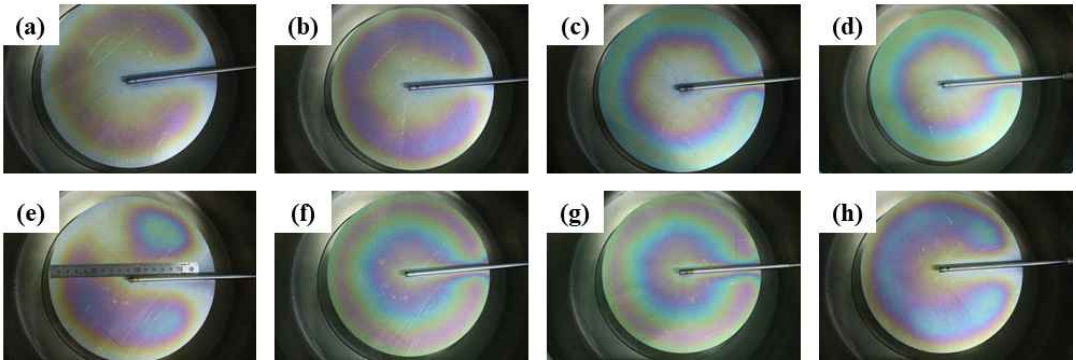

Figure 3.12. The effect of plasma power and nozzle diameter on the changes of surface distribution patterns of 1,2-diaminocyclohexane polymeric thin film. The plasma power was selected to be 50 and 80 W; (a-d) 50 W, and (e-h) 80 W. Also, nozzle diameter varied from 0.5 mm to 3.5 mm; (a, e) 0.5 mm, (b, f) 1 mm, (c, g) 2 mm, and (d, h) 3.5 mm. Plasma-polymerization was performed on the 19 cm diameter stainless steel plate and set up by 10 mTorr chamber pressure.

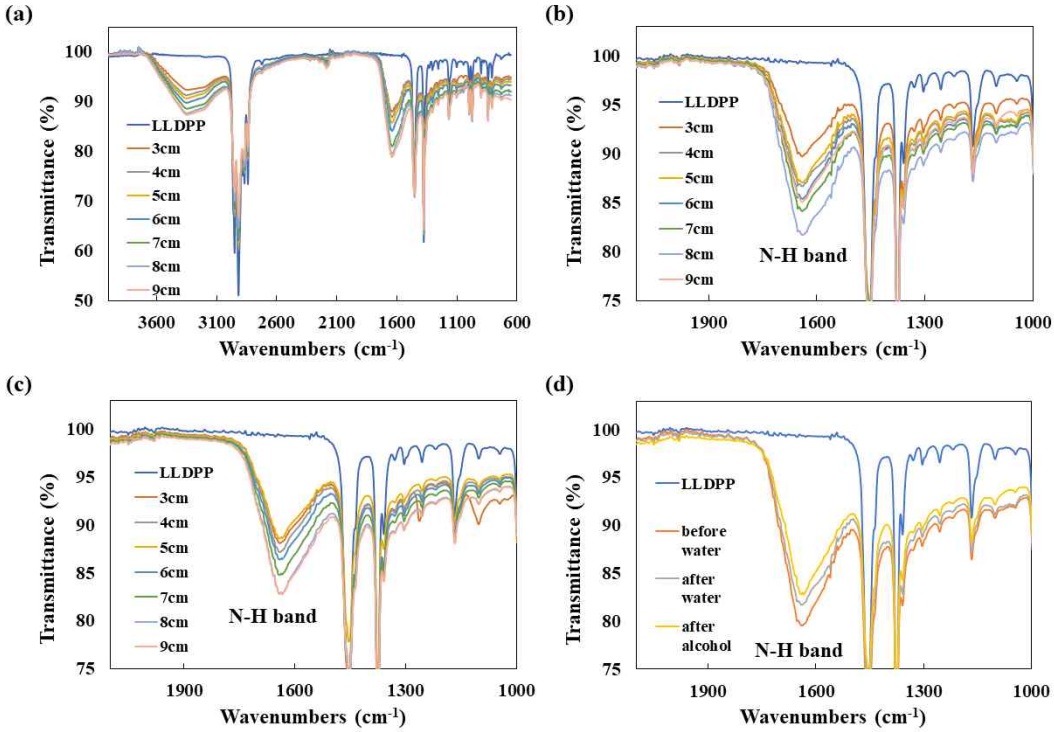

Figure 3.13. FT-IR results of 1,2-diaminocyclohexane plasma-polymerization after washed by water or 70% ethanol. (a) no washed. (b) deionized water at 25℃, 100 rpm for 1 h. (c) 70% ethanol for 5 min. (d) Comparison of each samples of 8 cm distance from center. Plasma-polymerization was carried out at 80 W power and 10 mTorr chamber pressure.

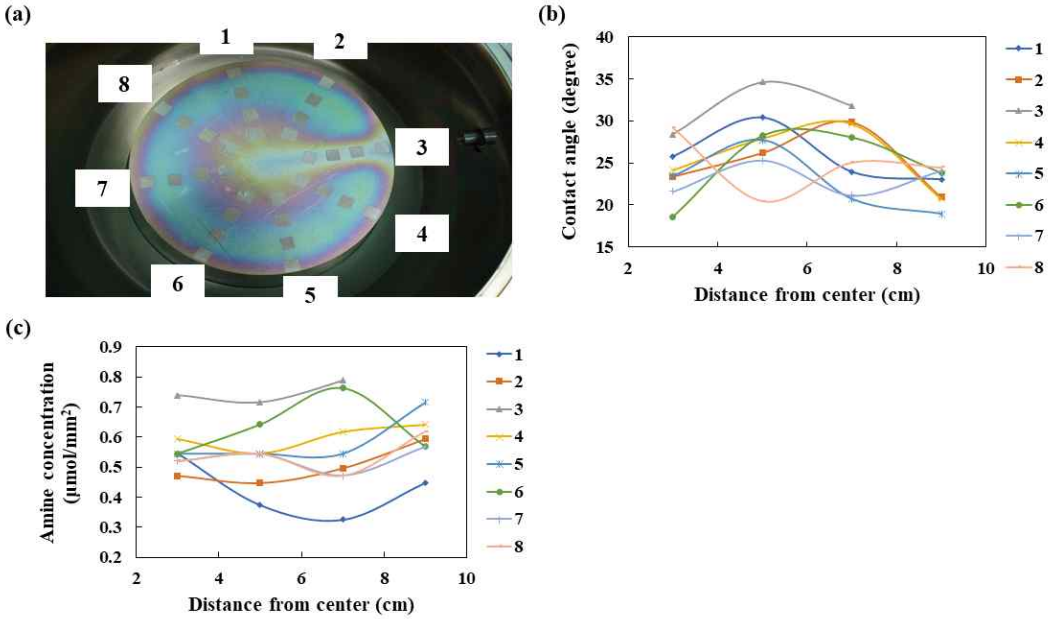

Figure 3.14. The effect of distance from center on the changes of amine concentration distributions. (a) Sample positions marked on surface. (b) Contact angles. (c) Plots of amine concentrations vs. distance from center. Plasma-polymerization was carried out at 80 W power and 10 mTorr chamber pressure.

3.4.1.4. Amine concentration analysis after amine plasma-polymerization

Amine plasma-polymerization was performed under optimized conditions for each monomer and established high and low concentrations required for the study. High concentration was around 100 nmol/mm^2, and low concentration was around 5 nmol/mm^2 (Table 3.2). The concentration of the amine was controlled by plasma-polymerization time. The concentration of the sample was measured under each condition using the orange II method (Figure 3.15(a)). As a result of measuring a sample having the same amine concentration using FT-IR, it was observed that a peak was generated at a wavelength of 1640 cm^{-1} indicating the amine (Figure 3.15(b)).

Figure 3.16 shows the contact angle values of surface modified HDPE surface. This result show that amine polymerization was increased of the hydrophilicity on the HDPE surface. In particular, AA and CPA showed that the hydrophilicity increased with the increase of the amine concentration on the surface.

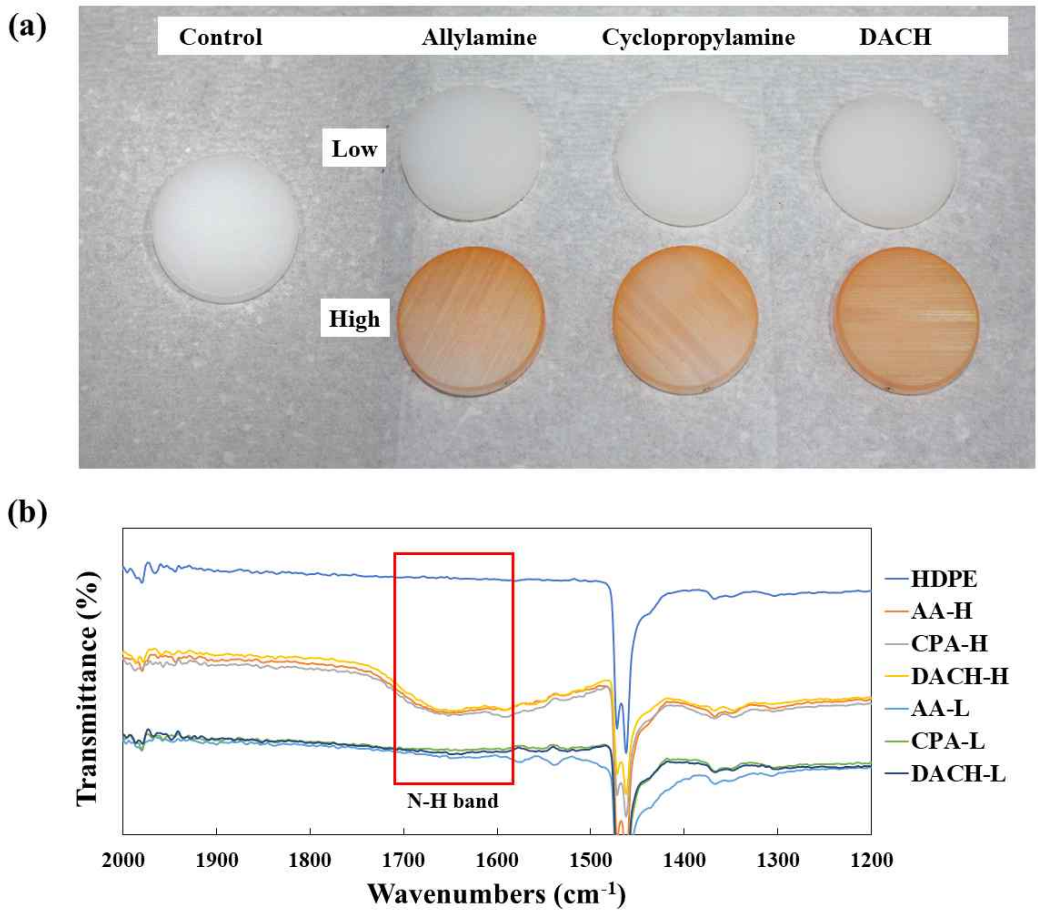

Figure 3.15. (a) HDPE disks with low and high amine concentration dyed by orange II. (b) FT-IR spectrum of disks treated with various monomers. (AA-H, allylamine high amine concentration; CPA-H, cyclopropylamine high amine concentration; DACH-H, 1,2-diaminocyclohexane high amine concentration; AA-L, allylamine low amine concentration; CPA-L, cyclopropylamine low amine concentration; DACH-L, 1,2-diaminocyclohexane low amine concentration).

Table 3.2. Low and high amine concentrations

Final amine concentration ($nmol/mm^2$)	AA	CPA	DACH
Low	6.01	5.65	4.45
High	103.2	105.1	113.5

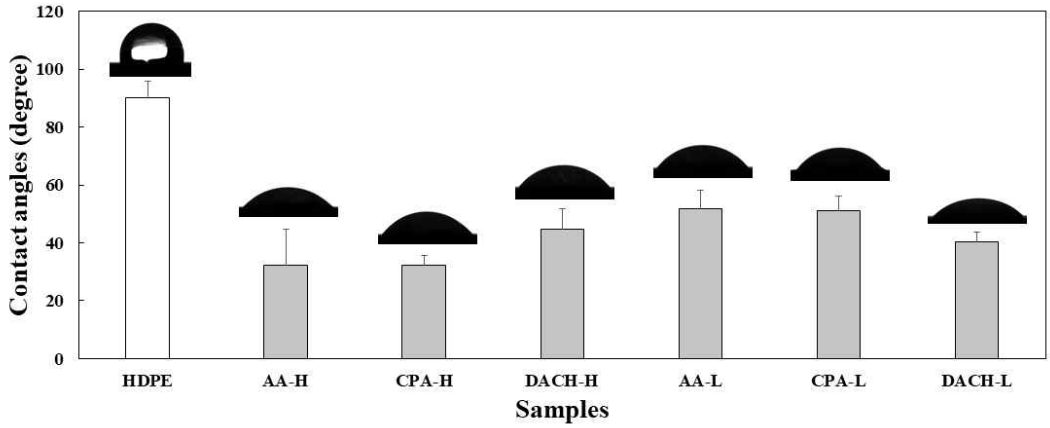

Figure 3.16. The effect of monomers on the changes of contact angles of the samples. (AA-H, allylamine high amine concentration; CPA-H, cyclopropylamine high amine concentration; DACH-H, 1,2-diaminocyclohexane high amine concentration; AA-L, allylamine low amine concentration; CPA-L, cyclopropylamine low amine concentration; DACH-L, 1,2-diaminocyclohexane low amine concentration)

3.4.2. Proliferation of mesenchymal stem cells

Samples were prepared by implementing two concentrations of amine coating using three monomers. MSCs were used in samples, and a total of 9×10^4 cells were used in each samples. Cell proliferation of AA and CPA were affected by concentration and showed a tendency to increase at high concentration. On the other hand, DACH showed no difference in cell proliferation by the concentration (Figure 3.17).

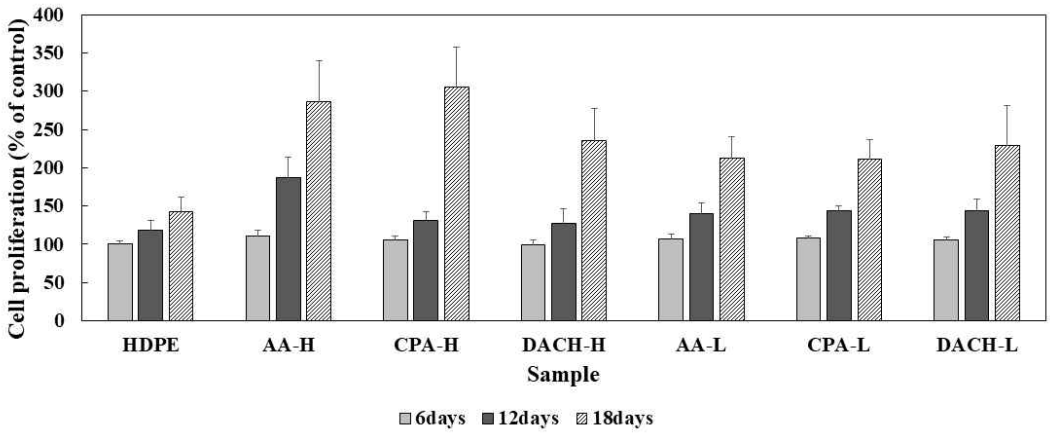

Figure 3.17. The effect of various monomers and amine concentrations on the MSCs proliferation. (AA-H, allylamine high amine concentration; CPA-H, cyclopropylamine high amine concentration; DACH-H, 1,2-diaminocyclohexane high amine concentration; AA-L, allylamine low amine concentration; CPA-L, cyclopropylamine low amine concentration; DACH-L, 1,2-diaminocyclohexane low amine concentration).

3.5. Discussions

Since synthetic polymer HDPE have favorable mechanical and physicochemical properties, they are frequently employed as a bio-implant in dental or orthopedic injuries [73, 74]. These kinds of polymeric materials have advantages such as ease of processing, appropriate mechanical strength/hardness and ease of modification [75]. Even though these materials have long history as a bio-inert material, they are some limitation for clinical application [76-80]. For example, these materials in implant application have problems in fast integration of healthy tissues and fibrosis by multiple corrective surgeries [76-80]. To overcome these obstacles, surface modification of implant can be considered to improve implant surface to have required characteristics without change of bulk properties [75]. For example, Sengupta *et al.* reported that HDPE surfaces were modified with plasma-treated polyetherimide (PEI) films of gold nanoparticles and arginine to have amine-decorated surface [75]. They argued that arginine-modified surfaces showed almost similar cell viability compared to the surfaces modified with fibronectin. Furthermore, Žáková *et al.* reported that carbon nanoparticles (CNPs) functionalized with amide-amine groups were grafted to the plasma activated surface of HDPE and these modified HDPE surfaces showed positive results in adhesion, proliferation and viability of vascular smooth muscle cells [81]. It seems to be that HDPE surfaces modified with amine groups provide better environment in cell adhesion or viability. From these points of view, we studied amine deposition onto HDPE surfaces using low-pressure plasma for dental implant application and optimal conditions were explored to deposit amine groups onto HDPE surfaces by the types of amine monomers.

In this study, three kinds of monomers having amine group such as AA, CPA, and DACH were used to modify HDPE surfaces because they have abundance of primary amine groups in their chemical structure and ease of deposition on the hydrophobic polymer surfaces. When AA and DACH as a monomer was used for plasma -polymerization, polymerization band was visually confirmed as shown in Figure 3.4, 3.5, 3.11, and 3.12. These results indicated that plasma-polymerization can be successfully occurred on the surface of HDPE by low-pressure plasma. Otherwise,

polymerization band was difficult to be distinguished when CPA as a monomer was used. Then, the final polymerization conditions were confirmed after checking the amine concentration by each polymerization condition with the LLDPP sample. Furthermore, amine density and chemical architecture on the surface of materials are considered as an important factor for the cell attachment and proliferation [75, 81]. The density of primary amine groups on the HDPE surfaces were determined as shown in Figure 3.6, 3.10, 3.14. The results shown that change the amine concentration of surface follow the distance from the center, i.e. the density of amine group was maximized at 7 cm from the center when AA was used as a monomer. Otherwise, the density of amine groups was significantly increased from 7 cm from the center in the case of CPA as a monomer. When DACH was used as a monomer, the density of amine group was fluctuated. These results indicated that conditions for amine deposition need to be optimized with the kind of monomer. Furthermore, these results indicated that amine-monomers formed stable thin film on the HDPE surfaces and these thin films have structure with high cross-linking degree. Furthermore, amine-deposited thin film on the HDPE surfaces was water-insoluble. Thompson and Mayhahn *et al*. also reported that polymer formation was affected by the power level, bleed rate of monomer, pressure and reactor geometry of low-pressure plasma [82]. They argued that the higher of plasma power level induced increased amount of monomers participated in plasma -polymerization and then polymers formed by plasma was cross-linked with a high degree. Our results also showed similar tendency to their results. Furthermore, amine-deposited thin film was quite stable before and after washing with deionized water or 70% (v/v) ethyl alcohol, i.e. as shown in Figure 3.13, amine-specific peaks were also observed after washing process even though peak intensity has been changed. These results indicated that amine-deposited thin film on the HDPE surface was stable in the fabrication process, washing step and cell culture step.

Since contact angle was decreased with the increase of AA or CPA monomer as shown in Figure 3.16, amine-deposited thin film on the surface of HDPE may contribute to the improvement of cell proliferation and then biocompatibility. Chen *et al*. reported that polytetrafluoroethylene (PTFE) treated with NH_3 + O_2 plasma increased the attachment of bovine aorta endothelial cells compared to PTFE itself and then cells

confluent grew on the PTFE surfaces [83]. In the case of DACH, contact angle was not significantly changed by the amine density on the HDPE surfaces even though cell growth on the DACH-deposited HDPE surfaces showed positive results. These results might be due to the molecular architecture of DACH. As shown in Figure 3.17, cell growth at high density of AA or CPA-deposited HDPE surfaces resulted in relatively higher cell growth than DACH, indicating that polymer thin film formation by low-pressure plasma was changed by the used monomer and then formed thin polymer films significantly affected to the cell growth.

3.6. Conclusions

In this study, amine polymeric thin films were deposited on the HDPE surface using low-pressure RF plasma through plasma-polymerization, and the following results were obtained.

1. The introduction of amine groups on the HDPE surface using low-pressure RF plasma was successful.
2. After amine plasma-polymerization, HDPE was modified to hydrophilic surface.
3. The optimization of amine plasma-polymerization process was established by changing of plasma process parameters.
4. MSCs proliferation enhanced by the increasing of amine groups on the HDPE surface.

From these results, we suggest that amine plasma-polymerization technique is potential and useful tool in biomaterial surface modification.

4. Part Ⅱ: Preosteoblast behaviors on Ti surface with modified by amine plasma-polymerization using APPJ device

4.1. Introduction

An atmospheric plasma jet (APPJ) is a plasma (so-called atmospheric pressure) whose pressure is nearly equal to that of the surrounding atmosphere. Schütze A *et al*. reported that APPJ generate high-velocity effluent streams of highly reactive species with specific heat, high-pressure and uniform glow plasma discharges [84]. APPJ is believed to be a superior candidate for surface modification in terms of accessibility and convenience compared to other plasma technologies, i.e. it does not require a separate reaction tray while low or high pressure plasma normally requires reaction tray to maintain low or high pressure [84]. For example, specific chamber is required to create the partial vacuum for low pressure plasma technology [85, 86]. Therefore, APPJ technologies can be used directly on the production line without specific chamber. Furthermore, APPJ technology can be used to activate, clean, thin and/or impart functional moieties on the surface of materials or metals [87-89]. In particular, the plasma-polymerization and/or surface modification using APPJ technology are similar to the effects obtained with the low-pressure plasma [90]. Furthermore, this technology has advantages such as coating of variety of surfaces, anti-corrosion and adhesion-promoting layers generation onto the metals without solvents [87-90]. For these reasons, this technology provides environmentally friendly solution compared to other kinds of methods for surface modification. Due to these advantages, plasma-surface modification (PSM) using APPJ technology has extensively investigated in the field of biomedical engineering due its effective and economical surface treatment option for many kind of materials. Especially, surface modifications, including plasma technology, are one of the key determinants of the long-term success of dental implants [91].

Titanium (Ti) is the most widely used material for dental implant materials [91, 92].

Various types of surface modification modalities for Ti such as sandblasting, acid-etching, and hydroxyapatite coating have been extensively investigated to improve biocompatibility and bone regeneration [92-97]. Recently, plasma technology has investigated to endow antibacterial capacity, pore formation, air-powder abrasive system, biofilm model formation, protein adsorption and functional group attachment on the dental Ti surface [98-102]. For example, some functional groups such as $-NH_2$, -OH and -COOH were deposited onto the surface Ti surface using RF glow discharges of non-depositing gases [99-102]. Since these functional groups are known to increase wettability of conventional polymers, they are frequently employed to improve adhesion and the growth of cells on polymer surfaces [103-106]. Among them, the amine ($-NH_2$) coating shows an excellent function of the surface of biomaterials in terms of wettability, which is an important factor for biocompatibility [107, 108]. Although amine coating on the dental Ti surface is effective for improving biocompatibility, it is necessary to avoid complex or toxic physicochemical methods such as anodizing or sandblasting. However, the use of APPJ technology for coating of Ti with amine groups has been rarely reported still now. Since its coating efficiency is frequently fluctuated by researcher, manufacturer and/or operating environment, the establishment of accurate condition of amine coating using APPJ is most important factor to build biocompatible Ti surface. Additionally, it has been reported that the required functionality for biocompatible Ti surfaces seriously varied with the amine concentration [109, 110]. However, there has been no report in the optimal condition of amine creation for bone regeneration. Therefore, the finding of optimal condition of amine deposition on the surface of Ti is important to success bone regeneration.

In this study, we investigate the optimal conditions of APPJ for amine polymerization on the Ti surface and their modified Ti surfaces were assessed using preosteoblast cells.

4.2. Materials

4.2.1. Titanium

Commercial Ti disk (Grade 4) used as a substrate material was purchased from Zapp AG, Germany. Ti disk was further processed to have dimension of 20 mm diameter and 1 mm thickness (Figure 4.1 (a)). Sample was cleaned by ultrasonically in acetone for 10 min and deionized water for 10 min 5 times.

4.2.2. Amine monomers

Cyclopropylamine (CPA, A13844, Alfa Aesar, 98% purity, Haverhill, MA, USA) was selected for use in plasma-polymerization (Figure 4.1 (b)).

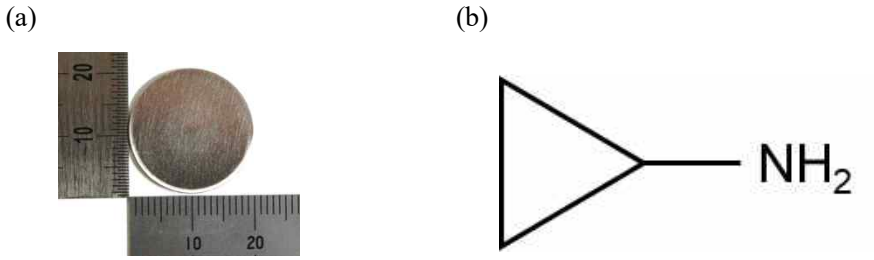

Figure 4.1. Experimental specimen and monomer. (a) Ti disk and (b) chemical structure of cyclopropylamine.

4.3. Methods

4.3.1. Atmospheric pressure plasma jet setup

APPJ is consisted of a quartz tube (100 mm length, 4 mm external diameter and 2 mm inner diameter), one electrode and two grounds. The electrode was excited by a AC voltage (12 k peak to peak voltage (V_{PP})) at fixed frequency of 50 kHz. He, the main gas of plasma generation, was flowed at 1 standard liter per minute (slm), and the bubbler containing the monomer for amine coating was bubbled with CPA through 10 standard cubic centimeter per minute (sccm) of helium at room temperature. The CPA precursor is mixed before entering the quartz tube and enters the reactor with He gas. An x-y stage was used for the entire plasma treatment of the sample. The x-y stage speed was 300 mm/min (Figure 4.2).

4.3.2. Gas species analysis in plasma plume

Light emitted from excited atoms and molecules was detected with an Optical Emission Spectrometer (OES, Avantes model of AvaSpec-ULS2048CL-EVO-RS, Oude Apeldoornseweg, Gelderland, Netherlands). The analysis performed between 200 nm and 900 nm in wavelength with 1.4 nm in resolution. For the optical fiber, Avantes model FC-UV400-2 was used (Figure 4.3).

4.3.3. Electrical characteristic of plasma discharge

Plasma electrical properties was recorded by Tektronix (Beaverton, OR, USA) MDO32 digital oscilloscope. To detect high voltage, Tektronix P6015A 1000:1 HV probe was used. Additionally, I_{PG} (phase-to-ground) current transformer (TCP0030A) was used to measure the current on the ground side (Figure 4.4).

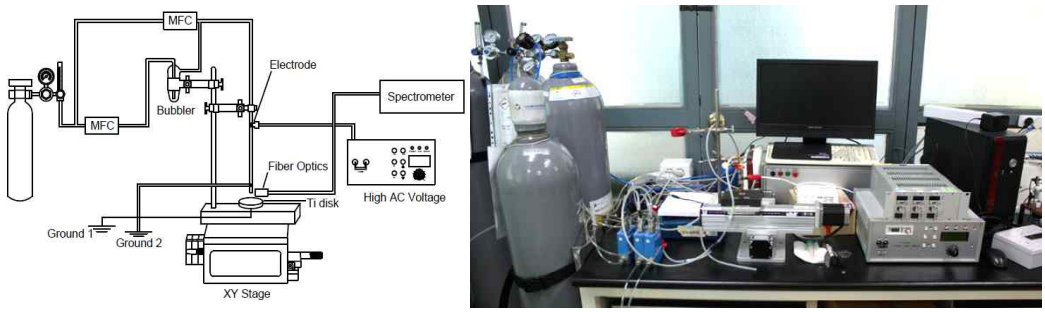

Figure 4.2. Schematic diagram and photograph of the atmospheric pressure plasma jet device components.

Figure 4.3. Gas species analyzing device. Optical emission spectrometer (left) and optical fiber (right).

Figure 4.4. Device for analyzed electrical characteristics of plasma discharge. Oscilloscope (left) and high voltage probe (middle) and current probe (right).

4.3.4. Surface characterizations

4.3.4.1. Contact angles

The GSX (Surfacetech, Gwangju-si, Korea) equipment was used to measure contact angle. After dropping 7 μL deionized water, the contact angle is automatically measured after 4 sec. The captured images were read by the Surfacetech software (version 1.1.5.6). Following this, these measurements were aggregated and averaged.

4.3.4.2. Surface topologies and roughness

Atomic Force Microscopy (AFM, XE-100, Parksystems, Suwon-si, Korea) was used to investigate the surface topography of APPJ treatment. The root-mean-square (RMS) roughness (Rq) were measured by XEI software (version 4.1.1) and each treatment was averaged over 4 scans at the center of the sample. The measurement using AFM used the non-contact mode, and the PPP-NCHR probe was used.

4.3.4.3. Surface chemistry

The surface chemistry of CPA coated Ti samples were examined using a High-Performance X-ray Photoelectron Spectroscopy (XPS, K-ALPHA+, Thermo Fisher scientific, Waltham, MA, USA). The system was equipped with a monochromatic Al K α radiation source, a 180° double focusing hemispherical analyzer, and an 128-channel detector. The survey spectra were collected in an energy range of 0−1350 eV and a resolution of 1 eV. The resulting spectra were then analyzed with the Avantage software (version 5.966).

4.3.5. Preosteoblast *in vitro* evaluations

4.3.5.1. Cell culture

MC3T3-E1 cells from clonal preosteoblastic cell line originated from newborn mouse calvaria was purchased from ATCC (CRL-2593, Manassas, VA, USA). Minimum essential medium α (α-MEM, A1049001, Gibco, Waltham, MA, USA) supplemented with 10% FBS and 1% antibiotics was used to culture these cells, and the medium was exchanged 2 d intervals. For cell culture, 1×10^5 cells were seeded in 100 mm dishes and sub-cultured about 70 % confluence of cells in dish. Cells were detached by use of 2 mL trypsin-EDTA solution and then 2 mL α-MEM growth medium was used to neutralize Trypsin-EDTA. Detached cells were transferred to 15 mL conical tube. Cells in a 15 mL conical tube were centrifuged using a Bechman coulter (Allegra X-15R, Brea, CA, USA) and the supernatant was removed. The cell pellet was resuspended in 5 mL of α-MEM growth medium and an appropriate aliquot of the suspended cells was plated in 100 mm culture dishes. In this study the third passages MC3T3-E1 cells were used. All processes were performed at 37°C in a CO_2 incubator (MCO-15AC, Sanyo Electric, Osaka, Japan) maintained with a 5% CO_2 mixed gas.

4.3.5.2. Cell proliferation

Cell proliferation before and after amine coating was compared using WST-8 (CM-VA2500, Cellomax Cell Viability Assay Kit, Precaregene, Anyang-si, Korea) reagent. Cell proliferation was performed using third sub-cultured MC3T3-E1 cells. Cells cultured in 100 mm dishes were isolated using trypsin-EDTA and neutralized with 2 mL of α-MEM growth medium. After centrifugation, the cells were counted through a cell counter (Countess™ II, Thermo Fisher scientific, Waltham, MA, USA) and diluted to a final concentration of 1×10^4 cells/mL.

Each of specimen (Con, 2, 4, 6, 8, and 10 min) was sterilized by 70% ethanol for 5 min. The specimens were put in 12 well plate and the cells were seeded at a density of 1×10^4 cells/mL on them. At the target point (1, 2, and 3 d), the cells were incubated with 100 μL of the WST-8 solution per well at 37℃ for 30 min. One hundred micro-liter aliquots of the solution from each well was aspirated and poured

onto a 96-well plate to measure the absorbance at 450 nm using an enzyme-linked immunosorbent assay (ELISA) reader (Epoch, BioTek, Winooski, VT, USA).

4.3.5.3. Cell viability

Cell viability before and after amine coating was compared using Live-Dead cell staining kit (K501, BioVison, Milpitas, CA, USA). Cell proliferation was performed using third sub-cultured MC3T3-E1 cells. Cells cultured in 100 mm dishes were isolated using trypsin-EDTA and neutralized with 2 mL of α-MEM growth medium. After centrifugation, the cells were checked through a cell counter and diluted to a final concentration of 1×10^5 cells/mL.

Each of specimen (Control, 2, 4, 6, 8, and 10 min) was sterilized by 70% ethanol at 5 min. The specimens were put into 12-well plate and the cells were seeded at a density of 1×10^5 cells/mL on them. 1 d later, all samples were washed with Dulbecco's Buffered Saline (DPBS, IBS-BP052, iNtRON Biotechnology, Seongnam-si, Korea). Staining solution was prepared as follows: 1 mL staining buffer was mixed with 0.25 μL Solution A (1 mM Live-Dye) and 1 μL solution B (1 mg/mL Pi). After the DPBS removed from samples, Live-Dead staining solution treated for 15 min in dark at room temperature. After staining, cells were imaged with an ECLIPSE Ni-U fluorescent microscope (Nikon, Tokyo, Japan), with 10× objective and a 20× objective for image taken.

4.3.5.4. Focal adhesion

Cells were grown on the substrates for 4 h. Thereafter, cells were fixed in 4% paraformaldehyde in PBS for 15 min, permeabilized with 0.1% triton X−100 solution (Sigma-Aldrich, Saint Louis, MO, USA) for 10 min. To prevent or reduce nonspecific binding of the primary and secondary antibodies to proteins, 1% bovine serum albumin (BSA, Sigma-Aldrich, Saint Louis, MO, USA) in DPBS was used for 30 min. After blocking step, primary antibody Paxillin was used overnight at 4℃ for immunocytochemistry. Next day, samples were washed 3 times by DPBS. Washed samples reacted with secondary antibody (Alexa fluor 488) for 1 h in dark at room

temperature. When the reaction is complete, the sample is washed and, then, 1:1 mixture of rhodamine and 4',6-diamidino-2-phenylindole (DAPI) was applied to the sample surface. This was covered with a cover glass. After 15 min, the sample was photographed using a fluorescence microscope (ECLIPSE Ni-U, Nikon, Tokyo, Japan).

4.3.5.5. Cell differentiation

The level of osteogenic differentiation induced by increase of the alkaline phosphatase (ALP) activity of the MC3T3-E1 cells were carried out as follows: cells were plated at 3×10^4 cells in 12-well plates and then, after 1 and 2 weeks, each specimen (Con, 2m, 4m, 6m, 8m, 10m) was assayed using a standard ALP test procedure. The cells were rinsed with PBS two times. The ALP activity in the cell lysates was determined by measuring the level of p-NP released from disodium p-NPP. The cells were lysed by adding a cell lysis buffer for 30 min. The lysis buffer was prepared by mixing 1% Xpert Protease Inhibitor Cocktail Solution (100X, GenDEPOT, Katy, Texas, USA), 1% Xpert Phosphatase Inhibitor Cocktail Solution (100X, GenDEPOT, Katy, Texas, USA) in RIPA Lysis and Extraction Buffer (89900, Thermo Scientific, Waltham, Massachusetts, USA). 150 μL cell lysate was collected and vortexed at 5 min intervals for 30 min. Centrifuge was carried out at 12,000 rpm for 10 min at 4℃. The supernatant was transferred into a eppendorf tube for determining the alkaline phosphate assay (100 μL) and protein concentration (20 μL).

For ALP analysis, ALP reaction reagent was prepared in a ratio of 2:1:2 (0.1 M glycine-NaOH buffer : 15 mM p-NPP : distilled water). For the ALP assay, ALP test premixture (100 μL of cell lysate solution, 100 μL of ALP reaction reagent) was added to each tube and incubated at 37℃ for 30 min. After adding 600 μL of 1.2 N NaOH to the tubes, the absorbance was measured by ELISA reader at 405 nm.

The protein concentration of the cell lysates was determined by using BCA protein assay reagent kit (Thermo Scientific). 25 μL of cell lysate and BSA standard were placed in a 96-well plate and 200 μL of BCA test reagent was added. In order to react the BCA reagent, it was reacted in a 37℃ incubator for 30 min and then measured at 570 nm using an ELISA reader. Protein concentration of the specimens

was determined by BSA standard curve. The ALP activities were normalized determined by the protein content of the cell lysate and expressed in μmol p-NP/min/μg protein.

4.3.5.6. Bone mineralization

To assess bone mineralization, the degree of bone differentiation of each sample was confirmed by staining with Alizarin red. Each sample was placed in 12 wells and then 3×10^4 cells were used for each well. Cell differentiation was performed for 1 or 2 weeks using a differentiation medium. At the end of the planned period, each sample was washed with DPBS to remove medium components and fixed with 4% paraformaldehyde for 15 min. After fixing, the sample was washed twice with DPBS and reacted at room temperature for 15 min at pH 4.2 with 2% Alizarin red reagent. After 15 min, the samples washed twice with DPBS was photographed. For comparative analysis of each sample, Alizarin red was eluted by adding 10% (w/v) cetylpyridinium chloride to 10 mM sodium phosphate reagent, and the eluted reagent was measured at 560 nm.

4.3.5.7. Western blotting

Total cell extracts were lysed, subjected to 10% SDS-PAGE, and transferred to polyvinylidene difluoride membranes. After blocking in 5% skim milk in Tris-buffered saline with 0.1% Tween 20, the membrane was incubated with specific antibodies followed by incubation with horseradish peroxidase-conjugated secondary antibodies. Antigen-antibody interactions were visualized by incubation with ECL chemiluminescence reagent (SuperSignal™ West Pico PLUS Chemiluminescent Substrate, 34580, Thermo Scientific™).

4.3.6. Statistical analysis

Statistical analysis was done using SPSS 26 statistics software (SPSS, IBM) and results are reported as means ± standard deviation. Statistical significance was measured by one-way ANOVA followed by Tukey's test if homogeneity of variances was upheld or violated, respectively. Statistical significance was assumed when $p < 0.05$.

4.4. Results

4.4.1. Surface characterizations

A Y-shape reactor was used to create an optimal reactor for applying amine groups to the surface of the sample. The Y-shape reactor was manufactured because it was judged to be a good design for the activation of amine monomers by plasma in such a way that the monomer enters the plasma flame generation position. To optimized the plasma-polymerization, the concentration of amines present on the surface was investigated by changing the plasma voltage, frequency, duty, and electrode position.

Figure 4.5(a), the plasma voltage was fixed at 14 kV and the change of amine concentration was investigated to the duty or plasma frequency. The amine concentration on the surface was increased with increasing frequency at a duty of 3 μs. Under the duty condition of 2.2 μs, the highest surface amine concentration was shown at 50 kHz, and then this was set as the standard.

In Figure 4.5(b), plasma-polymerization was carried out while changing the voltage and frequency, and the concentration of amine groups on the surface was measured by dividing it into before and after washing. As for the washing method, plasma-polymerized samples were placed in distilled water and washed for 1 h at 25℃ and 100 rpm in a shaking incubator. The result shows the highest value at 12 kV and 50 kHz conditions, confirming that amine polymerization was properly performed and the amines on the surface remained properly after washing procedure.

Figure 4.5(c) shows the results of amine polymerization by the flow rate of the monomer and the distance between the nozzle and the sample. The amine groups polymerized on the surface was decreased when the flow rate was increased from 10 sccm to 20 sccm at a distance of 4 mm. When the distance between the nozzle and the sample was decreased to 2 mm at a monomer flow rate of 20 sccm, the amine concentration on the surface was increased.

In Figure 4.5(d), amine groups on the surface were measured during the change of position of high voltage electrode. The voltage was fixed at 12 kV and the electrode positions was fixed at 52 mm from the tip of the nozzle. As shown in Figure 4.5(d), the amine concentration on the surface was increased with increasing frequency and

flow rate of He gas. On the other hand, the amine concentration on the surface decreased as the He gas flow rate increased when the position of the electrode was fixed at 37 mm from the tip of the nozzle.

In order to improve the concentration of amines present on the material surface and the generation of plasma, a ground was added to the part where the monomer entered in the Y-shape reactor.

Figure 4.6(a) was the result of measuring the amine concentration on the surface with the change of the electrode position and flow rate in the Y-shape reactor with application of double ground. The voltage was 12 kV, the frequency 50 kHz, the monomer flow rate was 20 sccm, and the distance between the nozzle and the sample was fixed at 2 mm. At the electrode positions 35 and 40 mm, the amine concentration on the surface increased with the He gas flow rate. On the other hand, at the electrode position of 45 mm, the amine concentration on the surface decreased as opposed to the increase in the He gas flow rate.

The voltage, frequency, and flow rate of the monomer were fixed as shown in Figure 4.6(a), and the distance between the nozzle and the electrode was set to 40 mm. Variables were time and He gas flow rate, and the amine concentration on the surface was measured by changing the time from 4 to 12 min at 4 min intervals and changing the He gas flow rate. The amine concentration on the surface increased with the increase of polymerization time between 4 and 8 min, but these was decreased at 12 min. At 4 min, the amine concentration on the surface decreased with the increase of the flow rate of He gas but, at 8 and 12 min, the amine concentration on the surface increased by the increase of the flow rate of He gas.

Figure 4.6(c) showed the changes of the amine concentration on the surface of the Ti disk used as a sample. Amine concentration was measured at number of points subjected to plasma-polymerization. Plasma-polymerization conditions were fixed at 12 kV, 50 kHz, a monomer flow rate of 20 sccm, a He gas flow rate of 400 sccm, a distance between the material and the nozzle was 2 mm, and a polymerization time of 8 min per location. The amine concentration was increased by the number of polymerization sites.

In Figure 4.6(d), plasma-polymerization was performed on the surface of the Ti disk

using optimized plasma-polymerization conditions based on the previous experiment and cell proliferation was tested. Samples used for cell proliferation were prepared by plasma-polymerization in a total of 5 places for each disk so that the entire surface was coated evenly. Cells were measured on 1, 3, and 6 d using 9.5×10^4 cells/well of MC3T3-E1 for each sample. There was no improvement by amine polymerization compared to the control.

The Y-shaped plasma reactor showed no difference compared to the untreated sample in the cell proliferation experiment because the surface amine concentration was low. To increase the surface amine concentration, reactor design changed by I-shape. The result of the new designed reactor was shown in Figure 4.7. The variables fixed for the experiment were the voltage 12 kV, the frequency 50 kHz, the distance between the nozzle and the sample 2 mm, and the He gas flow rate 1 slm. For polymerization, 5 locations were set on one disk, and polymerization was performed for 4 min per location. The amine concentration on the surface was higher in the sample with two groundings than in the sample with one ground. Depending on the flow rate of the monomer used, the surface amine concentration was increased up to 10 sccm, and the surface amine concentration was decreased at 15 and 20 sccm.

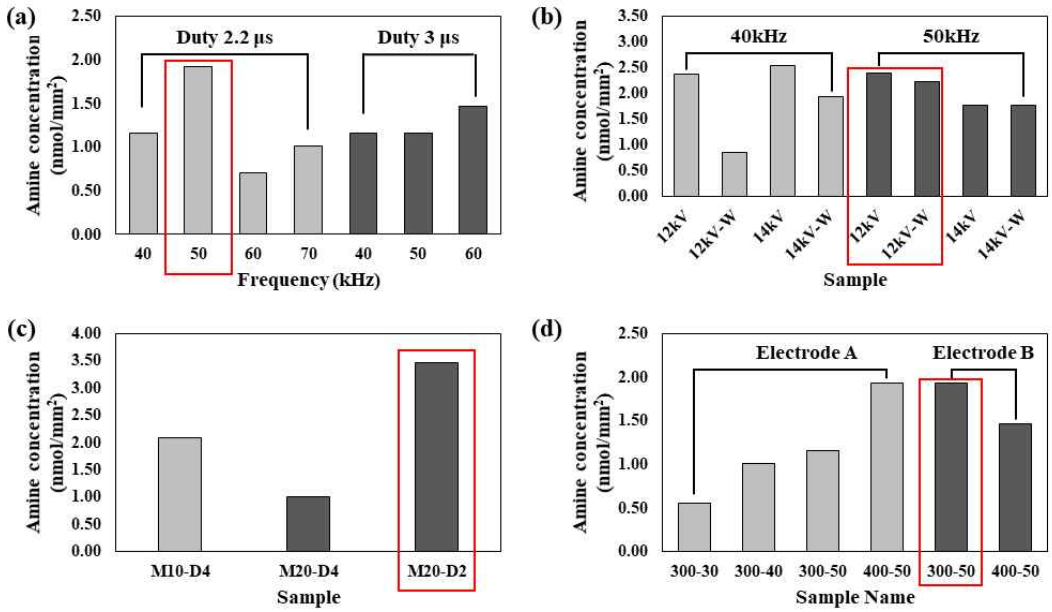

Figure 4.5. Amine concentrations as a function of (a) frequencies (distance between nozzle and sample is 4 mm, He flow rate 300 sccm, and CPA flow rate 2 sccm), (b) voltages (same condition as (a)), (c) CPA flow rate and distance at 14 kV and 50 kHz (M is CPA flow rate and D is distance of reactor and sample), (d) He flow rate and frequency (Electrode A was electrode position 52 mm and Electrode B was electrode position 37 mm; He 300 sccm and 30 kHz denote 300-30).

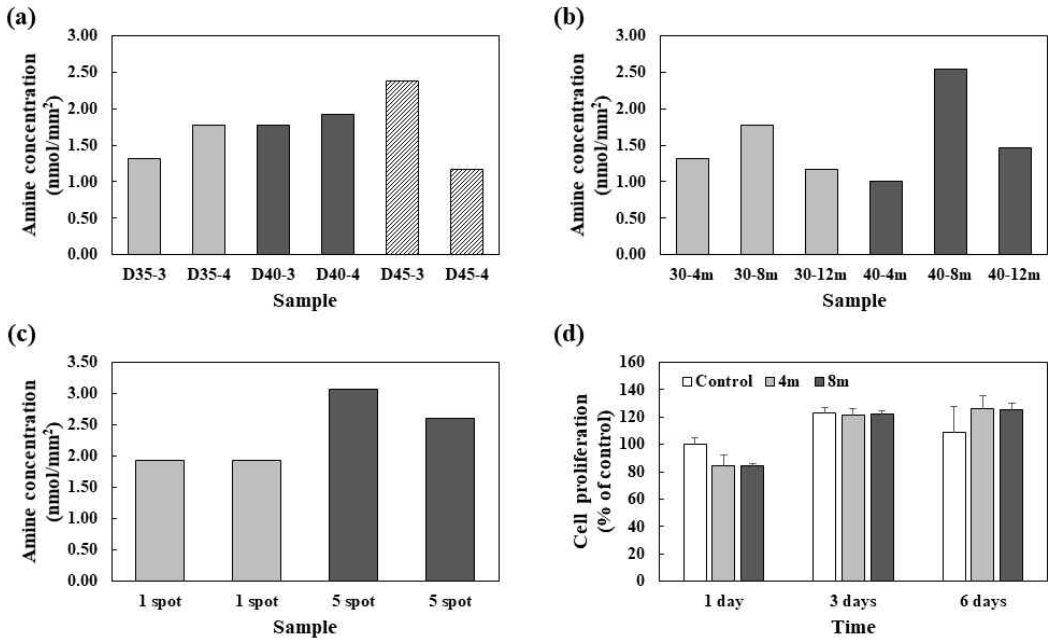

Figure 4.6. Amine concentrations as a function of (a) He flow rate and electrode position at 12 kV (distance between nozzle and sample 2 mm, frequency 50 kHz, monomer flow rate 20 sccm), (b) He flow rate and polymerization time (distance between nozzle and sample 2 mm, frequency 50 kHz, CPA flow rate 20 sccm), (c) number of plasma-polymerization sites on the amine concentration (voltage 12 kV, frequency 50 kHz, distance between nozzle and sample 2 mm, He flow rate 400 sccm, monomer flow rate 20 sccm). (d) The effect of plasma-polymerization time on the cell proliferation (voltage 12kV, frequency 50 kHz, distance between nozzle and sample 2 mm, He flow rate 400 sccm, monomer flow rate 20 sccm).

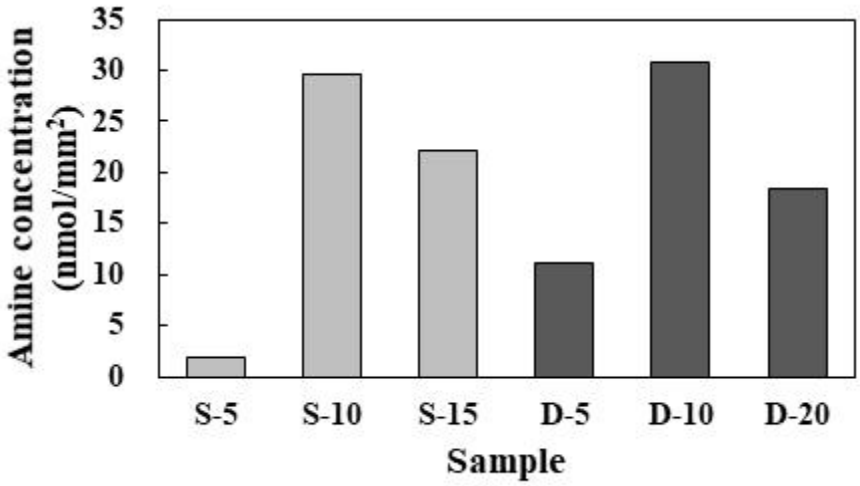

Figure 4.7. The effect of single or double grounds and the flow rate of monomers on the amine concentration (S, single ground; D, double ground; CPA flow rate 5 sccm denote S-5; -10, monomer flow rate 10 sccm; -15, monomer flow rate 15 sccm; -20, monomer flow rate 20 sccm).

In Figure 4.8, the shape of the plasma flame in the double ground was observed. The flow rate of the monomer was 10 and 20 sccm, and the flow rate of He gas was increased by 100 sccm from 400 to 1000 sccm. The variables fixed for the experiment were the voltage 12 kV, the frequency 50 kHz, the distance between the nozzle and the sample 2 mm. The shape of the flame with the flow rate of each monomer was affected by the flow rate of He gas, and the flame was surely generated as the flow rate of He gas increased. The lower the flow rate of the monomer, the stronger the plasma flame was generated.

The flow rate of He gas was set to 1 slm, and the optimum polymerization conditions were founded by voltage, frequency, and flow rate of monomers. Frequency, monomer flow rate, and polymerization time were fixed at 50 kHz, 10 sccm, and 2 min, respectively.

Figure 4.9(a) showed the result of the change in surface amine concentration with the increase in voltage. From 10 to 14 kV, the amine concentration on the surface increased as the voltage increased, and decreased at 16 kV. The results of the flow rate of the monomer at a voltage of 12 kV, a frequency of 50 kHz, and a polymerization time of 2 min were shown in Figure 4.9(b). The surface amine concentration showed the highest value at 15 sccm, but no significant difference was shown due to error values at other monomer flow rates.

Figure 4.9(c) showed the results by frequency at a voltage of 12 kV, a monomer flow rate of 10 sccm, and a polymerization time of 2 min. The concentration of the deposited amine with the increase of polymerization increased with the increase of the frequency, and there was no significant difference above 60 kHz. The results by polymerization time at a voltage of 12 kV, a frequency of 50 kHz, and a monomer flow rate of 10 sccm were shown in Figures 4.9 (d) and (e). The amine concentration on the surface increased with the increase of polymerization time, and in particular, it increased sharply between 8 and 10 min. The increase in the amine concentration on the surface with the change of polymerization time is clearly shown in the photos stained with Orange II reagent, and the orange color on the surface indicates the amine on the surface (Figure 4.9 (e)).

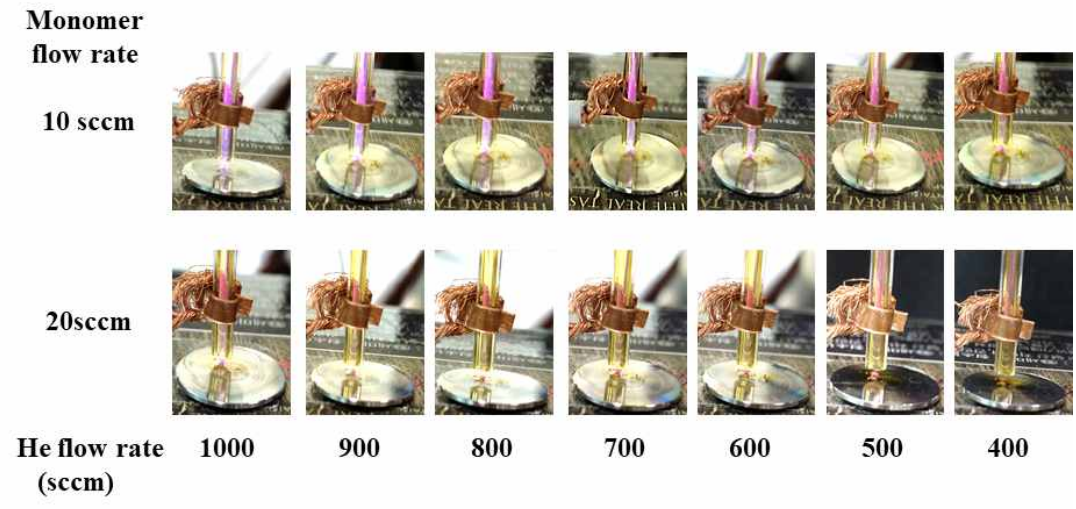

Figure 4.8. Generation of a plasma flame with increasing He gas flow rate at a fixed monomer flow rate. Monomer flow rate was fixed at 10 and 20 sccm.

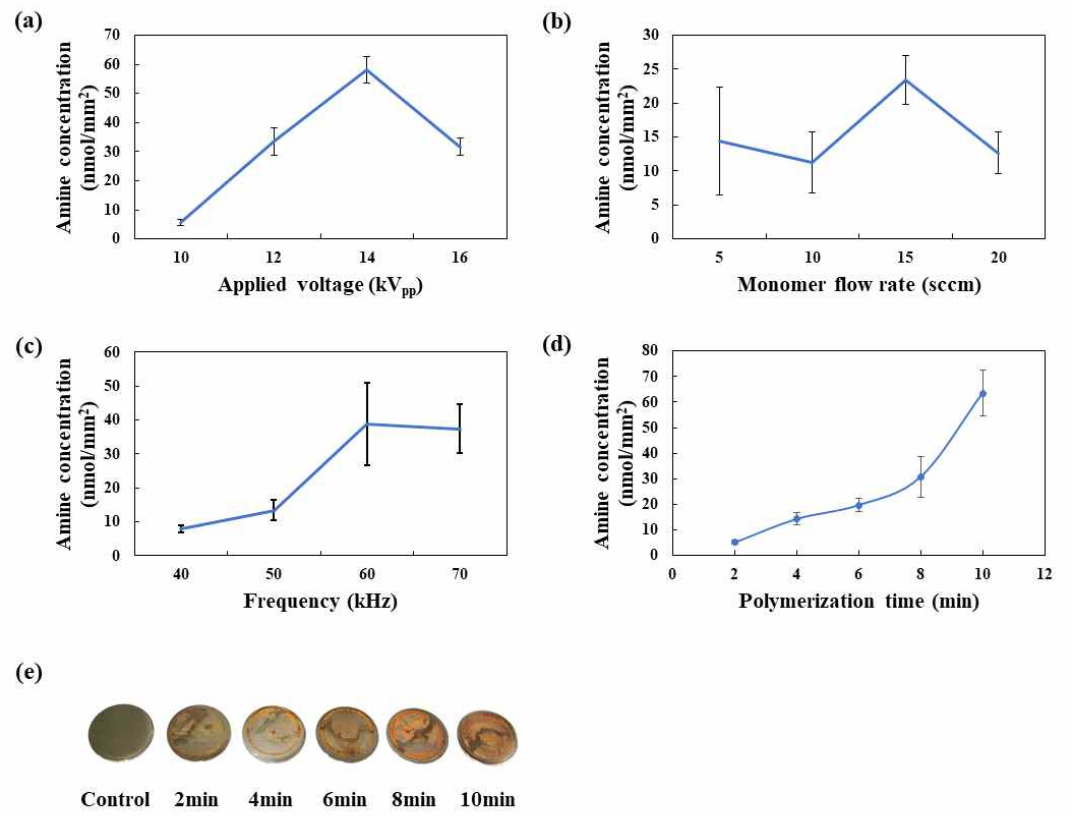

Figure 4.9. The effect of various parameters on the changes of amine concentration. (a) Applied voltage at 50 kHz frequency. (b) Monomer flow rate. (c) Frequency. (d) Plasma-polymerization time. (e) The effect of polymerization time on the changes of amine concentration on the disks.

High voltage, current, and plasma power were measured using an oscilloscope for plasma discharge and electrical characteristics. Figure 4.10 showed the measured waveform and plasma power with the change of frequency at 12 kV voltage.

As shown in Figure 4.10(e), the plasma power was increased by frequency increased except 60 kHz.

Plasma discharge with the voltage change at a frequency of 50 kHz was measured the waveform with the oscilloscope (Figure 4.11). As the voltage increased, the plasma power was increased.

Figure 4.12 showed the effect of monomer rate on the changes of plasma power. Waveform did not show change by the flow rate of the monomer, but the plasma power decreased as the flow rate of the monomer increased.

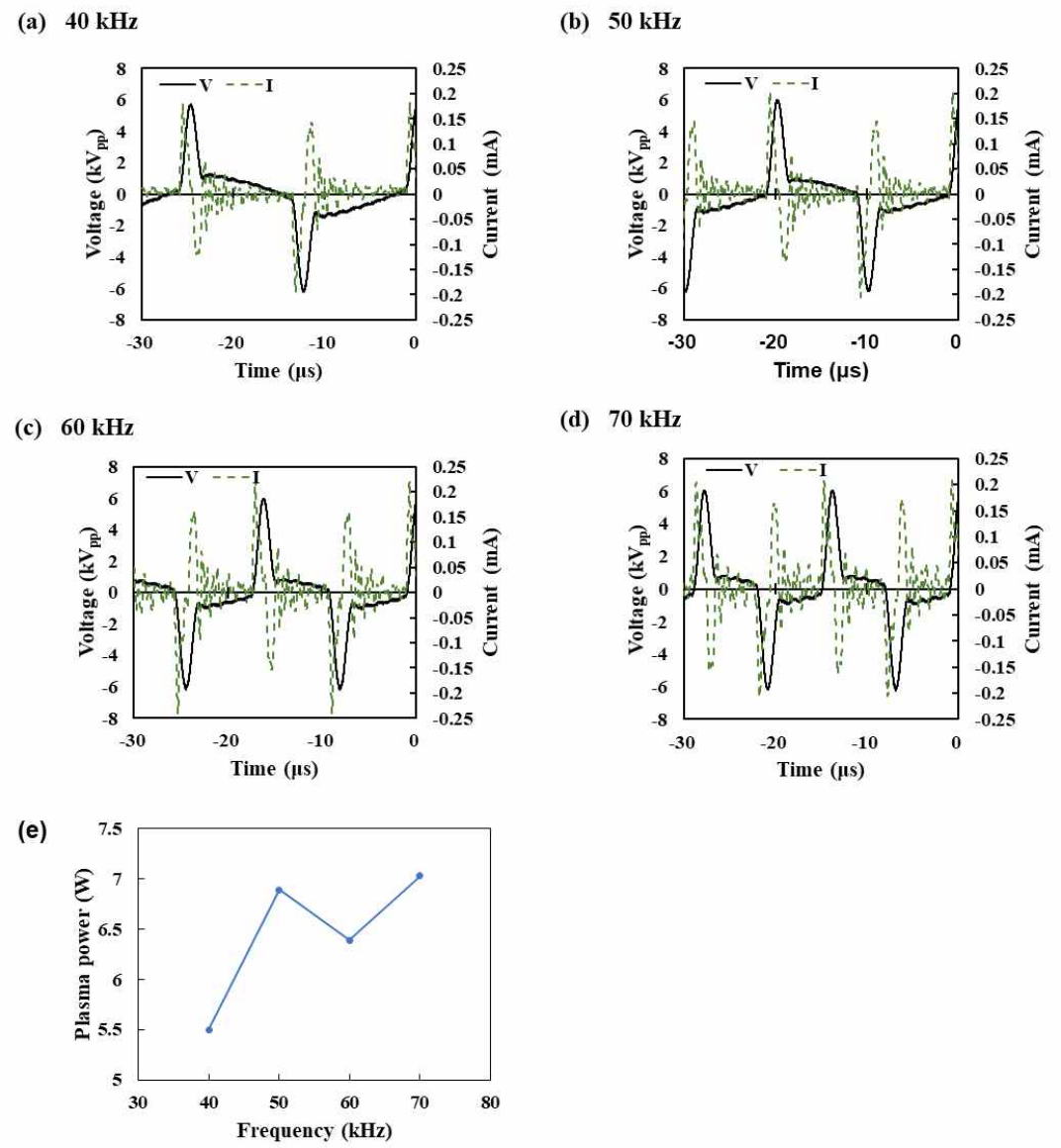

Figure 4.10. The effect of frequency on the changes of waveform 12 kV voltage. (a) 40 kHz, (b) 50 kHz, (c) 60 kHz, and (d) 70 kHz. (e) plasma power vs. frequency. The waveform was measured by changing the frequency by every 10 kHz from 40 to 70 kHz.

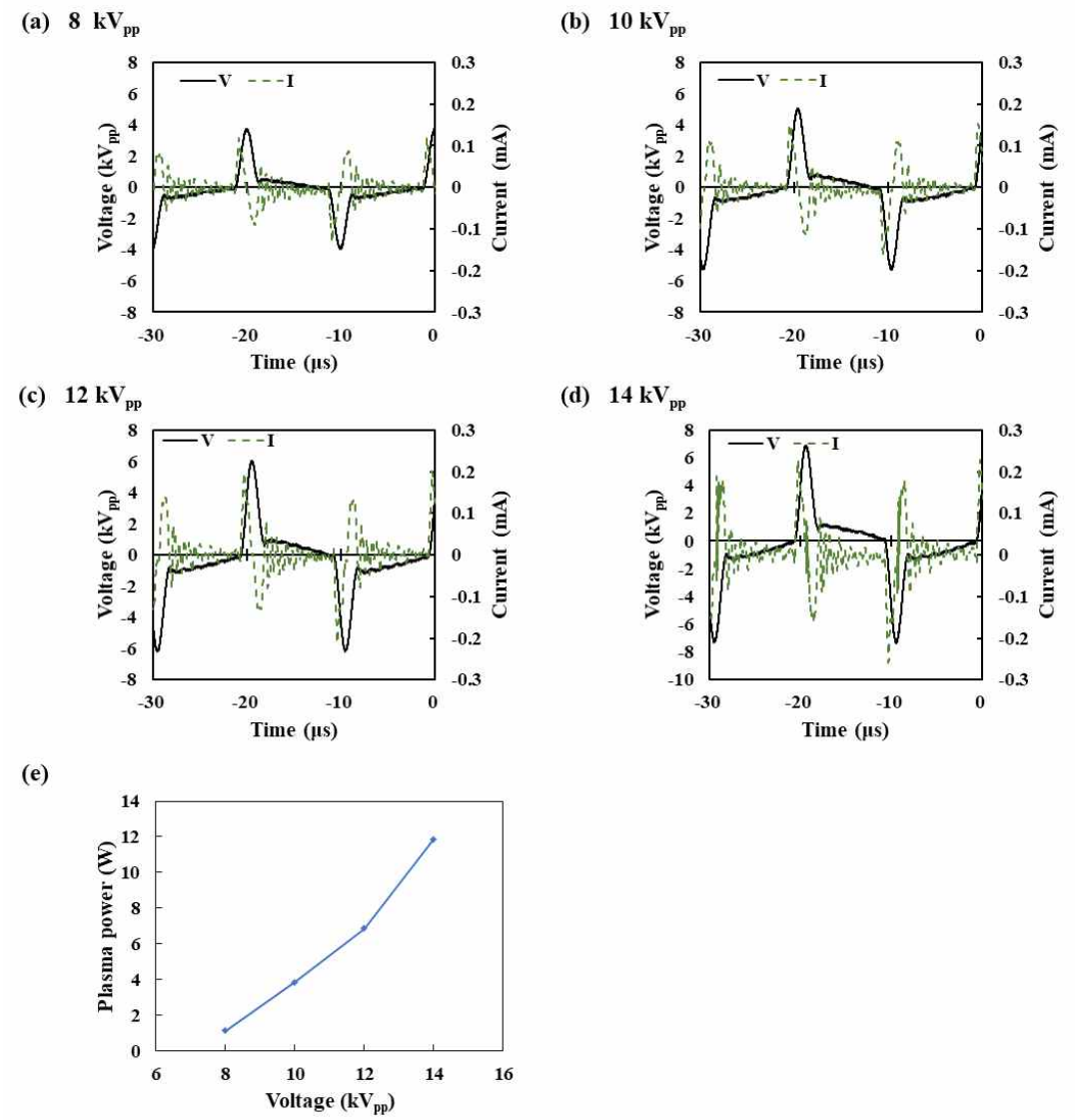

Figure 4.11. The effect of voltages on the changes waveform at 50 kHz frequency (a) 8 kV, (b) 10 kV, (c) 12 kV, and (d) 14 kV. (e) Plots of voltage vs. plasma power. The voltage was measured from 8 to 14 kV in every 2 kV increments.

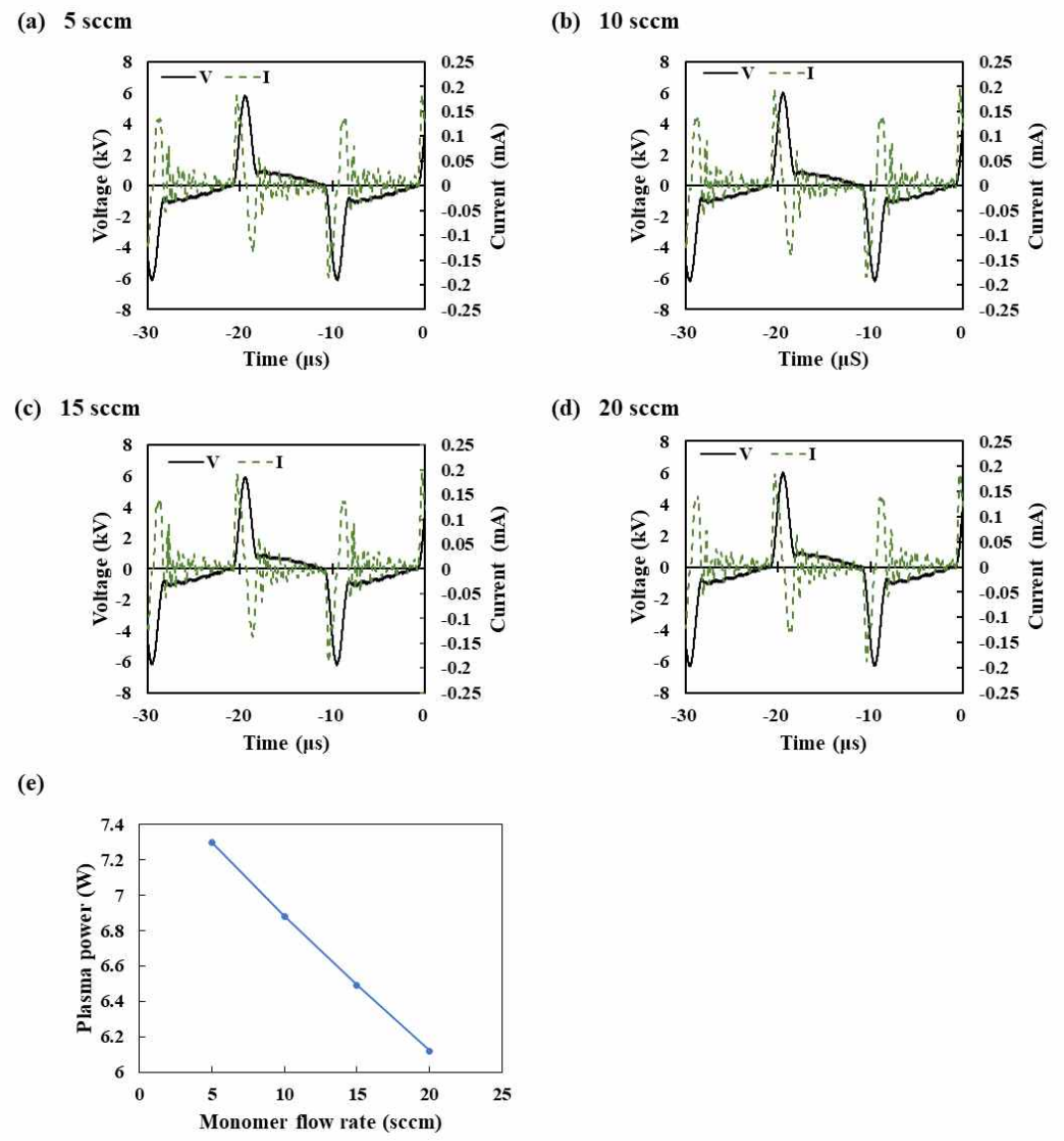

Figure 4.12. The effect of monomer flow rate on the changes of waveform at 12 kV voltage and 50 kHz frequency. (a) 5 sccm, (b) 10 sccm, (c) 15sccm, and (d) 20 sccm. (e) Plots of monomer flow rate vs. plasma power. The voltage was fixed at 12 kV and the frequency was set at 50 kHz, and the flow rate of the monomer was increased from 5 to 20 in steps of 5 sccm.

According to the previous experiment, the voltage, frequency, He flow rate, monomer flow rate, and the distance between the nozzle and the sample used for plasma -polymerization were selected as shown in Table 4.1. The contact angle was measured to confirm the hydrophilicity under the selected conditions. After surface treatment by plasma-polymerization, the contact angle of the surface of Ti disk decreased from 59° to 12°, and the hydrophilicity increased. To confirm the maintenance of hydrophilicity, it was sterilized in 70% ethanol for 5 min, dried overnight, and the contact angle was measured. The measured contact angle dried for overnight was 34° or less in the samples polymerized for 4 min or more, and then hydrophilicity was maintained even after sterilization (Figure 4.13).

The spectrum of the plasma flame was analyzed using OES to confirm the activated nitrogen element through the plasma. There was no significant difference between He gas only and the spectrum of the gas mixed with the monomer as shown in Figure 4.14.

To investigate the change in surface roughness by plasma-polymerization sample surface was measured by AFM. The surface of the Ti disk confirmed by AFM showed smooth surface by the polymer film. The roughness of the sample after polymerization was significantly reduced compared to the control. Also, the roughness was decreased as the polymerization time increased as shown in Figure 4.15.

XPS was used to characterize the elemental composition on amine plasma-polymerized surface. Ti element and oxygen element were significantly decreased as shown in Figure 4.16. In addition, nitrogen and carbon, which were constituent elements of the amine thin film, was increased (Figure 4.16). As shown in Figure. 4.17(a), two different carbon peaks were modified at the C 1s binding energy. Pristine Ti surface XPS peak was changed from C-O-C (286.0 eV) and O-C=O (288.4 eV) to =C-N+ (286.2 eV) and −C=N+ (287.5 eV). The N 1s peak of the amine-coated Ti disk was shown in Figure. 4.16 (b). The -NH(399.8 eV), -N-H+(401.0 eV) peaks present in the control were replaced with =N-(398.2 eV), -N-(C=O)- (400.0 ev).

Table 4.1. Conditions of plasma discharge

Selected condition	Voltage (kV_{pp})	Frequency (kHz)	He flow rate (slm)	Monomer flow rate (sccm)	Distance of between nozzle and sample (mm)
	12	50z	1	10	2

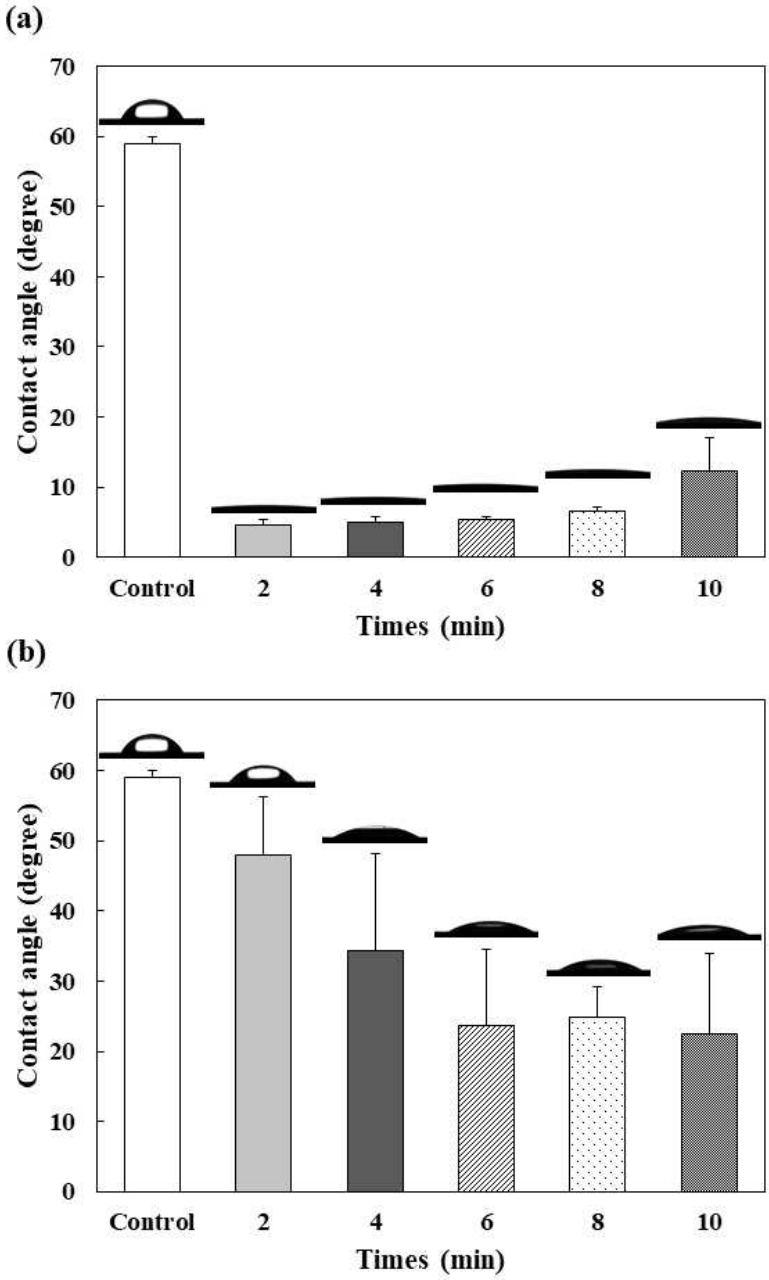

Figure 4.13. Contact angles measurement. (a) before sterilization, (b) after sterilization.

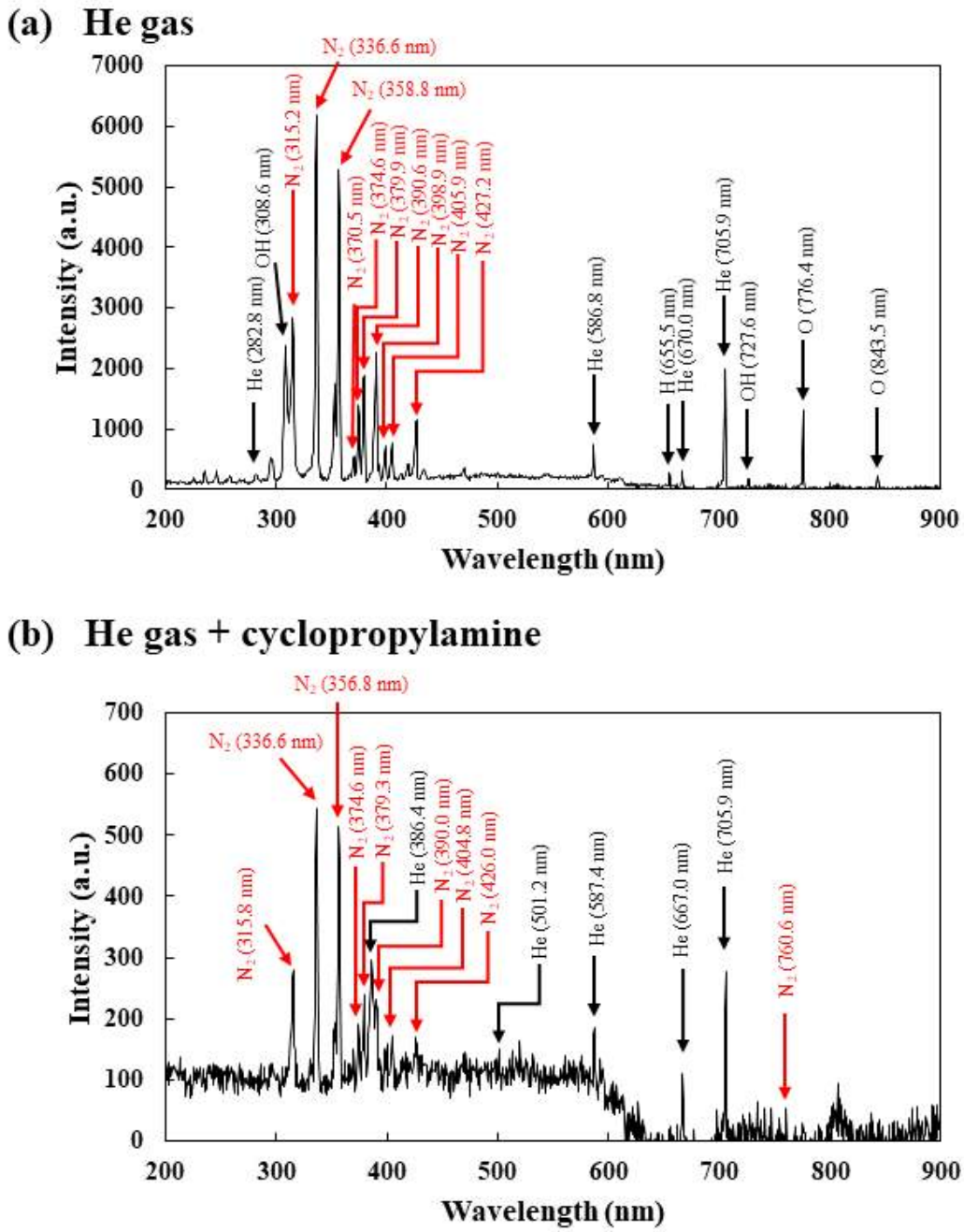

Figure 4.14. Optical emission spectroscopy of plasma flame. (a) He gas plasma, (b) amine plasma-polymerization plasma.

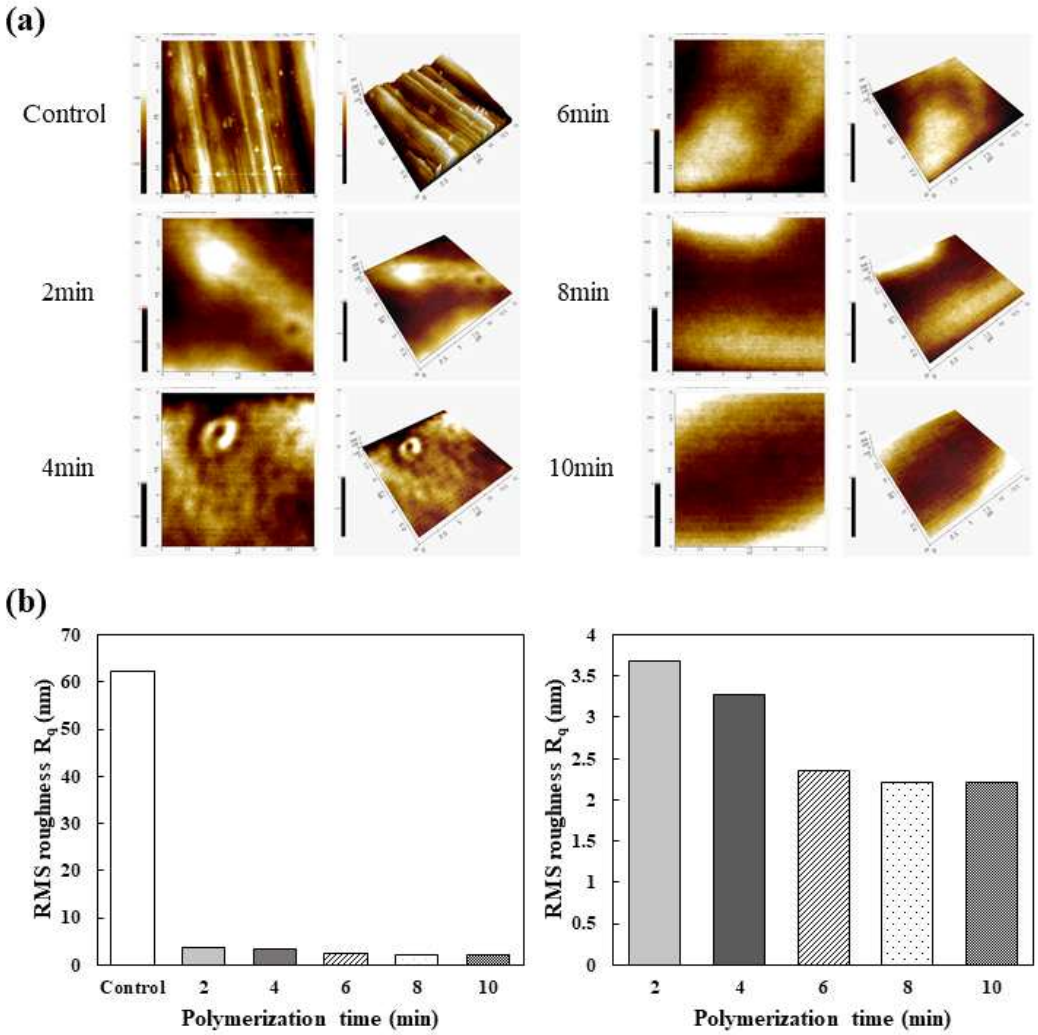

Figure 4.15. Changes of surface topologies with increased plasma-polymerization times (a) and root mean square roughness (b).

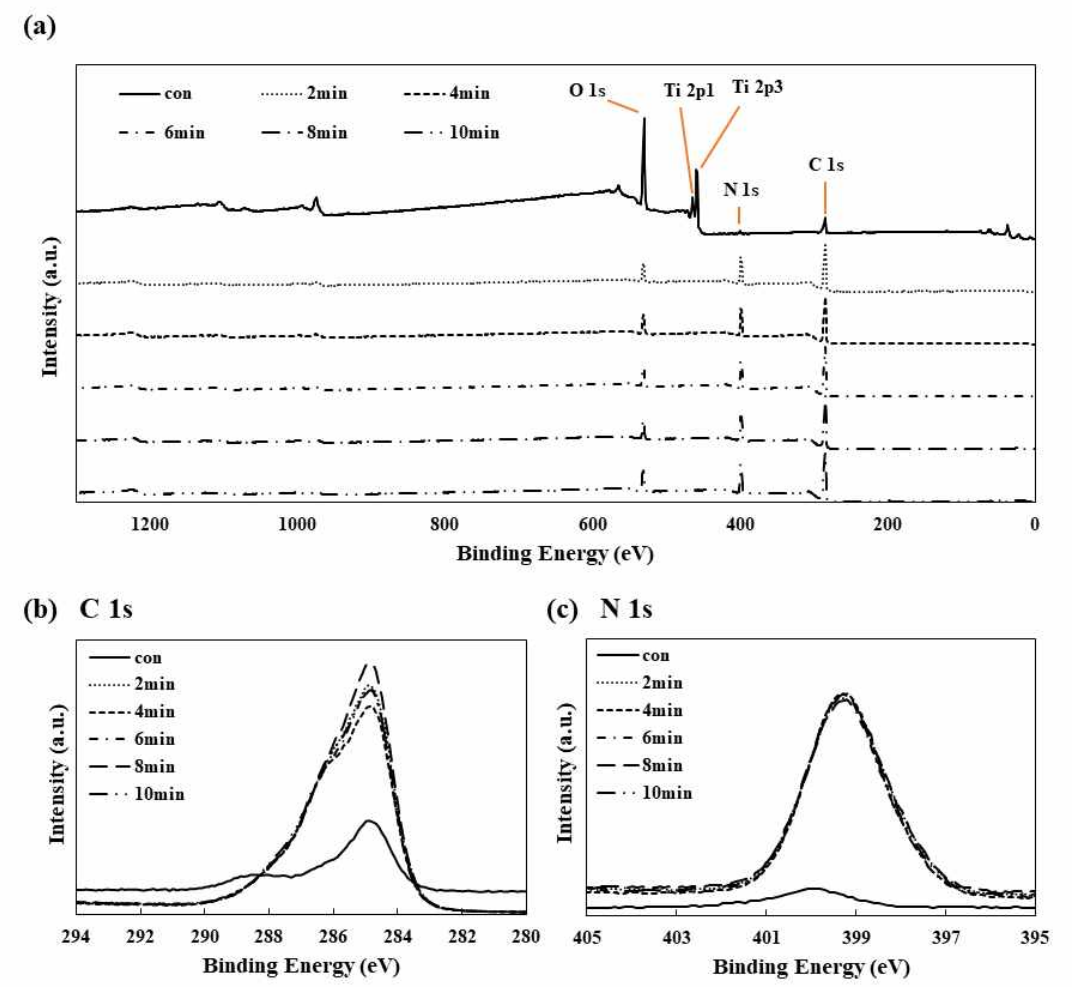

Figure 4.16. Analysis of elements on the surface using XPS, (a) XPS wide spectrum, (b) carbon element, and (c) nitrogen element.

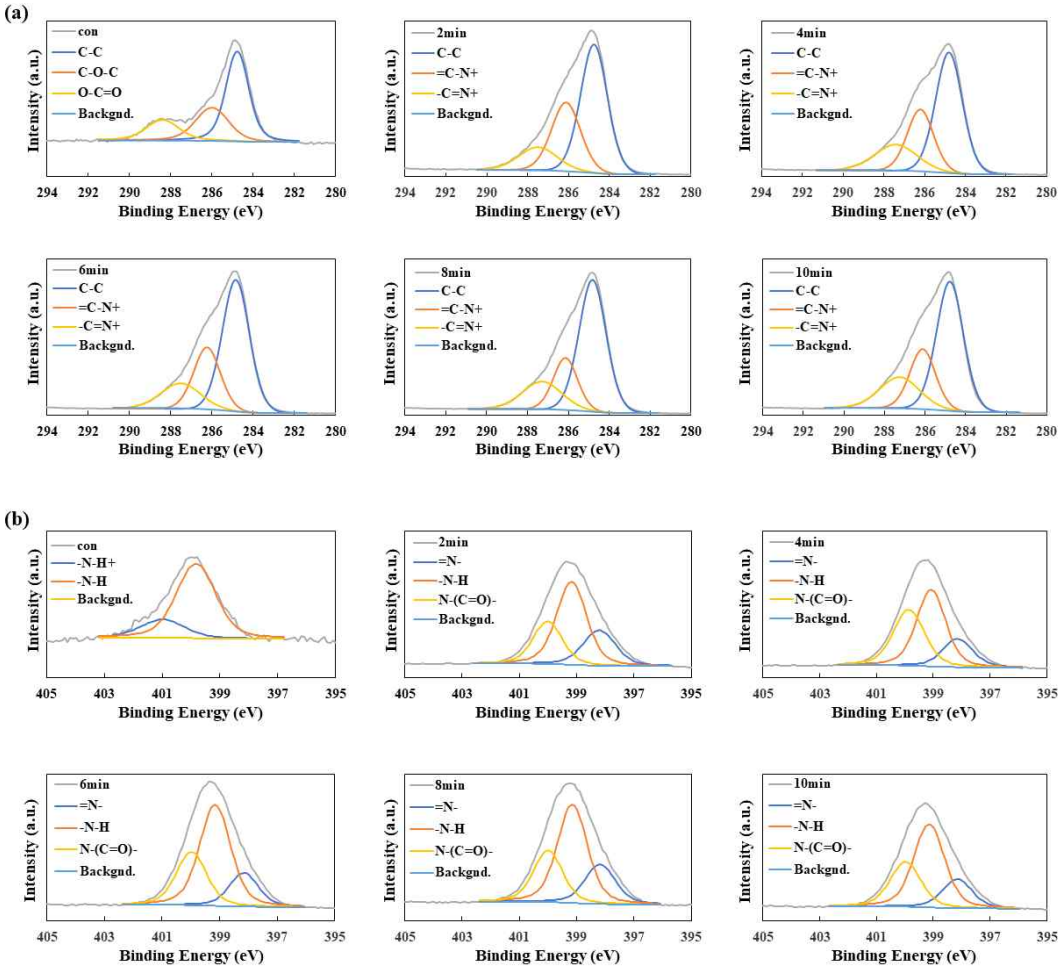

Figure 4.17. Analysis of amine plasma-polymerization surface elements using XPS. (a) C 1s. (b) N 1s.

4.4.2. Biological responses of MC3T3-E1 cells

In order to confirm initial adhesion of cells, MC3T3-E1 cells were seeded on the surface of the sample. These were fixed and fluorescently stained after 4 h. Cell morphology was stained with Rhodamine, and the initial adhesion factor was fluorescently stained with Paxillin antibody. There was no significant difference in cell shape at fluorescent staining, but green fluorescent Paxillin was stronger at the surface of plasma-polymerization compared to the untreated control. (Figure 4.18)

Cell proliferation on the amine coated surface by plasma-polymerization was compared after for 3 d incubation using WST-8 reagent. The results were statistically processed using SPSS 26. The 4 min polymerization sample on the 3 d showed a significant difference from the control, 8, and 10 min samples as shown in Figure 4.19.

The cytotoxicity of the plasma-polymerization surface was tested through Live-Dead staining. After culturing the cells on the sample surface for 24 h, the reagent was treated. As shown in Figure 4.20, cells stained with green were not significantly changed after plasma-polymerization, indicating that surface with plasma-polymerization has no intrinsic cytotoxicity against cells.

ALP, an initial differentiation factor, was examinated on 7 and 14 d to confirm the differentiation pattern of cells as shown in Figure 4.21. At 7 d, ALP was increased at 4 min, but there was no significant difference at the 14 d.

To compare calcification, samples were stained with Alizarin red reagent as shown in Figure 4.22. After 7 d of differentiation, 4, 6, and 10 min treated samples showed a decrease compared to the control, and in 14 d differentiated samples, 8 and 10 min treated samples showed decreased compared to other samples.

The results of western blot showed that ALP was higher in the 6 and 8 min amine plasma treatment surface on 7 d as shown in Figure 4.23. Furthermore, the higher ALP value was observed on 14 d in the 6, 8, and 10 min of amine plasma treatment surface. OPN was strongly expressed on 7 d at 2, 6, 8, and 10 min. Furthermore, OPN was strongly expressed strongly expressed on 14 d at control, 2 and 4 min. RUX2 showed no significant difference in all samples.

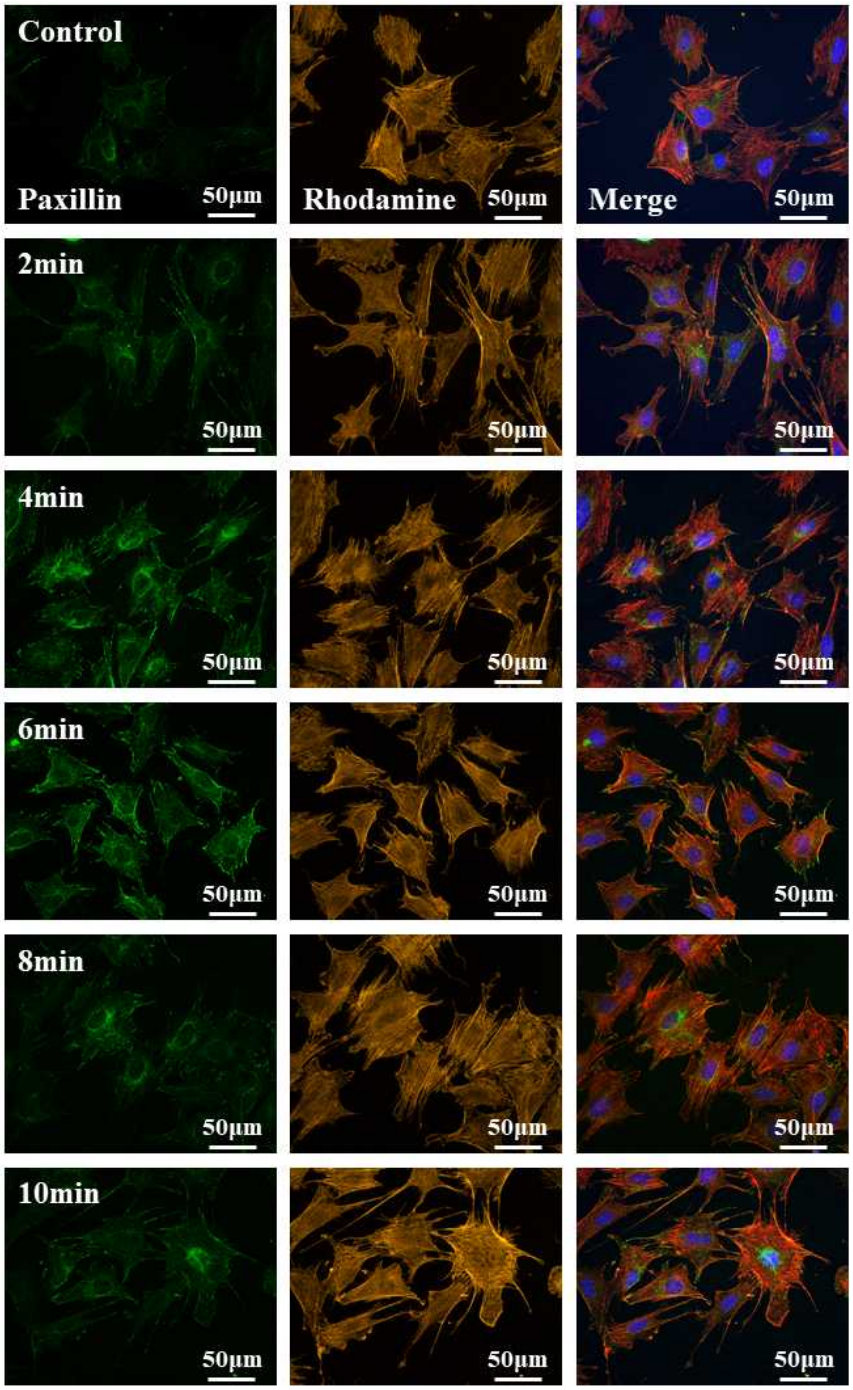

Figure 4.18. Fluorescence images of early-adherent cells (green is Paxillin; orange is Rhodamine; blue is DAPI, 4hr after seeding).

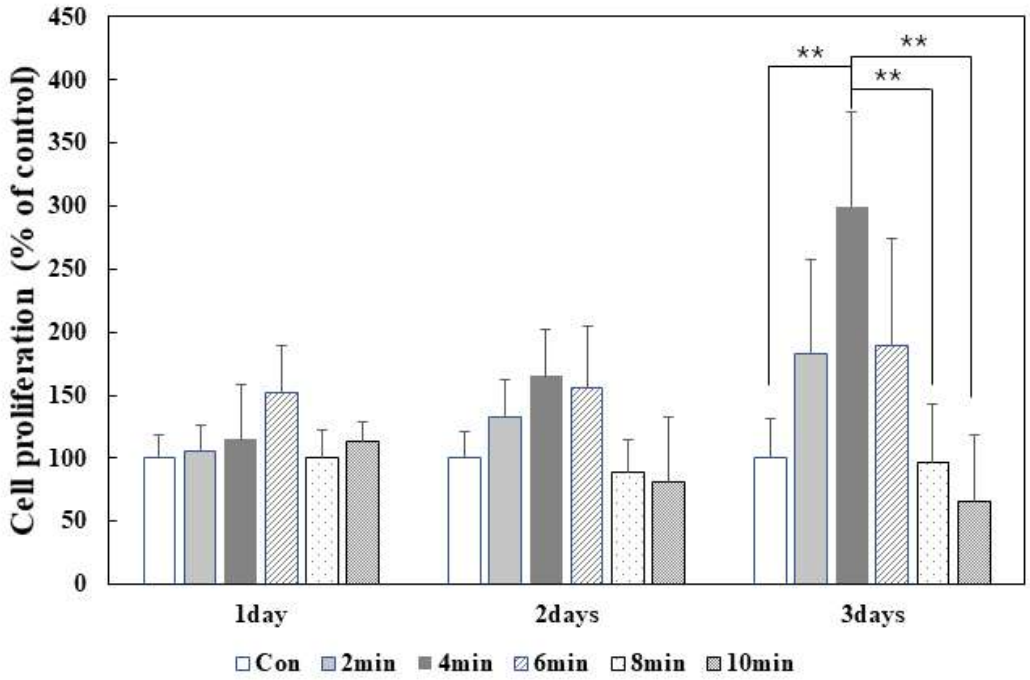

Figure 4.19. Proliferation of MC3T3-E1 cells on amine plasma-polymerized surfaces. (**p<0.01).

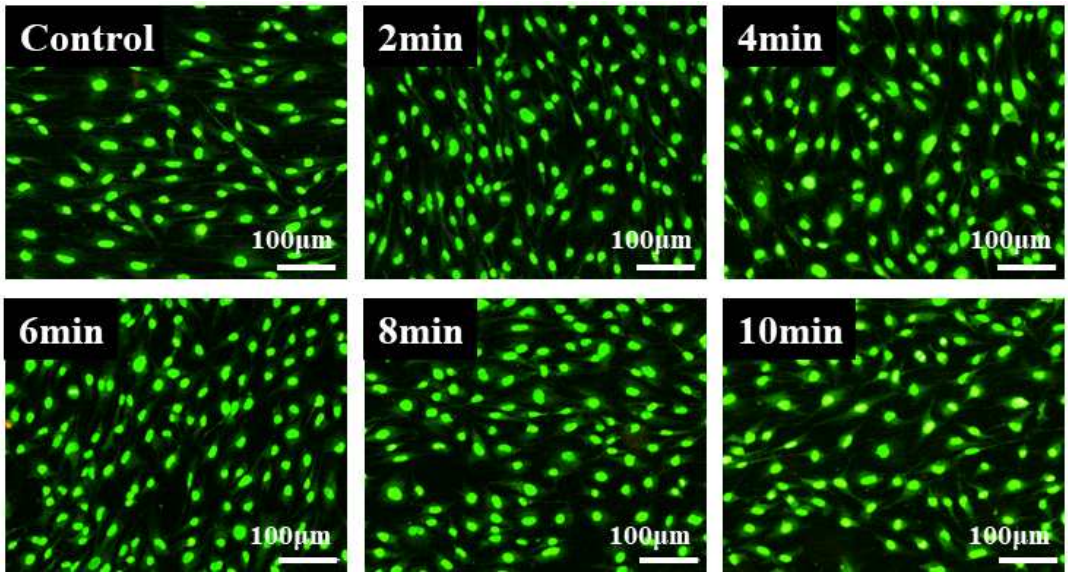

Figure 4.20. Live-dead cell staining of MC3T3-E1 cells on the amine plasma-polymerization surface. (Live cell is green and dead cell is red).

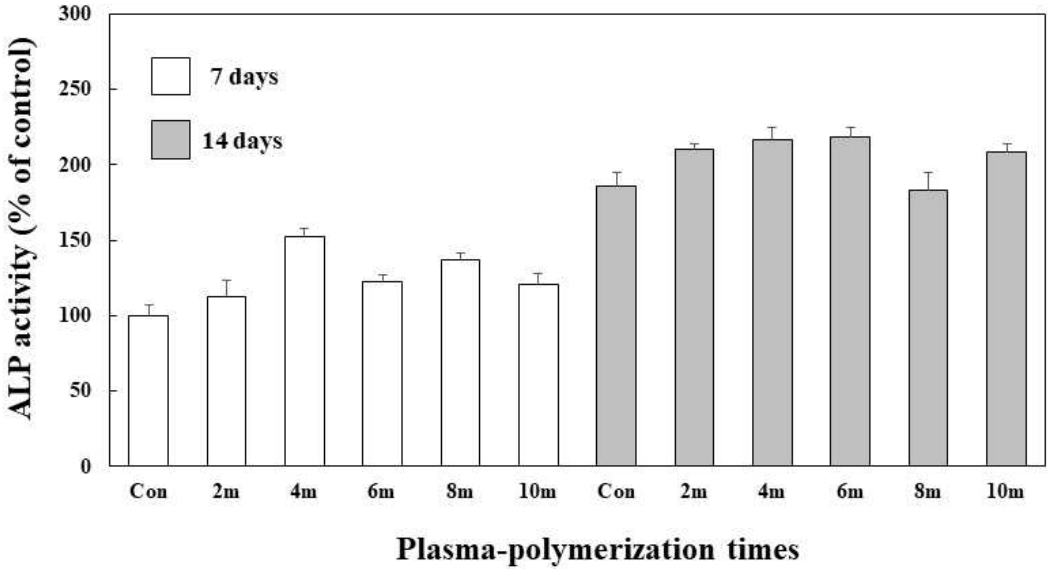

Figure 4.21. The effect of treatment time on the changes of ALP activity at 7 and 14 d.

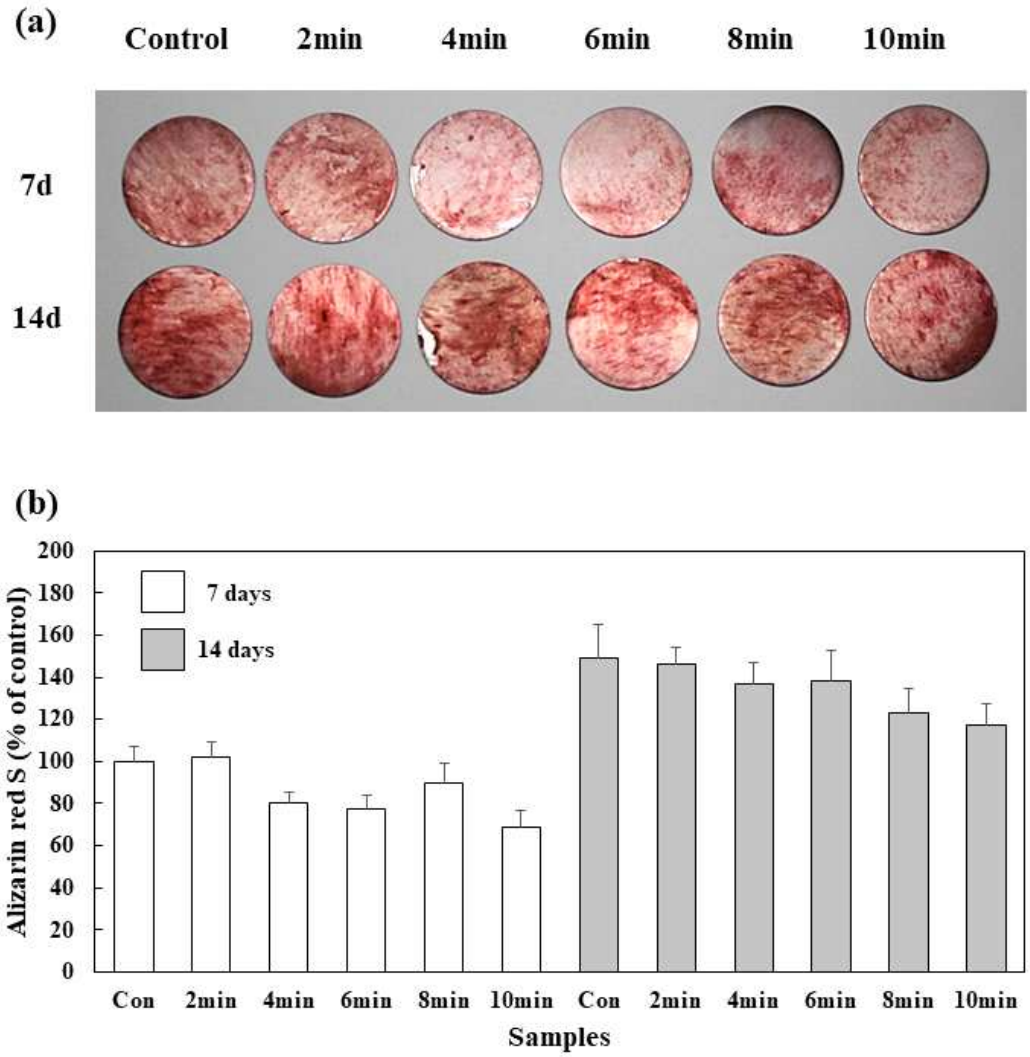

Figure 4.22. The effect of treatment time on the changes of calcium deposition. (a) Alizarin red S staining, (b) Plots of treatment time vs. Alizarin red S.

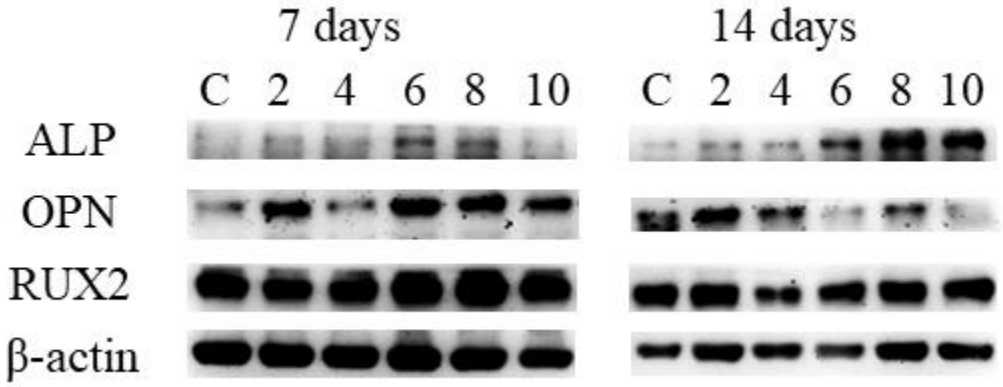

Figure 4.23. Western blot analysis of osteogenic protein expression.

4.5. Discussions

In present study, we designed and developed of atmospheric pressure DBD plasma jet to apply the amine plasma-polymerization of Ti implant surface. This plasma device was advanced form improvement of based on equipment fabricated in previous research.

Surface modification of Ti implant is very important role in osseointegration surrounding the bone tissue. Therefor, we performed the surface modification of Ti surface, and investigated the preosteoblast biological response. The contact angle was decreased as shown in Figure 4.13 (a), indicating that the hydrophilicity and biocompatibility were improved after amine plasma-polymerization. Furthermore, the sterilization procedure increase contact angle of all samples more than two times. In particular, 2 min polymerization sample showed a marked decrease in hydrophilicity and increase in the contact angle from 4.7˚ to 48˚. This result indicated that the contact angle increased due to the reduction of the amine concentration on the surface. The increase of the contact angle was interpreted through the research of D. Magisaans and coworkers. D. Magindaan *et al.* reported that a wettability gradient was formed with the concentration gradient of the applied amine functional groups by plasma-polymerization. [111, 112]. In samples treated longer than 4 min, the contact angle was maintained to 34° or less, and hydrophilicity was not changed significantly. The amine polymerization film was maintained during the sterilization process at 70% (v/v) ethanol. Furthermore, the 4 min polymerization sample showed the best cell proliferation at 3 d of culture (Figure 4.19). Cell proliferation result showed that the deposition of the CPA-based plasma-polymerization under all examined plasma exposure durations improved initial attachment and proliferation of MC3T3-E1. K. V. Chan *et al.* research show that cyclopropylamine plasma-polymerization was no clear trend of deposition time in HFF cell attachment and proliferation as a function [113].

To investigate the cytotoxicity, the toxicity of the amine plasma-treated surface was examined using the Live-Dead staining reagent. No red fluorescence was observed, indicating that toxicity of the amine plasma-treated surface was negligible. Furthermore, no decrease in green fluorescence indicated that live cells were maintained compared to control. Therefore, it was confirmed that the amine plasma-treated surface increased the

proliferation of cells with negligible toxicity against cells as shown in Figure 4.20.

To compare the differences in differentiation on the amine plasma-treated surface, A various technique such as ALP activity, Alizarin red S staining, and western blot were used. An initial differentiation factor, ALP activity on the amine plasma-treated Ti sample tended to slightly increase at 7 and 14 d compared to the untreated control sample. On 7 d, 4 min sample showed the higher APL activity was observed compared to the other plasma-treated samples. On 14 d, the 8 min sample showed a lower value than other plasma-treated samples, and showed negligible difference compared to control as shown in Figure 4.21. Alizarin red staining showed that the plasma-treated Ti samples had lower values compared to the untreated control on 7 and 14 d. These results indicated that calcium production of plasma-treated Ti sample was lower than that of the control as shown in Figure 4.22. Western blot results showed that ALP on 7 d was higher in the 6 and 8 min amine plasma treatment sample as shown in Figure 4.23. At 14 d, ALP was higher in 6, 8, and 10 min at amine plasma treatment sample. M. F. Griffin *et al.* and X. Liu *et al.* research show that amine plasma-polymerization surface was much more expressed than carboxyl, methyl, hydroxyl chemical groups in ALP and Osteocalcin [114, 115]. The difference in these results was depending on various variables such as the type of monomer, the type of the base material, and the measurement time. F. Mwale *et al.* also reported that osteogenic differentiation factors such as ALP and RUX2 were decreased even in amine plasma treated sample [116].

OPN expressed in the differentiation stage was strongly expressed at 2, 6, 8, and 10 min on 7 d and at con, 2 and 4 min on 14 d. The OPN expression increased in the osteogenic phase, which represents adhesion of osteocytes to the matrix and proliferation/differentiation of osteocytes [117]. The above result could be considered that the change into osteocytes does not occur well in the process of cell differentiation. This phenomenon was considered to be caused by subtle differences in surface chemistry, and further studies are required.

4.6. Conclusions

In this study, the amine group was deposited on Ti disk surface by APPJ, and the following results were concluded.

1. The APPJ device for amine plasma-polymerization was well designed and optimized.
2. Ti surface by plasma-polymerization was increased of hydrophilicity and decreased of surface roughness.
3. The amine polymeric thin film deposited by APPJ was maintained after washing with 70% ethanol and cell culture medium.
4. The amino-functionalized Ti surface has been enhanced proliferation of MC3T3-E1 cells.
5. The cell differentiation on the Ti surface by amine plasma-polymerization was slightly enhanced compared to those of the untreated Ti surface.

From these results, amine plasma-polymerization by APPJ is a promising candidate for dental Ti implant clinical applications.

5. Part Ⅲ: Feasibility of CAP on the erradication of *P. gingivalis* bioflim for periodontitis treatment

5.1. Introduction

Periodontitis, a serious infection of the gums, may cause frequent tooth loss and a variety of disease problems in other organs. [118, 119]. This can lead to inflammation of the gums or destruction of bones, ultimately resulting in serious damage to dental health. In particular, due to pathogens in the gums and/or oral cavity, a sticky biofilm is formed on the tooth surface and finally a hard biofilm is formed [119]. The biofilm on the teeth that causes periodontitis is difficult to remove with regular brushing and/or flossing. To remove the biofilm on the gums, a mechanical cleaning procedure is now a common treatment option. However, mechanical cleaning procedures are usually time-consuming and require local anesthesia [119, 120]. Otherwise, systemic chemotherapy with antibiotics has delivery problems. In other words, antibacterial agents are difficult to penetrate deep into the gingiva at the treatment site and cause drug resistance problems to the treated antibiotic [120]. Nakajima *et al.* reported the development of an ion-gel of a deep eutectic antimicrobial agent for improved penetration into deep tissues and therapeutic efficacy [120]. They reported that the ion gel effectively penetrated the gingival/gingival sulcus within a short period of time and that the delivered dose was adequate to inactivate *P. gingivalis*. Lu *et al.* reported that systemic antibiotics using amoxicillin and metronidazole were helpful in the treatment of periodontitis through scalping/root planning [121]. They claimed that the microbial benefits were lost after six months of treatment. Polymeric biomaterials for antibacterial and antifouling dental applications have also been investigated for sustained drug release to inhibit biofilm formation [122]. However, these materials must be approved for an extended period of biocompatibility and essential biomaterial features for longevity of the material in the oral cavity.

Cold atmospheric plasma (CAP) has been extensively investigated in the field of antibacterial and anticancer therapy over the past few decades [123-125]. Intrinsic properties of CAP in biological systems are the generation of reactive oxygen species

(ROS) and/or reactive nitrogen species (RNS) and antibacterial/anticancer activity of ROS/RNS [123-125]. While adequate levels of ROS/RNS in biological systems are required to maintain cell proliferation and differentiation, excessive levels of ROS/RNS in biological systems usually induce oxidative stress on target cells or bacteria, inhibiting their growth [126-128]. In particular, CAP can be considered to be an ideal device for the treatment of local diseases such as periodontitis as side effects on surrounding cells/tissues are minimized compared to systemic chemotherapy [128, 129]. These clinical properties of CAP make it a safe treatment option for local disease.

In this study, the ROS generation ability of the CAP device and the antibacterial activity against an *in vitro* periodontitis model were investigated. For the *in vitro* periodontitis model, *P. gingivalis* was grown on titanium (Ti) disk to create a bacterial biofilm, and then the biofilm was used to evaluate the biological capacity of the CAP instrument. In addition, the ROS-generating ability of CAP was evaluated *in vitro* and then their antibacterial activity was compared.

5.2. Materials

Sand-blasted, large grit, acid etched (SLA)-treated Ti disks were used as a model of dental implant. SLA-treated Ti disks have dimension 5 mm diameter and 3 mm height in dimension.

Brain heart infusion (BHI) broth, yeast extract, bacto agar, resazurin, cysteine HCl, hemin and vitamin K_1 was purchased from Sigma-Aldrich Chem. Co., (St. Louis, MO, USA). Singlet oxygen sensor green (SOSG) was purchased from Invitrogen (Thermo Fisher Scientific Co. Ltd., Eugene, Oregon, USA). The live/dead cell staining kit was purchased from Biovision (Milpitas, CA, USA). Organic solvents such as ethyl alcohol and hexamethyldisilazane were as HPLC grade.

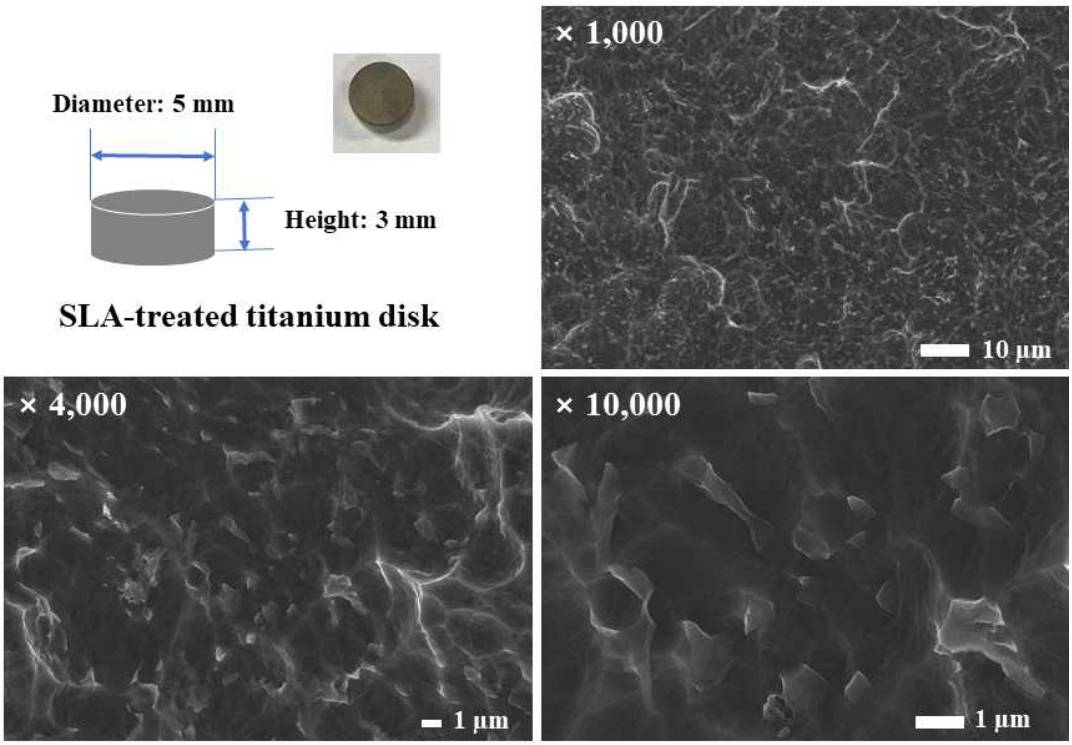

Figure 5.1. Surface morphologies of SLA treated Ti disks.

5.3. Methods

5.3.1. CAP setup

To treat bacteria on Ti disks, FEDBD-G (Power&plasma, Incheon, Korea) was used as shown in Figure 5.2. They consist of a gas supply system, a plasma jet, a mass flow controller (MFC) and a high voltage AC. power supply. Under atmospheric conditions, a stable discharge was produced at a 9 kHz radio frequency in this instrument, and the discharge power was adjusted to 6.39 W/11.30 kV. For plasma treatment, 2 L/min of Ar gas was supplied from the gas supply system, and a gas with a purity of 99.9% or higher was used in this experiment. A Ti disk with bacteria was placed on the XY stage as shown in Figure 5.2. The distance between the plasma jet nozzle and the top of the Ti disk was adjusted to 5 mm. Characterization of frequency and power of CAP was presented in Table 5.1.

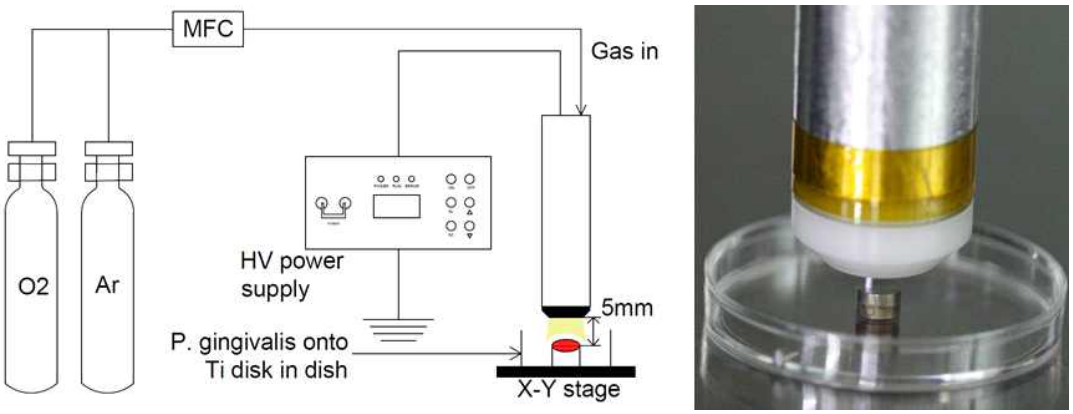

Figure 5.2. Schematic diagram and actual image for treating cold atmospheric plasma on the Ti surface with *P. gingivalis* grown.

Table 5.1. Characterization of frequency and power of CAP

Intensity-energy level ratio	Peak-Peak (kV)	Frequency (kHz)*	Plasma Power (W)
9-5	11.04	9	3.50
9-7	13.30	9	6.39
9-9	13.91	9	6.99

* Frequency was measured as 111 μs. 1/111 μs = 9.009 kHz.

5.3.2. Gas species analysis in plasma plume

To analyze the optical emission spectrum of the CAP, the optical properties of the plasma jet were measured using a fiber optic spectrum analyzer (Avantes AvaSpec-ULS2048CL-EVO-RS, spectral range 200 to 1100 nm) (Figure 3). An optical fiber (Avantes, Fiber-optic cable, FC-UV400-2) was placed at a distance of 10 mm from the plasma jet nozzle (Figure 5.3).

Figure 5.3. Gas species analyzing device. Optical emission spectrometer (left) and optical fiber (right).

5.3.3. *P. gingivalis* culture

P. gingivalis (KCOM 2796) was provided from the Korean Collection for Oral Microbiology (Gwangju, Korea). BHI growth medium for *P. gingivalis* KCOM 2796 is as follows; 1 L solution HCl containing 30 g BHI broth, 5 g yeast extract, 4.0 mL resazurin solution (0.025% (w/v) in PBS), 0.5 g cysteine HCl, hemin 1.0 mL of solution (5 mg/mL in water) and 0.2 mL of vitamin K1 (10 mg/mL in water). This solution was adjusted to pH 7.2. For the agar medium, Bacto agar (20 g) was added to the growth medium. Bacteria were cultured for 1 d in anaerobic conditions (GasPak-EZ Anaerobic Vessel System; Becton Dickinson Microbiology Systems, Cockeysville, MD, USA). The number of bacteria was assessed spectrophotometrically in BHI medium containing 1×10^6 colony forming units (CFU)/mL. A sterile Ti disk was placed in a 12-well plate and then bacteria were inoculated. They were incubated in an anaerobic environment for 3~5 d until bacterial confluence on the disk surface. Medium was changed every 48 h during incubation.

5.3.4. *P. gingivalis* CFU assay

Carefully wash *P. gingivalis* KCOM 2796 on Ti disks with sterile PBS (0.01 M, pH 7.4, Welgene) as previously described to remove plankton or loosely attached bacteria. The CAP treatment conditions were an Ar gas flow rate of 2 L/min, a voltage of 11.3 kV, and a frequency of 9 kHz for 1, 3, and 5 min. After treatment, the treated sample was placed in a 15 mL tube with 10 mL of PBS, and the remaining *P. gingivalis* KCOM 2796 on the Ti disk was separated by sonication for 5 min. Then, the obtained suspension was serially diluted on an agar plate with BHI medium, incubated in anaerobic conditions, and incubated at 37°C. for 48 h, and then the number of CFU was counted.

5.3.5. Human gingival fibroblast culture

Human gingival fibroblast (HGF-1, CRL-2014, Manassas, VA, USA) cells to be used in the experiment were purchased from ATCC. As a culture medium, dulbecco's modified eagle's medium (DMEM, 11995065, Gibco) supplemented with 10% FBS and 1% antibiotics was used, and the medium was exchanged every 2 d. For cell culture, 8×10^5 cells were seeded in 100 mm dishes and subcultured when 80% confluence was reached. 2 mL of trypsin-EDTA solution was used to detach the adherent cells and used 2 mL of DMEM growth medium for neutralize Trypsin-EDTA. Detached cells were transferred to 15 mL conical tube. Cells in a 15 mL conical tube were centrifuged using a Bechman coulter (Allegra X-15R) and the supernatant was removed. The cell pellet was resuspended in 5 mL of DMEM growth medium and an appropriate aliquot of the suspended cells was plated in 100 mm culture dishes. In this study the third passages HGF-1 cells were used. All processes were performed at 37°C in a CO_2 incubator (MCO-15AC, Sanyo Electric) maintained with a 5% CO_2 mixed gas.

5.3.6. Morphological analysis

For morphological observation of *P.gingivalis* on the Ti disks, bacteria on the Ti disks were treated as follows. Samples were immersed for 3 h into mixed solution of 2.5% (v/v) paraformaldehyde and 2.5% (v/v) glutaraldehyde. They were washed with

phosphate-buffered saline (PBS, pH 7.4) and then immersed again into 1% (w/v) of OsO_4 aqueous solution (O5055, Sigma-aldrich) for 30 min. Following this, they washed with PBS and then immersed into ethyl alcohol/water mixtures for dehydrated. For dehydration process, samples were immersed into these solutions for 5 min each ethyl alcohol/water mixtures with 70, 90, 95, and 100% (v/v), respectively. Dehydrated samples were immersed into hexamethyldisilazane solution for 10 min and then dried in room temperature. Samples were observed with field-emission scanning electron microscope at 15 kV (FE-SEM, S-4800, Hitachi Instruments Ltd., Tokyo, Japan).

5.3.7. ROS generation in PBS

ROS generation by CAP treatment in aqueous solution was monitored with a reagent singlet oxygen sensor green (SOSG, S36002, Thermo Fisher Scientific Co. Ltd., Eugene, Oregon, USA). SOSG stock solution was prepared by dissolving it into methyl alcohol (5 mM). Plasma jets under various conditions were exposed to 1 mL PBS using CAP equipment. To this solution, 1 μL SOSG stock solution was added and then measured fluorescence intensity at 400 nm of excitation wavelength and 525 nm of emission wavelength using fluorescence spectrophotometer (RF-5301PC, Shimadzu Co., Kyoto, Japan). This procedure was carried out under dark conditions. ROS values are average ± S.D. (standard deviation) from individual four measurements.

5.3.8. Live and dead cell Staining

For live/dead staining of bacteria, staining solution was prepared as follows: 1 μL live dye (1 mM) and 1 μL dead dye solution (1 mg/mL propidium iodide) (PI) was added to 1 ml staining buffer. To observe the viability of bacteria, bacteria on the surface of Ti disks was treated with CAP equipment as described above. Then, bacteria on the Ti disks were briefly washed with PBS and then incubated for 10 min with 1 mL of the live/dead cell staining solution at 37°C. Following this, bacteria on the Ti disks were observed with a confocal laser scanning microscope under dark conditions (Zeiss LSM 800 confocal laser scanning microscope, Carl Zeiss Microscopy, NY, USA).

5.4. Results

5.4.1. Gas species analysis in plasma plume

The OES of the plasma jet plume measured in the CAP equipment was measured. UV range (200 nm to 400 nm) and visible light range (690 nm to 950 nm) as shown in Figure 5.4.

5.4.2. *P. gingivalis* biofilm formation

P. gingivalis was grown on Ti disk surface under anaerobic conditions. As shown in Figure 5.5(a), it was confirmed that *P. gingivalis* was overlapped on the surface of the Ti disk in the FE-SEM image. Then it formed a biofilm-like shape. No bacteria appeared on Ti disk without *P. gingivalis* (Figure 5.5(b)). Otherwise, *P. gingivalis* on Ti disks was well-visualized stained with live dyes as shown in Figure 5.5(c).

5.4.3. Generation of ROS by CAP

Figure 5.6 shows ROS generation in PBS using CAP processing to test the ROS generating ability of CAP devices. As shown in Figure 5.6(a), ROS generation according to treatment time in aqueous solution is shown, which indicates that the ROS level gradually increases with treatment time. Also, ROS level gradually increased according to the energy level as shown in Figure 5.6(b). These results indicate that the CAP device efficiently generates ROS in aqueous solution.

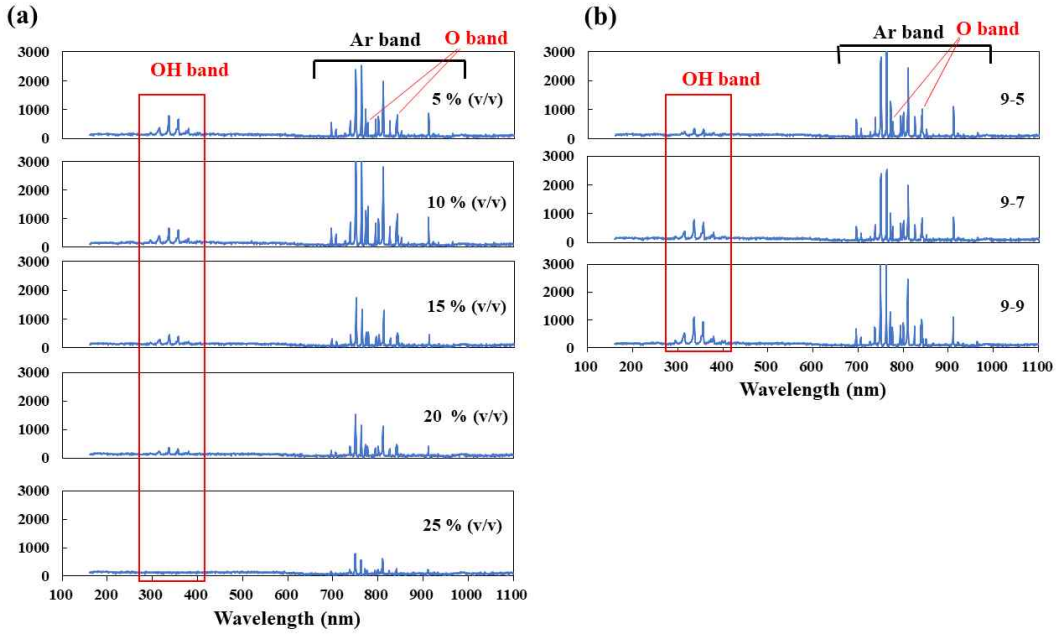

Figure 5.4. Optical emission spectroscopy spectra of the CAP pillars. (a) Effect of oxygen supply. (b) Effect of energy level.

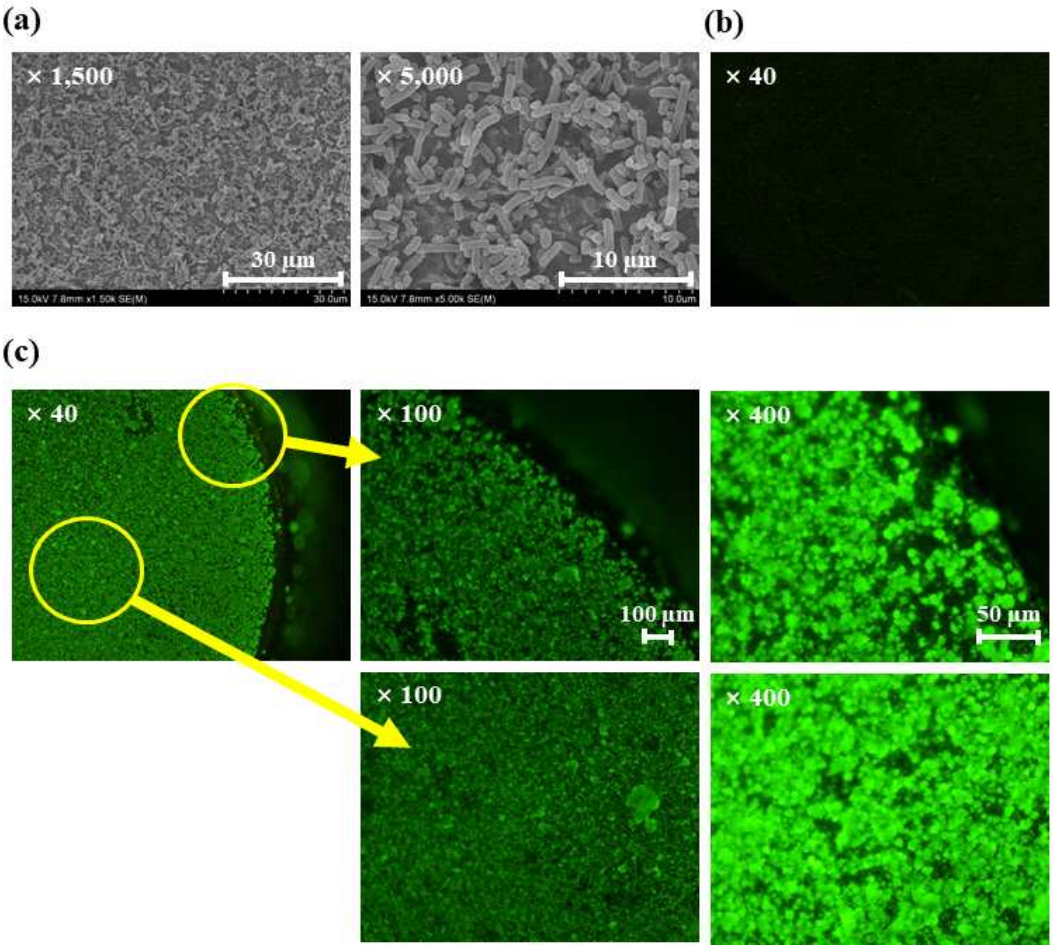

Figure 5.5. Morphological observations of biofilm formation on the surface of Ti disks. (a) FE-SEM image. (b) Uninoculated Ti surface. (c) Fluorescence image of *P. gingivalis* on Ti disks surface.

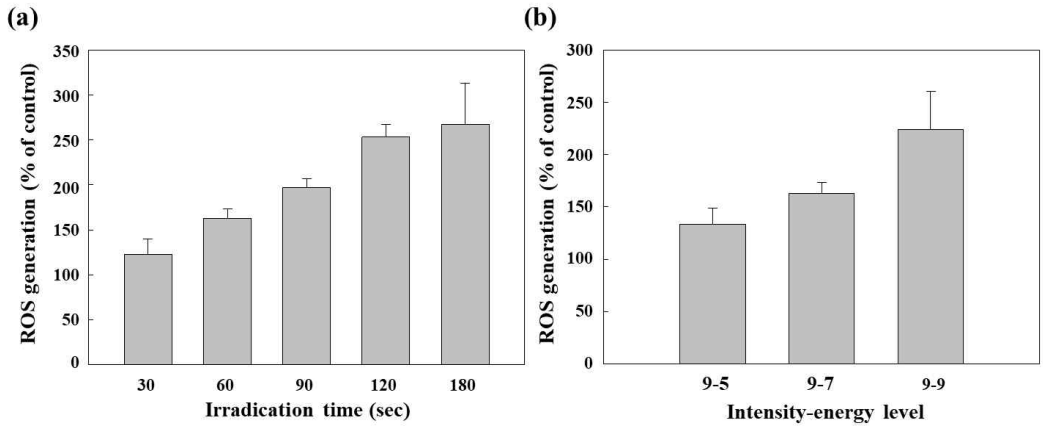

Figure 5.6. ROS generation in PBS (0.01 M, pH 7.4) by CAP treatment. (a) Effect of treatment time (intensity, 9, energy level, 7). (b) Effect of energy level (treatment time was 60 sec). Relative ROS levels were measured with SOSG reagents.

5.4.4. Antibacterial activity of CAP

Figure 5.7 shows CFU of *P. gingivalis* to evaluate the biofilm eradication potential of CAP devices. As shown in Figure 5.7(a), the number of CFU of *P. gingivalis* gradually decreased according to CAP treatment time and energy level. Figures 5.7(b) and (c) show the estimated number of CFU as a function of treatment time and energy level, respectively. The experiment was independently conducted 4 times and presented by statistical analysis.

5.4.5. Live and dead cell activity of *P. gingivalis*

In addition, to observe live and dead bacteria, viable and/or stained *P.gingivalis* of Ti discs were stained with green dye for live bacteria and red dye for dead bacteria. As shown in Figure 5.8, live bacteria were observed with green dye and dead bacteria were observed with red dye. As the treatment time increased, the number of dead bacteria in red increased relative to the treatment time, whereas the control group or shorter treatment time showed a higher degree of surviving bacteria. These results suggest that the CAP device has the potential to eradicate *P. gingivalis* biofilms from Ti disks. Furthermore, these results indicate that the CAP device could be an effective means to eradicate bacterial biofilms on the implant surface.

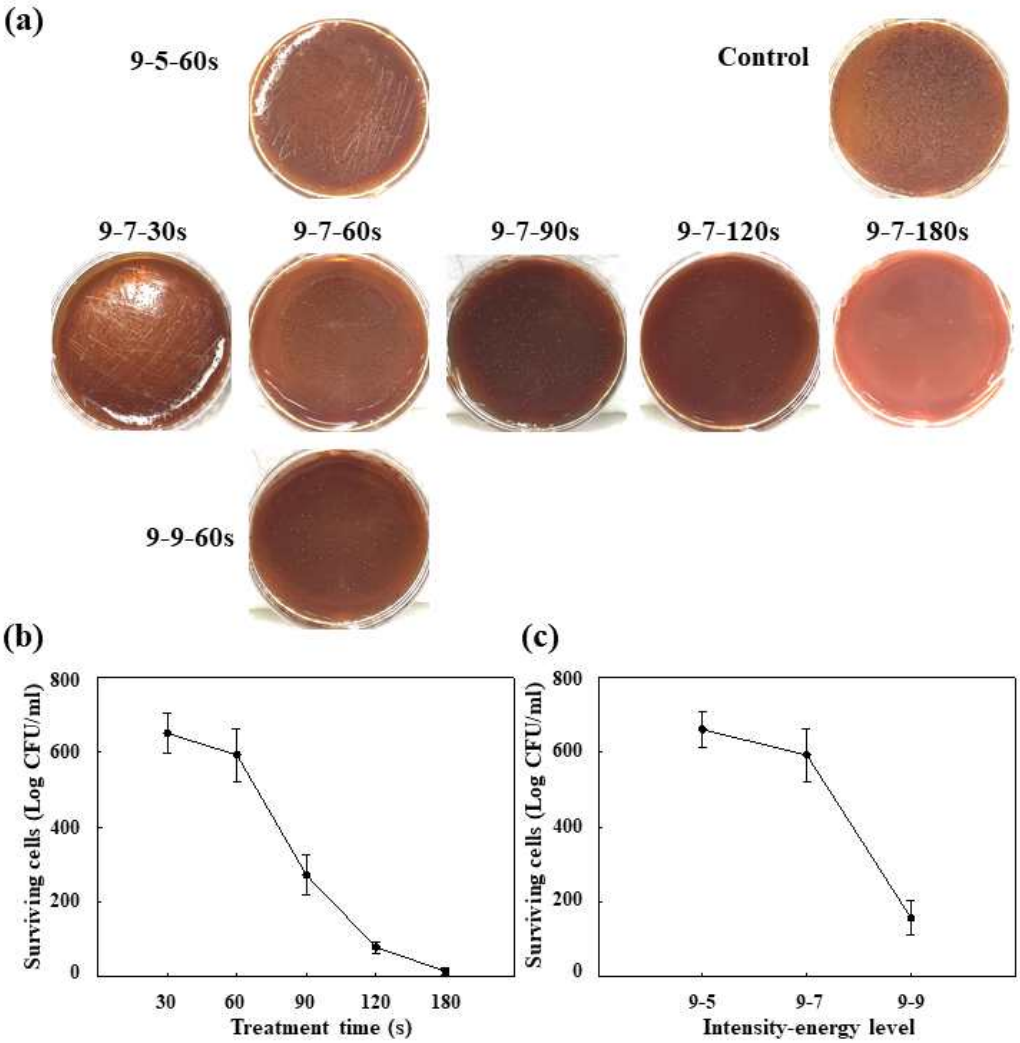

Figure 5.7. CFU analysis of *P. gingivalis*. (a) Images of surviving bacteria after CAP treatment. (b) Effect of treatment time on viability of *P. gingivalis* (9-7 in Table 5.1). (c) Effect of energy on viability of *P. gingivalis* (treatment time: 60 sec).

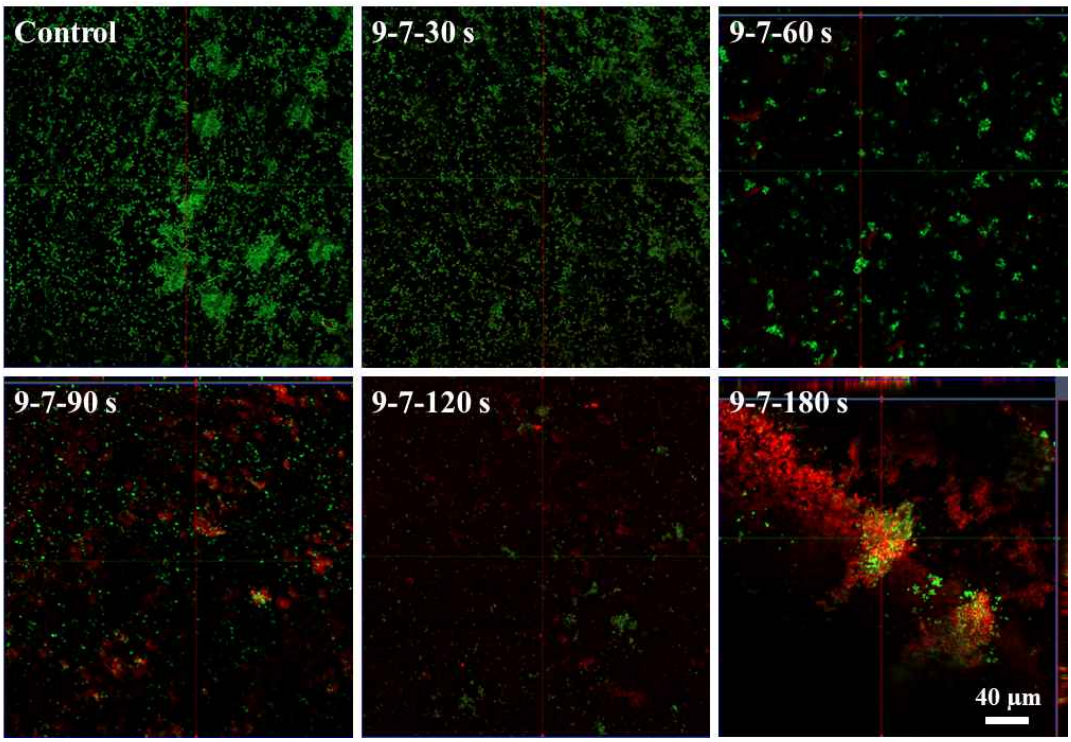

Figure 5.8. Effect of CAP device treatment time on *P. gingivalis* survival rate of Ti disk. *P. gingivalis* on Ti disk was treated with the CAP device and then stained with *P. gingivalis* live and dead cell dyes. Green and red represent live and dead bacteria, respectively.

5.4.6. Viability of HGF-1 cells after CAP treatment

The effect of the CAP device on the viability of HGF-1. This experiment was intended to study the deleterious effects of CAP devices on the gingiva. As shown in Figure 5.9(a) and (b), the viability of HGF-1 gradually decreased according to the treatment time and energy level. In particular, the viability of HGF-1 was significantly inhibited at 120 sec of CAP treatment. In addition, higher energy levels induced progressive inhibition of HGF-1. The inhibitory effect of the CAP on *P. gingivalis* was due to the generation of ROS in aqueous solution by CAP treatment as shown in Figure 5.9(c) and (d). The intracellular ROS level gradually increased with the treatment time and energy level. Although plasma irradiation conditions of 9-9 resulted in higher ROS levels and increased bactericidal effect, the viability of HGF-1 was also lower than that of other protocols. Furthermore, these results indicate that the CAP device generates ROS in aqueous solution in biological systems and affects the survival of normal cells in the gingiva. In addition, CAP treatment can affect the viability of normal cells by raising the temperature of the aqueous solution. Furthermore, these results indicate that an appropriate CAP treatment time is important for eradicating *P.gingivalis* biofilms on Ti implant surfaces, although longer CAP treatment times are more effective in eradicating *P. gingivalis* biofilms from Ti disk.

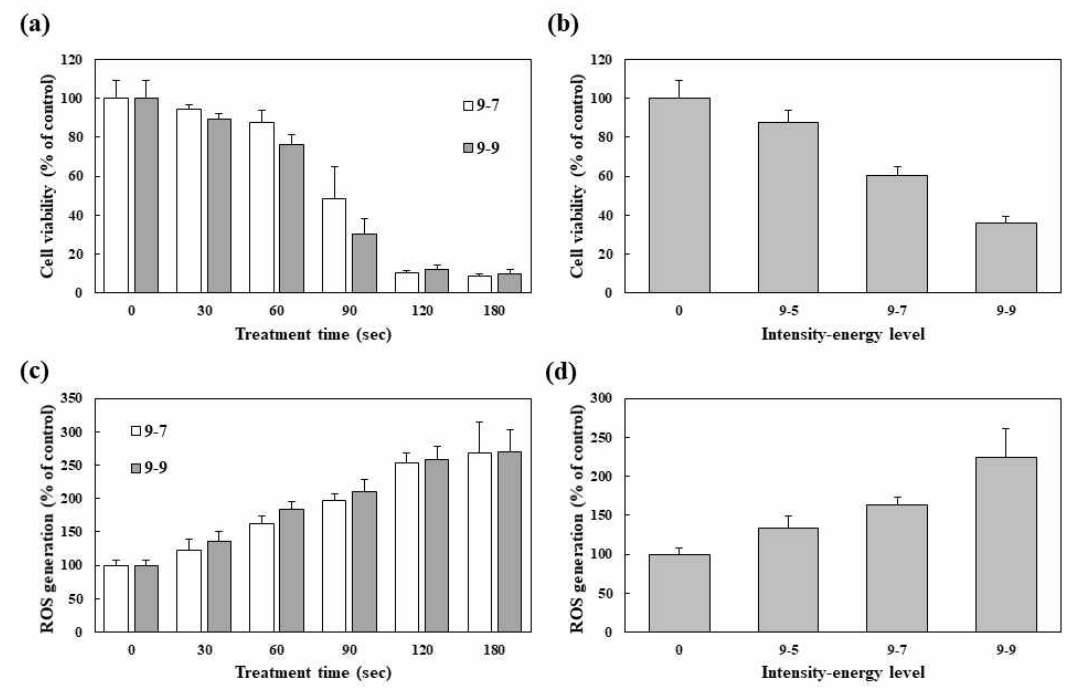

Figure 5.9. Viability and intracellular ROS levels of HGF-1 after CAP treatment. Effect of treatment time (a) and energy level (b) on viability of HGF-1. Effect of treatment time (c) and energy level (d) on intracellular ROS levels in HGF-1.

5.5. Discussions

Gargles and mouthwashes using antibiotics such as povidone iodine and cetylpyridinium chloride are difficult to eradicate biofilms [130, 131]. The use of mouthwash antibiotics has a problem with drug resistance [131]. In particular, it is difficult for antibiotics to be delivered to the biofilm of teeth or implants through mouthwash. For this reason, mechanical removal is still considered a suitable candidate for periodontal disease [132]. However, mechanical disruption of biofilms can lead to immunological changes in patients with periodontitis [133]. Furthermore, mechanical disruption of biofilms is associated with remaining problems of biofilm dysbiosis and host inflammation in some patients [133]. Otherwise, ultrasound equipment for periodontal disease also has a problem with a risk of recurrence [134]. The ROS produced by CAP treatment has a bactericidal effect and can be used to remove the biofilm formed by periodontitis. Because CAP treatment is limited to within 100 μm from the biological surface, CAP treatment is mainly limited to epidermal diseases or bacterial biofilm diseases [135]. Additionally, the lifetime of ROS generated by CAP treatment is generally very short in biological systems [136]. CAP treatment is an ideal candidate for eradicating periodontal biofilm. Our group previously reported that the CAP instrument efficiently inhibits the growth of oral squamous cancer cells by overproduction of ROS in vitro [137]. However, there have been few reports on the effects of ROS generation and periodontitis biofilm eradication by the CAP device [138]. Abnormal levels of ROS can be used to eradicate bacteria and/or cancer cells [138, 139]. For example, Thakur *et al*. reviewed that ROS produced by nanoceria has excellent antibacterial activity [139]. Also, Jean *et al*. reported that ROS-generating chemicals such as piperlongumine induce oxidative stress in epithelial cancer [140]. In their report, piperlongumine, excessively produced in cancer cells, causes abnormal ROS levels to induce apoptosis in cancer cells. In particular, Bekeschus reviewed the use of plasma technology for treatment through inactivation of pathogens [141]. In addition, CAP treatment is known to effectively eliminate antibiotic-resistant *Staphylococcus aureus* by RAW 264.7 cells by increasing intracellular ROS/RNS levels [142]. Because CAP equipment is suitable for surface or near-surface treatment of biological systems

and biomaterials, the CAP equipment for *P. gingivalis* biofilm eradication on Ti disk surface was studied. Our group previously reported that atmospheric pressure plasma jets (APPJ) could be used to efficiently kill *Staphylococcus aureus* [143]. In addition, APPJ induces rupture of bacterial cell morphology and then inhibits growth. Kim *et al.* reported that cold atmospheric microwave plasma is effective in eradicating planktonic bacteria and biofilm formation in *P. aeruginosa* [144]. Our results showed that *P. gingivalis* biofilms could be eradicated by treatment with the CAP device as shown in Figures 5.7 and 5.8. These results are related to ROS generation by the CAP device, as shown in Figure 5.6. A concentrated aqueous solution of ROS produced by plasma is known. It is effective in inhibiting microbial infection [145, 146]. In our results, normal cells and/or tissues of the gingiva may be affected by ROS generation from the CAP device. That is, ROS formation progressively increased with treatment time and energy level of the CAP device, which induced low viability of HGF-1 *in vitro*. However, other scientists have reported that long-term exposure to plasma activated water does not cause side effects. In other words, there were no changes in the organs and tissues of mice in histopathological examination in which plasma activated water was ingested for 90 d [147]. In our study, we investigated CAP in the presence of medium on HGF-1 because normal cells are usually surrounded by extracellular matrix and are not directly exposed to plasma irradiation. In any case, an appropriate processing time and energy level should be determined to maximize the eradication efficiency of bacterial biofilms and to minimize deleterious effects on normal cells.

5.6. Conclusions

The CAP device was designed to eradicate biofilm formation by *P. gingivalis* for application in the treatment of periodontitis. True power of plasma jet plume from the CAP device gradually increased with increasing intensity/energy level ratio. The OES of the plasma jet plume in the CAP instrument showed that the peaks of Ar^+, OH and O^- ions were observed in the UV range (200 nm to 400 nm) and the visible light range (690 nm to 950 nm). A biofilm of *P.gingivalis* was formed on the Ti disk and the viability of *P.gingivalis* was confirmed. The generation of ROS in aqueous solution by the CAP device gradually increased with the treatment time and energy level. Increased ROS levels induced a decrease in surviving *P. gingivalis* according to treatment time and energy level. In addition, CAP treatment of *P. gingivalis* biofilms on Ti disk also induced apoptosis of bacterial cell. Longer treatment times and higher energy levels of the CAP device decreased HGF-1 viability. Appropriate treatment time and energy levels are then required to maximize the bactericidal effect while minimizing cytotoxicity to normal cells or tissues. These results suggested that CAP devices are promising candidates for eradicating biofilms with antimicrobial effects through ROS generation in CAP devices.

6. ABSTRACT (KOREAN)

의생명 응용을 위한 아민 플라즈마 중합 및 플라즈마 살균에 관한 최적공정 탐색

이창민
지도교수 : 김병훈
치의생명공학과
조선대학교 대학원

최근 플라즈마 기술은 생체 물질 표면개질, 살균, 암 치료 등 다양한 생물 의학 분야에 광범위하게 적용되었다. 본 연구에서는 생체적합성을 향상시키기 위해 의료용 HDPE 고분자 및 치과용 티타늄 임플란트 소재에 아민 플라즈마 표면개질을 수행하였다. 또한, 저온 대기압 플라즈마 제트를 이용하여 임플란트 주위염의 원인인 *P. gingivalis*를 살균하였다.

HDFE 폴리머는 골 결손 재건에서 골 대체 재료로 널리 사용되고 있다. 그러나 HDPE는 소수성을 가지고 있어 세포 접착 및 증식과 같은 생체 활성이 좋지 않다. 이에 알릴아민(AA), 시클로프로필아민(CPA), 1,2-디아미노시클로헥산(DACH) 단량체를 사용하여 HDPE 표면에 아민 플라즈마 중합을 수행하여 표면 기능화를 유도하였다.

첫 번째 연구의 목적은 표면 특성 분석을 통해 아민 플라즈마 중합 과정을 최적화한 다음 중간엽 줄기세포(MSC) 증식을 조사하였다.

플라즈마 중합의 최적화는 챔버 압력, 플라즈마 출력, 단량체 주입 노즐 직경 및 플라즈마 챔버 내 샘플 위치와 같은 공정 조건을 변화시켜 조사하였다. HDPE에서 아민 플라즈마 중합 후 FT-IR, XPS, AFM 및 접촉각을 사용하여 표면 특성을 확인하였다. 또한, HDPE 표면의 아민 농도는 Orange Ⅱ법으로 조사하였고, MSC 증식은 MTT assay로 평가하였다.

첫 번째 연구 결과는 다음과 같다.

1. FT-IR 분석 결과, HDPE에 증착된 아민 고분자 박막이 물 또는 알코올로 부분적으로 제거되었음을 확인하였다.
2. HDPE의 접촉각은 단량체의 종류에 관계없이 노즐과의 거리가 멀어질수록 감소하였다. HDPE 표면의 아민 농도는 노즐로부터의 거리에 따라 변화하였다. 거리에 따른 아민 농도 분포는 각 단량체에 따라 다른 패턴을 보였으나 7cm 거리에서는 분산이 감소하였다.
3. HDPE 표면의 아민 농도는 5 nmol/mm^2 와 100 nmol/mm^2 로 나누었다. FT-IR 결과 1640cm^{-1}의 N-H band에서 아민 농도의 증가에 따라 흡광도가 증가함을 보였다. 접촉각은 AA와 CPA 단량체에서 농도가 증가함에 따라 감소했지만 DACH 단량체에서는 차이가 없었다.
4. MSC 증식은 처리되지 않은 샘플에 비해 아민 플라즈마 처리된 샘플에서 향상되었다. 특히, 18일째에서 AA 및 CPA 단량체를 사용한 플라즈마 중합 HDPE의 세포증식은 무처리 HDPE에 비해 2배 이상 증가하였다. 낮거나 높은 아민 농도에서 AA 및 CPA 단량체의 경우 표면의 아민 농도가 증가함에 따라 세포증식은 증가하였다. 그러나 DACH 단량체의 경우 아민 농도 증가에 따른 차이는 없었다.

이러한 결과로부터 우리는 아민 플라즈마 중합 기술이 뼈 조직 공학에 적용할 수 있는 가능성과 유용성을 알 수 있었다.

두 번째 연구에서는 치과용 티타늄(Ti) 임플란트의 표면개질에 적용하기 위한 대기압 플라즈마 제트 (APPJ) 장치를 설계 및 제작하였다. 플라즈마 표면개질(PSM)은 CPA 모노머를 사용하여 Ti 임플란트 소재에 아민 플라즈마 중합을 수행하였다. APPJ 설계를 최적화하기 위해 플라즈마 반응기의 형상, He 가스 유량, CPA 단량체 유량, 인가 전압, 주파수, 전극 위치 및 접지 전극과 같은 설계 변수를 고려하였다. 그리고, Ti 임플란트 소재표면을 아민 농도, 접촉각, XPS, AFM으로 조사하였고, 체외 시험은 MC3T3-E1 조골모세포의 증식, 초기 부착 및 분화를 통하여 평가하였다.

두 번째 연구 결과는 다음과 같다.

1. I-형 반응기는 Y-형 반응기보다 시료 표면에 더 많은 아민기를 증착시켰다. 접지의 증가에 따른 표면의 아민 농도 변화는 5 sccm 이상에서는 보이지 않았다. 모노머 유속이 증가함에 따라 표면의 아민 농도는 15 sccm까지 증가하였지만 20 sccm에서는 감소하였다.

2. 반응기에 인가되는 전압이 증가할수록 표면의 아민 농도는 증가하였으나 16 kV에서는 감소하였다. 주파수가 증가함에 따라 표면의 아민 농도가 증가하였고 60 kHz 이상에서는 증가 또는 감소의 변화가 없었다.
3. 최적화 조건은 전압 12 kV, 주파수 50 kHz, He 가스 유량 1 slm, 모노머 유량 10sccm 이었다. 접촉각은 대조군인 59˚에 비해 아민 플라즈마 중합 후 12.3˚이거나 그 이하로 낮았다. 1일 후, 플라즈마 중합된 Ti 표면의 접촉각은 34˚ 이하로 확인되었다.
4. 아민 중합된 Ti 표면의 거칠기는 크게 감소하였고, 표면의 RMS 거칠기도 감소하였다. XPS 분석은 질소와 탄소가 깨끗한 Ti 표면에 비해 아민 중합된 Ti 표면에서 증가함을 나타냈다.
5. 세포 증식을 실험한 결과, 4분 시료가 2일과 3일에 가장 높은 증식을 보였다. 형광염색을 이용하여 초기 세포 부착 형태를 관찰한 결과 세포 형태에는 큰 차이가 없었으나 아민 표면 시료에서 초기 부착 인자인 paxillin의 발광이 더 강하게 발현되었다. Live-Dead cell 시약을 이용하여 세포독성을 확인한 결과, 아민 중합 표면에 독성은 없었다.
6. 아민 중합된 Ti 표면의 세포 분화는 14일 동안 30% 미만으로 증가하였다. 아민 중합 시료의 골석회화는 미처리 시료에 비해 감소하였다. Western blot을 통하여 ALP와 OPN이 일부 아민 중합 시료에서 강하게 발현되었음을 보았다. RUX2는 모든 샘플에서 유의미한 차이를 보이지 않았다.

우리는 Ti 임플란트의 골유착 강화에 적용할 수 있는 간단하고 저렴한 APPJ 장치를 성공적으로 개발했으며 최적의 아민 플라즈마 중합을 유도하였다. APPJ는 향후 상업용 Ti 임플란트의 표면처리에 활용될 수 있을 것으로 기대된다.

세 번째 연구에서는 FEDBD 플라즈마에 의한 SLA 처리된 Ti 표면의 살균 효과를 조사하였다. *P. gingivalis*는 임플란트 주위염을 유발하는 주요 미생물로 잘 알려져 있다. 따라서 우리는 *P. gingivalis* 바이오필름에 대한 살균 및 제거 실험을 수행하고 사람 치은섬유모세포-1(HGF-1)의 세포독성을 평가하였다.

세 번째 연구 결과는 다음과 같다.

1. 플라즈마 가스의 산소 혼합 비율과 플라즈마 세기의 증가에 따라 OH 라디칼의 생성은 증가하였다.

2. 플라즈마 조사 시간과 플라즈마 강도가 증가할수록 활성산소종(ROS)의 생성이 증가하였다.
3. 플라즈마 조사 시간과 플라즈마 강도가 증가할수록 *P. gingivalis*의 콜로니와 바이오필름이 감소하였다.
4. 플라즈마 조사 60초까지는 HGF-1 생존율에 유의한 영향이 없었으나 90초 이후에는 생존율이 감소하였다. 세포 내부의 ROS가 증가함에 따라 세포 생존율이 감소하였다.

플라즈마 멸균은 *P. gingivalis* 멸균 실험을 통해 임플란트 주위염 치료에 매우 효과적인 방법임을 확인하였다.

결론적으로 플라즈마 기술을 이용한 표면개질 및 살균은 생체 활성이 낮은 생체물질에 대한 기능화 도입 및 살균 효과를 제공할 수 있다. 플라즈마 기술은 생물의학 분야에서 무한한 응용이 가능할 것으로 생각된다.

7. References

[1] R. Langer, and J. P. Vacanti, Tissue engineering, Science **260** (1993) 920–926.

[2] A. R. Amini, C. T. Laurencin, and S. P. Nukavarapu, Bone tissue engineering: recent advances and challenges, Crit Rev Biomed Eng. **40** (2012) 363-408.

[3] G. L. Koons, M.i Diba, and A. G. Mikos, Materials design for bone-tissue engineering, Nat. Rev. Mater. **5** (2020) 584-603.

[4] T. A. St John *et al.*, Physical and monetary costs associated with autogenous bone graft harvesting, Am. J. Orthop. **32** (2003) 18-23.

[5] C. F. Lord, M. C. Gebhardt, W. W. Tomford, and H. J. Mankin, Infection in bone allografts. Incidence, nature, and treatment, J Bone Joint Surg Am. **70** (1988) 369-376.

[6] W. W. Tomford, R. J. Starkweather, and M. H. Goldman, A study of the clinical incidence of infection in the use of banked allograft bone, J Bone Joint Surg Am. **63** (1981) 244-248.

[7] J. H. Kwon, S. S. Kim, B.-S. Kim, W. J. Sung, S. H. Lee, J. I. Lim, Y. Jung, S.-H. Kim, S. H. Kim, Y. H. Kim, Histological Behavior of HDPE Scaffolds Fabricated by the “Press-and-Baking” Method, J. Bioact. Compat. Polym. **20** (2005) 361-376.

[8] R. Cenzi, A. Farina, L. Zuccarino, F. Carinci, Clinical outcome of 285 Medpor grafts used for craniofacial reconstruction, J Craniofac. Surg. **16** (2005) 526-530.

[9] N. C. Paxton, M. C. Allenby, P. M. Lewis, M. A. Woodruff, Biomedical applications of polyethylene, Eur. Polym. J. 118 (2019) 412-428.

[10] N. Pande, N. P. S. Chauhan, and S. Kale, “Plasma polymerization and plasma modification of surface for biomaterials applications,” Fundamental Biomaterials: Polymers, Sawston, UK: Woodhead Publishing, 2018, ch. 8, pp. 171-178.

[11] J. A. Gan, and C. C. Berndt, “Plasma surface modification of metallic biomaterials,” Surface Coating and Modification of Metallic Biomaterials, Sawston, UK: Woodhead Publishing, 2015, ch. 4, pp. 103-157.

[12] P. K. Chua, J. Y. Chena, L. P. Wanga, N. Huang, Plasma-surface modification of biomaterials, Mater. Sci. Eng. R-Rep. 36 (2002) 143-206.

[13] I. T. Ozbolat, “Applications of 3D Bioprinting,” 3D Bioprinting, Cambridge, MA, USA: ACADEMIC PRESS, 2017, ch. 9, pp. 271-312.

[14] T. W. Bauer, and G. F. Muschler, Bone graft materials. An overview of the basic

science, Clin. Orthop. Rel. Res. **371** (2000) 10-27.

[15] R. S. Valtanen, Y. P. Yang, G. C. Gurtner, W. J. Maloney, and D. W. Lowenberg, Synthetic and Bone tissue engineering graft substitutes: What is the future?, Injury **5252** (2021) S72-S77.

[16] M. Okamoto, R. Domura, R. Sakai and S. Arakawa, "Smart surfaces chemistry and coating materials for tissue engineering," Smart materials for tissue engineering: fundamental principles 1st e.d. London, U.K: RSC Publishing, 2017, ch. 2, pp. 25-44.

[17] G. Gautam, S. Kumar and K. Kumar, "Processing of biomaterials for bone tissue engineering: State of the art," Mater. Today: Proc., to be published, https://doi.org/10.1016/j.matpr.2021.09.459.

[18] D. S. Kohane and R. Langer, Polymeric Biomaterials in Tissue Engineering, Pediatr. Res. 63 (2008) 487-491.

[19] A. Ivkovic, I. Marijanovic, D. Hudetz, R. M. Porter, M. Pecina, and C. H. Evans, Regenerative medicine and tissue engineering in orthopaedic surgery, Front. Biosci. **1** (2011) 923-944.

[20] R. Kannan, G. Wei and P. X. Ma, "Synthetic polymeric biomaterials for tissue engineering," Tissue Engineering Using Ceramics and Polymers, 3rd ed. Sawston, UK: Woodhead Publishing, 2021, ch. 2, pp. 41-74.

[21] M. S. Lopes, A.L. Jardini, R. M. Filho, Poly (Lactic Acid) Production for Tissue Engineering Applications, Procedia Eng. **42** (2012), 1402-1413.

[22] C. R. Chu, R. D. Coutts, M. Yoshioka, F. L. Harwood, A. Z. Monosov, and D. Amiel, Articular cartilage repair using allogeneic perichondrocyteseeded biodegradable porous polylactic acid (PLA): A tissue-engineering study, J. Biomed. Mater. Res. **29** (1995) 1147-1154.

[23] H. Sun, L. Mei, C. Song, X. Cui, and P. Wang, The in vivo degradation, absorption and excretion of PCL-based implant, Biomaterials **27** (2006) 1735-1740.

[24] F. Hajiali, S. Tajbakhsh, and A. Shojaei, Fabrication and properties of polycaprolactone composites containing calcium phosphate-based ceramics and bioactive glasses in bone tissue engineering: a review, Polym. Rev. **58** (2018) 164-207.

[25] B. D. MacArthur, and R. O. C. Oreffo, Bridging the gap, Nature **433** (2005) 19.

[26] N. C. Paxton, M. C. Allenby, P. M. Lewis, and M. A. Woodruff, Biomedical applications of polyethylene, Eur. Polym. J. **118** (2019) 412-428.

[27] J. Y. Wang, K. Wang, X. Gu, and Y. Luo Polymerization of hydrogel network on microfiber surface: synthesis of hybrid water-absorbing matrices for biomedical applications, ACS Biomater. Sci. Eng. **2** (2016) 887-892.

[28] A. J. T. Teo, A. Mishra, I. Park, Y. J. Kim, W. T. Park, and Y. J. Yoon, Polymeric biomaterials for medical implants and devices, ACS Biomater. Sci. Eng. **2** (2016) 454-472.

[29] J. W. Nicholson, Titanium Alloys for Dental Implants: A Review, Prosthesis **2** (2020) 100-116.

[30] M. Özcan and C. Hämmerle, Titanium as a reconstruction and implant material in dentistry: advantages and pitfalls, materials **5** (2012) 1528-1545.

[31] A. Jemat, M. J. Ghazali, M. Razali, and Y. Otsuka, Surface modifications and their effects on titanium dental implants, Biomed Res. Int. **2015** (2015) 791725.

[32] T. Xue1 *et al.*, Surface modification techniques of titanium and its alloys to functionally optimize their biomedical properties: thematic review, Front. Bioeng. Biotechnol. **8** (2020) 1261-1279.

[33] I. Langmuir, Oscillations in ionized gases, Proc. Natl. Acad. Sci. U.S.A. **14** (1928) 627-637.

[34] G. Aziz, N. De Geyter, and R. Morent, “Incorporation of Primary Amines via Plasma Technology on Biomaterials,” Advances in Bioengineering, London, UK: IntechOpen, 2015, ch. 2, pp. 21-47.

[35] R. Jung, and Z. T. Jung, “Plasma in the dental laboratory”, relyon-plasma.com. https://www.relyon-plasma.com/plasma-in-the-dental-laboratory/?lang=en (accessed December 3, 2021)

[36] A. Marshall, “Explanation of low pressure plasma cleaning,” inseto.co.uk. https://www.inseto.co.uk/explanation-of-low-pressure-plasma-cleaning-ikb-014/ (accessed Dec. 3, 2021).

[37] T. H. Chen, F. Y. Chung, W. F. Jiang, and C. Huang, A study of plasma power effects on surface activation of polystyrene, Vacuum **186** (2021) 110069.

[38] S. Rimpelová, N. S. Kasálková, P. Slepička, H. Lemerová, V. Švorčík, and T. Ruml, Plasma treated polyethylene grafted with adhesive molecules for enhanced adhesion and growth of fibroblasts, Mater. Sci. Eng. C **33** (2013) 1116-1124.

[39] N. Kasálková et al., Cell adhesion and proliferation on plasma-treated and poly(ethylene glycol)-grafted polyethylene, J. Adhes. Sci. Technol. **24** (2010) 743-754.

[40] R. Morent, N. De Geyter, C. Leys, L.Gengembre, and E. Payen, Study of the ageing behaviour of polymer films treated with a dielectric barrier discharge in air, helium and argon at medium pressure, Surf. Coat. Technol. **201** (2007) 7847-7854.

[41] S. P. Huertas, K. Terpiłowski, M. Tomczyńska-Mleko, S. Mleko, Ł. Szajnecki, Time-based changes in surface properties of poly (ethylene terephthalate) activated with air and argon-plasma treatments, Colloid Surf. A **558** (2018) 322-329.

[42] R. Bitar, P. Cools, N. De Geyter, and R. Morent, Acrylic acid plasma polymerization for biomedical use, Appl. Surf. Sci. **448** (2018) 168-185.

[43] S. B. Adler, Mechanism and kinetics of oxygen reduction on porous $La_{1-x}Sr_xCoO_{3-\delta}$ electrodes, Solid State Ion. **111** (1998) 125-134.

[44] S. Lerouge, M. R. Wertheimer and L'H. Yahia, Plasma Sterilization: A Review of Parameters, Mechanisms, and Limitations, Plasmas Polym. **6** (2001) 175-188.

[45] M. Laroussi, C. Tendero, X. Lu, S. Alla, and W. L. Hynes, Inactivation of bacteria by the plasma pencil, Plasma Process. Polym. **23** (2006) 470-473.

[46] R. E. J. Sladek and E. Stoffels, Deactivation of Escherichia coli by the plasma needle, J. Phys. D-Appl. Phys. **38** (2005) 1716.

[47] M. K. Singh, A. Ogino and M. Nagatsu, Inactivation factors of spore-forming bacteria using low-pressure microwave plasmas in an N_2 and O_2 gas mixture, New J. Phys. **11** (2009) 115027.

[48] M. Y. Alkawareek *et al.*, Eradication of *Pseudomonas aeruginosa* biofilms by atmospheric pressure non-thermal plasma, PLoS One **7** (2012) e44289.

[49] S. Kitazaki, A. Tanaka, N. Hayashi, Sterilization of narrow tube inner surface using discharge plasma, ozone, and UV light irradiation, Vacuum, **110** (2014), 217-220.

[50] T. Nishikawa, N. Abe, A. Yonesu, and N. Hayashi, Reprint of: Sterilization of small vial using electron cyclotron resonance plasma, Vacuum, **167** (2019) 586-590.

[51] R. Zhou, R. Zhou, P. Wang, B. Luan, X. Zhang, Z. Fang, Y. Xian, X. Lu, K. K. Ostrikov, and K. Bazaka, Microplasma Bubbles: Reactive Vehicles for Biofilm Dispersal, ACS Appl. Mater. Interfaces **11** (2019) 20660-20669.

[52] M. A. Mackinder, K. Wang, B. Zheng, M. Shrestha, and Q. H. Fan, Magnetic field enhanced cold plasma sterilization, Clin. Plasma Med. **17-18** (2020) 100092.

[53] G. Altankov, V. Thom, T. Groth, K. Jankova, G. Jonsson, and M. Ulbricht, Modulating the biocompatibility of polymer surfaces with poly(ethylene glycol): effect of fibronectin, J. Biomed. Mater. Res. **52** (2000) 219-230.

[54] R. Sbarbati, D. Giannessi, M. C. Cenni, G. Lazzerini, F. Verni, and R. De Caterina, Pyrolytic carbon coating enhances teflon and dacron fabric compatibility with endothelial cell growth, Int. J. Artif. Organs **14** (1991) 491-498.

[55] S. K. Singh, M. K. Singh, P. P. Kulkarni, V. K. Sonkar, J. J. A. Gra´cio, and D. Dash, Amine-Modified Graphene: Thrombo-Protective Safer Alternative to Graphene Oxide for Biomedical Applications, ACS Nano **6** (2012) 2731-2740.

[56] A. Nanci *et al.*, Chemical modification of titanium surfaces for covalent attachment of biological molecules, J. Biomed. Mater. Res. **40** (1998) 324-335.

[57] P. Rossini, P. Colpo, G. Ceccone, K. D. Jandt, and F. Rossi, Surfaces engineering of polymeric films for biomedical applications, Mater. Sci. Eng. C **23** (2003) 353-358.

[58] J. H. Lee, J. W. Park, and H. B. Lee, Cell adhesion and growth on polymer surfaces with hydroxyl groups prepared by water vapour plasma treatment, Biomaterials **12** (1991) 443-448.

[59] I. Gancarz, G. Poźniak, M. Bryjak, and W. Tylus, Modification of polysulfone membranes 5. Effect of n-butylamine and allylamine plasma, Eur. Polym. J. **38** (2002) 1937-1946.

[60] S. Bhatt, J. Pulpytel, M. Mirshahi, and F. Arefi-Khonsari, Catalyst-free plasma-assisted copolymerization of poly(ε-caprolactone)-poly (ethylene glycol) for biomedical applications, ACS Macro Lett. **1** (6) (2012) 764-767.

[61] S. Bhatt, J. Pulpytel, M. Mirshahi, and F. Arefi-Khonsari Nano thick poly (ε -caprolactone)-poly (ethylene glycol) coatings developed by catalyst free plasma assisted copolymerization process for biomedical applications, RSC Adv. **2** (2012) 9114-9123.

[62] E. Sardella, E.R. Fisher, J.C. Shearer, M.G. Trulli, R. Gristina, and P. Favia, N_2/H_2O plasma assisted functionalization of poly(ε-caprolactone) porous scaffolds: acidic/basic character versus cell behavior, Plasma Process. Polym., **12** (2015) 786-798.

[63] A. Baitukha *et al.*, Optimization of a low pressure plasma process for fabrication of a Drug Delivery System (DDS) for cancer treatment, Mater. Sci. Eng. C **105** (2019) 110089.

[64] K. S. Siow, S. Kumar, and H. J. Griesser, Low-pressure plasma methods for generating non-reactive hydrophilic and hydrogel-like bio-Interface coatings – a review, Plasma Process. Polym., **12** (2015) 8-24.

[65] E. Sardella, F. Palumbo, G. Camporeale, and P. Favia, Non-equilibrium plasma processing for the preparation of antibacterial surfaces, Materials, **9** (2016), 515.

[66] W. T. Couldwell, C. B. Stillerman, and W. Dougherty, Reconstruction of the skull base and cranium adjacent to sinuses with porous polyethylene implant: preliminary report, Skull Base Surg. **7** (1997) 57-63.

[67] J. K. Liu, O. N. Gottfried, C. D. Cole, W. R. Dougherty, and W. T. Couldwell, Porous polyethylene implant for cranioplasty and skull base reconstruction, Neurosurg. Focus **16** (2004) 1-5.

[68] C. S. Kim, K. H. Jung, H. Kim, C. B. Kim, and I. K. Kang, Collagen-grafted porous HDPE/PEAA scaffolds for bone reconstruction, Biomater. Res. **20** (2016) 1-9.

[69] J. M. Rodríguez, S. J. Renou, M. B. Guglielmotti, and D. G. Olmedo, Tissue response to porous high density polyethylene as a three-dimensional scaffold for bone tissue engineering: An experimental study, J. Biomater. Sci.-Polym. Ed. **30** (2019) 486-499.

[70] Y. Wu *et al.*, Engineering cartilage substitute with a specific size and shape using porous high-density polyethylene (HDPE) as internal support, J. Plast. Reconstr.

Aesthet. Surg. **63** (2010) e370-375.

[71] L. Mazini, M. Ezzoubi, and G. Malka, Overview of current adipose-derived stem cell (ADSCs) processing involved in therapeutic advancements: flow chart and regulation updates before and after COVID-19, Stem Cell Res. Ther. **12** (2021) 1-17.

[72] S. Noel, B. Liberelle, L. Robitaille, and G. De Crescenzo, Quantification of primary amine groups available for subsequent biofunctionalization of polymer surfaces, Bioconjugate Chem. **22** (2011) 1690-1699.

[73] K. Agarwal, R. B. Dhirawani, S. Singha, and A. Agrawal, High-Density Polyethylene Material versus Autogenous Grafts in Craniofacial Augmentation Procedures. Ann. Maxillofac. Surg. **9** (2019) 10-14.

[74] A. Rai, A. Datarkar, A. Arora, and D. G. Adwani, Utility of high density porous polyethylene implants in maxillofacial surgery, J. Maxillofac. Oral Surg. **13** (2014) 42-46.

[75] P. Sengupta, and B. L. V. Prasad. Surface Modification of Polymers for Tissue Engineering Applications: Arginine Acts as a Sticky Protein Equivalent for Viable Cell Accommodation, ACS Omega **3** (2018) 4242-4251.

[76] Z. Z. Can, A. R. Ercocen, I. Apaydın, E. Demirseren, and B. Sabuncuoglu, Tissue Engineering of high density porous polyethylene implant for three-dimensional reconstruction: An experimental study, Scand. J. Plast. Reconstr. Surg. Hand Surg. **34** (2000) 9−14.

[77] S. P. James, R. K. Oldinski, M. Zhang, and H. Schwartz, “UHMWPE/Hyaluronan Microcomposite Biomaterials,” UHMWPE Biomaterials Handbook, 2nd ed. Cambridge, MA, USA: Academic Press, 2009, ch. 18, pp 259−276.

[78] S. Deshpande, and A. Munoli, Long-term results of high-density porous polyethylene implants in facial skeletal augmentation: An Indian perspective. Indian J. Plast. Surg. **43** (2010) 34−39.

[79] Y. H. Kim, and T. Y. Jang, Porous high-density polyethylene in functional rhinoplasty: Excellent long-term aesthetic results and safety. Plast. Surg. **22** (2014) 14−17.

[80] I. Fernandez-Bueno *et al.*, Safety and biocompatibility of a new high-density polyethylene-based spherical integrated porous orbital implant: an experimental study in

rabbits. J. Ophthalmol. **2015** (2015) 1-7.

[81] P. Žáková *et al.*, Cytocompatibility of amine functionalized carbon nanoparticles grafted on polyethylene. Mater. Sci. Eng. C, **60** (2016) 394-401.

[82] L. F. Thompson and K. G. Mayhan, The Plasma Polymerization of Vinyl Monomers. Ⅱ. A Detailed Study of the Plasma Polymerization of Styrene, J. Appl. Polym. Sci. **16** (1972) 2317-2341.

[83] M. Chen, P. O. Zamora, P. Som, L. A. Peña, and S. Osaki, Cell attachment and biocompatibility of polytetrafluoroethylene (PTFE) treated with glow-discharge plasma of mixed ammonia and oxygen, J. Biomater. Sci.-Polym. Ed. **14** (2003) 917-935.

[84] A. Schutze, J. Y. Jeong, S. E. Babayan, Jaeyoung Park, G. S. Selwyn, and R. F. Hicks, The atmospheric-pressure plasma jet: a review and comparison to other plasma sources. IEEE Trnas. Plasma Sci, **62** (1998) 1685-1694.

[85] R. A. Wolf, "Plasma for surface modification," Atmospheric pressure plasma for surface modification, Hoboken, NJ, USA: Wiley, 2012, ch. 2, pp. 27-53.

[86] M. Fazeli, J. Florez, and R. Simão, Improvement in adhesion of cellulose fibers to the thermoplastic starch matrix by plasma treatment modification, Compos. Pt. B-Eng. **163** (2019) 207−216.

[87] K. Gotoha, E. Shohbuke, Y. Kobayash, and H. Yamada, Wettability control of PET surface by plasma-induced polymer film deposition and plasma/UV oxidation in ambient air, Colloid Surf. A-Physicochem. Eng. Asp. **556** (2018) 1-10.

[88] H. W. Herrmann, I. Henins, J. Park, and G. S. Selwyn. Decontamination of chemical and biological warfare (CBW) agents using an atmospheric pressure plasma jet (APPJ). Phys. Plasmas **6** (1999) 2284-2289.

[89] G. S. Selwyn,, and R. Hicks, "Atmospheric pressure plasma cleaning of contamination surfaces. 1997 mid-year progress report," Univ. of California, Los Angeles, CA, USA, Prog. Rep. EMSP-54914−97, Jun. 1997.

[90] M. Noeske, J. Degenhardt, S. Strudhoff, and U. Lommattzsch, Plasma jet treatment of five polymers at atmospheric pressure: surface modifications and the relevance for adhesion, Int. J. Adhes. Adhes. **24** (2004) 171−177

[91] T. Albrektsson, P. I. Branemark, H. A. Hansson, and J. Lindstrom, Osseointegrated titanium implants.Requirements for ensuring a long-lating direct bone-to-implant

anchorage in man, Acta Orthop. Scand. **52** (1981) 155−170.

[92] Y. Yang *et al.*, Enhancing osseointegration using surface-modified titanium implants, JOM-J. Miner. Met. Mater. Soc. **58** (2006) 71-76.

[93] Y, Liu *et al.*, "Engineered titanium surface promoting osseointegration," Biomaterials and Biomedical Engineering, Stafa-Zuerich, Switzerland, Trans Tech Publications, 2008, pp. 115−134.

[94] S. K. Nishimoto *et al.*, The effect of titanium surface roughening on protein absorption, cell attachment, and cell spreading, Int. J. Oral Maxillofac. Implants **23** (2008) 675-680.

[95] Y. Yang, K. H. Kim, and J. L. Ong, A review on calcium phosphate coatings produced using a sputtering process--an alternative to plasma spraying, Biomaterials **26** (2005) 327-337.

[96] Y. Yang, K. Bessho, and J. L. Ong, in, "Plasma-Sprayed Hydroxyapatite-Coated and Plasma-Sprayed Titanium-Coated Implants," Biomaterials in Orthopedics, 2nd ed. Boca Raton, FL, USA: CRC Press, 2004, ch. 17, p. 401-424.

[97] X. Zhu, J. L. Ong, S. Kim, and K. Kim, Surface characteristics and structure of anodic oxide films containing Ca and P on a titanium implant material, J. Biomed. Mater. Res. **60** (2002) 333-338.

[98] M. Annunziata, L. Canullo, G. Donnarumma, P. Caputo, L. Nastri, and L. Guida, Bacterial inactivation/sterilization by argon plasma treatment on contaminated titanium implant surfaces: *In vitro* study, Med. Oral Patol. Oral Cir. Bucal **21** (2016) 118-121.

[99] Y. Z. Yang, J. M. Tian, J. T. Tian, Z. Q. Chen, X. J. Deng, and D. H. Zhang, Preparation of graded porous titanium coatings on titanium implant materials by plasma spraying, J. Biomed. Mater. Res. **52** (2000) 333-337.

[100] P. L. Parham Jr, C. M. Cobb, A. A. French, J. W. Love, C. L. Drisko, and W. J. Killoy, Effects of an air-powder abrasive system on plasma-sprayed titanium implant surfaces: an in vitro evaluation, J. Oral Implant. **15** (1989) 78-86.

[101] A. O. Matos *et al.*, Three-species biofilm model onto plasma-treated titanium implant surface, Colloid Surf. B-Biointerfaces 152 (2017) 354-366.

[102] P. Cacciafesta, K. R.Hallam, A. C. Watkinson, G. C. Allen, M. J. Miles, and K.

D. Jandt, Visualisation of human plasma fibrinogen adsorbed on titanium implant surfaces with different roughness. Surf. Sci. 491 (2001) 405-420.

[103] T. R. Gegenbach, X. Xie, R. C. Chatelier, and H. J. Griesser, Evolution of the surface composition and topography of perfluorinated polymers following ammonia-plasma treatment, J. Adh. Sci. Technol. **8** (1994) 305-328.

[104] B. D. Ratner, A. Chikoti, and G. P. Lopez, "Plasma Deposition and Treatment for Biomaterial Applications," Plasma Deposition, Treatment, and Etching of Polymers, 1st ed. Cambridge, MA, USA: Academic Press, 1990, ch. 7, pp. 463-516.

[105] W. R. Gombotz, and A. S. Hoffmann, "Immobilization of Biomolecules and Cells on and Within Synthetic Polymeric Hydrogels," Hydrogels in Medicine and Pharmacy, 1st ed. Boca Raton, FL, USA: CRC Press. 1986, ch. 5, pp. 95-126.

[106] S. I. Ertel, A. Chilkoti, T. A. Horbetti and B. D. Ratner, Endothelial cell growth on oxygen-containing films deposited by radio-frequency plasmas: the role of surface carbonyl groups, J. Biomater. Sci.-Polym. Ed. **3** (1992) 163-183.

[107] A. Manakhov *et al.*, Carboxyl-anhydride and amine plasma coating of PCL nanofibers to improve their bioactivity. Mater. Des. **132** (2017) 257-265.

[108] H. J. Griesser, R. C. Chatelier, T. R. Gengenbach, G. Johnson, and J. G. Steele, Growth of human cells on plasma polymers: Putative role of amine and amide groups, J. Biomater. Sci.-Polym. Ed. 5 (1994) 531-554.

[109] Y. H. Choi and S. H. Hong, Effect of the amine concentration on phase evolution and densification in printed films using Cu(II) complex ink, Langmuir **31** (2015) 8101−8110.

[110] X. Y. Gao, J. Ashok, S. Widjaja, K. Hidajat, and S. Kawi, Ni/SiO_2 catalyst prepared via Ni-aliphatic amine complexation for dry reforming of methane: Effect of carbon chain number and amine concentration. Appl. Catal. A-Gen. **503** (2015) 34-42.

[111] D. Mangindaan, W. H. Kuo, and M. J. Wang, Two-dimensional amine-functionality gradient by plasma polymerization, Biochem. Eng. J. **78** (2013) 198-204.

[112] D. Mangindaan, W. H. Kuo, H. Kurniawan, and M. J. Wang, Creation of biofunctionalized plasma polymerized allylamine gradients, J. Polym. Sci. Pt.

B-Polym. Phys. **51** (2013) 1361-1367.

[113] K. V. Chan, M. Asadian, I. Onyshchenko, H. Declercq, R. Morent, and N. De Geyter, Biocompatibility of cyclopropylamine-based plasma polymers deposited at sub-atmospheric pressure on poly (ε-caprolactone) nanofiber meshes, Nanomaterials **9** (2019) 1215.

[114] X. Liu, Q. Feng, A. Bachhuka, and K. Vasilev, Surface modification by allylamine plasma polymerization promotes osteogenic differentiation of human adipose-derived stem cells, ACS Appl. Mater. Interfaces **6** (2014) 9733-9741.

[115] M. F. Griffin, A. Ibrahim, A. M. Seifalian, P. E. M. Butler, D. M. Kalaskar, and P. Ferretti, Chemical group-dependent plasma polymerisation preferentially directs adipose stem cell differentiation towards osteogenic or chondrogenic lineages, Acta Biomater. **50** (2017) 450-461.

[116] F. Mwale, H. T. Wang, V. Nelea, L. Luo, J. Antoniou, and M. R. Wertheimer, The effect of glow discharge plasma surface modification of polymers on the osteogenic differentiation of committed human mesenchymal stem cells, Biomaterials **27** (2006) 2258-2264.

[117] S. K. Han, H. M. Kim, N. Y. Choi, H. G. Kim, and J. D. Ha, The influence of fibronectin and/or RGDS tetrapeptide on osteopontin expression in cultures of rat calvarial osteoblasts, J. of Korean Orthop. Assoc. **37** (2002) 145-151.

[118] D. Clark, E. Kotronia, and S. E. Ramsay, Frailty, aging, and periodontal disease: Basic biologic considerations. Periodontol. 2000 **87** (2021) 143-156.

[119] K. C. Howard, O. A. Gonzalez, and S. Garneau-Tsodikova. *Porphyromonas gingivalis*: where do we stand in our battle against this oral pathogen?, RSC Med. Chem. **12** (2021) 666-704.

[120] M. Nakajima, E. E. L. Tanner, N. Nakajima, K. N. Ibsen, and S. Mitragotri, Topical treatment of periodontitis using an iongel, Biomaterials **276** (2021) 121069.

[121] H. Lu, L. He, D. Jin, Y. Zhu, and H. Meng, The effect of adjunctive systemic antibiotics on microbial populations compared to scaling and root planing alone for the treatment of periodontitis: A pilot randomized clinical trial. J. Periodont. (2021) 1-14.

[122] P. Ramburrun, N. A. Pringle, A. Dube, R. Z. Adam, S. D'Souza, and M. Aucamp, Recent advances in the development of antimicrobial and antifouling biocompatible materials for dental applications, Materials **14** (2021) 3167.

[123] D. Braný, D. Dvorská, E. Halašová, and H. Škovierová, Cold atmospheric plasma: a powerful tool for modern medicine, Int. J. Mol. Sci. **21** (2020) 2932.

[124] M. Izadjoo, S. Zack, H. Kim, and J. Skiba, Medical applications of cold atmospheric plasma: State of the science. J. Wound Care **27** (2018) S4-S10.

[125] G. Isbary *et al.*, Cold atmospheric plasma devices for medical issues. Expert Rev. Med. Devices **10** (2013) 367-377.

[126] P. M. Girard *et al.*, Synergistic effect of H_2O_2 and NO_2 in cell death induced by cold atmospheric He plasma. Sci. Rep. **6** (2016), 29098.

[127] F. Girard *et al.*, Correlations between gaseous and liquid phase chemistries induced by cold atmospheric plasmas in a physiological buffer, Phys. Chem. Chem. Phys. **20** (2018) 9198-9210.

[128] Y. Li *et al.*, Evaluation of cold plasma treatment and safety in disinfecting 3-week root canal enterococcus faecalis biofilm in vitro, J. Endod. **41** (2015) 1325-1330.

[129] B. Kleineidam, M. Nokhbehsaim, J. Deschner, and G. Wahl, Effect of cold plasma on periodontal wound healing-an in vitro study. Clin. Oral Investig. **23** (2019) 1941-1950.

[130] X. Mao *et al.*, Cetylpyridinium chloride: mechanism of action, antimicrobial efficacy in biofilms, and potential risks of resistance, Antimicrob. Agents Chemother. **64** (2020) e00576-20.

[131] D. Lepelletier, J. Y. Maillard, B. Pozzetto, and A. Simon, Povidone Iodine: properties, mechanisms of action, and role in infection control and Staphylococcus aureus decolonization, Antimicrob. Agents Chemother. **64** (2020) e00682-20.

[132] K. D. Bastendorf, N. Strafela-Bastendorf, and A. Lussi, Mechanical removal of the biofilm: Is the curette still the gold standard?, Monogr. Oral Sci. **29** (2021) 105-118.

[133] W. Johnston *et al.*, Mechanical biofilm disruption causes microbial and immunological shifts in periodontitis patients, Sci. Rep. **11** (2021) 9796.

[134] C. Tomasi, A. Bertelle, E. Dellasega, and J. L. Wennström, Full-mouth ultrasonic debridement and risk of disease recurrence: a 1-year follow-up, J. Clin. Periodontol. **33** (2006) 626-631.

[135] L. I. Partecke *et al.*, Tissue tolerable plasma (TTP) induces apoptosis in pancreatic cancer cells in vitro and in vivo. BMC Cancer **12** (2012) 473.

[136] J. Park, J. Lee, and C. Choi, Mitochondrial network determines intracellular ROS dynamics and sensitivity to oxidative stress through switching inter-mitochondrial messengers, PLoS One. **6** (2011) e23211.

[137] C. M. Lee, Y. I. Jeong, M. S. Kook, and B. H. Kim, Combinatorial effect of cold atmosphere plasma (CAP) and the anticancer drug cisplatin on oral squamous cell cancer therapy, Int. J. Mol. Sci. **21** (2020) 7646.

[138] N. Jha, J. J. Ryu, E. H. Choi, and N. K. Kaushik, Generation and role of reactive oxygen and nitrogen species induced by plasma, lasers, chemical agents, and other systems in dentistry, Oxidative Med. Cell. Longev. **2017** (2017) 7542540.

[139] N. Thakur, P. Manna, and J. Das, Synthesis and biomedical applications of nanoceria, a redox active nanoparticle. J. Nanobiotechnol. **17** (2019) 84.

[140] H. H. Jang *et al.*, Piperlongumine-eluting gastrointestinal stent using reactive oxygen species-sensitive nanofiber mats for inhibition of cholangiocarcinoma cells, Nanoscale Res. Lett. **14** (2019) 58.

[141] S. Bekeschus, A. Kramer, and A. Schmidt, Gas plasma-augmented wound healing in animal models and veterinary medicine, Molecules **26** (2021) 5682.

[142] C. Duchesne *et al.*, Cold atmospheric plasma promotes killing of staphylococcus aureus by macrophages. mSphere **6** (2021) e0021721.

[143] Y. O. Park *et al.*, In vitro bactericidal efficacy of atmospheric-pressure plasma jet on titanium-based implant infected with *Staphylococcus aureus*, Jpn. J. Appl. Phys. **56** (2017) 01AC01.

[144] E. J. Kim, J. E. Hyun, Y. H. Kang, S. J. Baek, and C. Y. Hwang, In vitro antibacterial and antibiofilm effects of cold atmospheric microwave plasma against *Pseudomonas aeruginosa* causing canine skin and ear infections, Vet. Dermatol., Nov 2021, doi: 10.1111/vde.13030.

[145] A. Privat-Maldonado *et al.*, ROS from physical plasmas: Redox chemistry for biomedical therapy, Oxidative Med. Cell. Longev. **2019** (2019) 9062098.

[146] R. Zhou *et al.*, Plasma-activated water: generation, origin of reactive species and biological applications, J. Phys. D-Appl. Phys. **53** (2020) 303001.

[147] V. Nastasa *et al.*, Toxicity assessment of long-term exposure to non-thermal plasma activated water in mice. Int. J. Mol. Sci. **22** (2021) 11534.

감사의 글

박사과정에 들어와 생소한 3D 프린팅 및 세포실험을 통하여 여러 가지 기술을 배우고 새로운 세상을 볼 수 있는 기회를 얻었습니다. 박사과정 중에서 여러 가지 일도 많았지만 새로운 사실을 알아가면서 성장할 수 있는 충실한 시간이었습니다.

오늘의 제가 있기까지 세심한 지도와 독려로 이끌어주신 평생의 스승이자 제 인생에서 가장 든든한 지원자이신 지도교수 김병훈 교수님의 은혜와 사랑에 고개 숙여 감사드립니다. 그리고 바쁘신 가운데도 열과 성의를 다해 심사해주신 최한철 교수님, 전남대학교 국민석 교수님, 김희중 교수님, 안상건 교수님 감사합니다. 세심한 부분까지의 지적과 수정을 통하여 부족한 저의 논문에 많은 도움을 주셨습니다.

언제나 저에게 아낌없는 조언을 해주신 전남대학교 김도형 교수님, 전남대학교 김명선 교수님, 미국에 계신 김도훈 교수님, 이헌 선배님, 처음 실험실에 와서 실험실 생활에 적응할 수 있게 도움을 준 명성운 박사님, 희상씨, 항상 웃는 얼굴로 실험실 분위기를 띄워주면서 실험장비의 사용법을 알려준 영욱이와 수영이, 실험과 연구로 바쁜 와중에도 많은 도움을 주신 정영일 박사님, 배인호 박사님, 김양경 박사님, 실험 준비에 도움을 준 김현준씨, 조혜리씨, 항상 같이 실험하면서 많은 도움을 준 국은별 선생님, 박지선 선생님, 김희연, 김창영, 김기준, 김호태에게 감사의 뜻을 전하고 싶습니다.

오늘이 있기까지 끊임없는 관심으로 언제나 힘이 되어준 사랑하는 가족과 친구들에게 깊은 감사의 말씀을 전하고 싶습니다.

2022. 01.

이 창 민 올림